NASA CR 159691

National Aeronautics
and Space Administration

A Computer Code for Estimating Installed Performance of Aircraft Gas Turbine Engines

Vol. I - Final Report

By Edward J. Kowalski

December 1979

Advanced Airplane Branch
Boeing Military Airplane Company
Seattle, Washington 98124

Prepared for

National Aeronautics and Space Administration
NASA-Lewis Research Center

Contract NAS3-21238

FOREWORD

This report documents the work accomplished during NASA LeRC Contract No. NAS3-21238. It was the purpose of this contract to develop a supervisory computer program which would tie together the routines (either presently existing or to be developed) to access the installation of a propulsion system. The contract was divided into seven tasks:

- Task A - Data Base
- Task B - Supervisory Program
- Task C - Nacelle Weight and Drag
- Task D - Nozzle Boattail Drag
- Task E - Pitot Inlets
- Task F - Two-Dimensional Inlets
- Task G - Axisymmetric Inlets

In TASK A, standardized formats for:

- Inlet performance and drag
- Nozzle internal performance and aftbody drag

were compiled for the data base described in this contract. In TASK B, a supervisory computer program was developed which evaluates the installation penalties associated with the inlets and nozzles of TASK A. The NASA NAVY Engine Program (NNEP), modified through the contract NAS3-21205 to predict bare engine weight, was used as this computer program's driver routine. The supervisory computer program also has the capability to determine the changes in inlet performance due to perturbations in engine cycle characteristics and/or inlet design parameters. In TASK C, computer procedures were developed for estimating nacelle weight and drag. In TASK D, a computer procedure was developed for estimating boattail drag for the nozzle data base of TASK A. In TASKS E, F, and G, a theoretically-based computer proceure was supplied to estimate conceptual design, performance and weight for pitot inlets, mixed and external compression axisymmetric and two-dimensional inlets.

Mr. L. J. Winslow was Program Manager for the Boeing Company. E. J. Kowalski was principal investigator. The following individuals contributed to the work accomplished during this contract: G. W. Klees, general consulting; R. A. Atkins, Jr., computer programming; S. G. Kyle and R. J. Pera, inlet performance; R. W. Rankin, inlet and nacelle weight; A. Hagen, A. Killinger, J. Welti, document preparation.

TABLE OF CONTENTS

LIST OF ILLUSTRATIONS

LIST OF ILLUSTRATIONS (cont.)

LIST OF ILLUSTRATIONS (cont.)

LIST OF ILLUSTRATIONS (cont.)

LIST OF ILLUSTRATIONS (cont.)

LIST OF ILLUSTRATIONS (cont.)

LIST OF ILLUSTRATIONS (cont.)

LIST OF TABLES

A	Area, ft^2 (m^2)
A_C	Inlet capture area, $ft^2(m^2)$
ALT	Altitude, ft(m)
A_o	$A_{o_I} - A_{o_{BLD}}$
$A_{o_{BLD}}$	Freestream tube area of bleed air entering the inlet, $ft^2(m^2)$
$A_{o_{BYP}}$	Free stream tube area of bypass air entering the inlet, $ft^2(m^2)$
A_{o_E}	Free stream tube area of engine demanded air entering the inlet, $ft^2(m^2)$
A_{o_I}	Free stream tube of air entering inlet, $ft^2(m^2)$
$A_{o_{SPL}}$	Free stream tube of air entering inlet, $ft^2(m^2)$
AR	Aspect ratio

A_w	Wetted area, $ft^2(m^2)$
A_{10}	Maximum cross sectional area, $ft^2(m^2)$
C_D	Drag coefficient
C_{F_G}	Nozzle gross thrust coefficient
C_P	Pressure coefficient
C_0	Angularity loss coefficient
$C_{D_{PAP}}$	Incremental drag coefficient due to tail fore-and-aft location
C_{D_R}	Incremental drag coefficient due to radial tail orientation
D	Drag, lb_f(Nt)
	Diameter, ft(m)
g_o	Acceleration of gravity, 32.174 ft/sec^2 ($9.806\ m/sec^2$)

h	Height, ft(m)
IMS_T	Integral mean slope parameter, truncated
	$IMS_T = -\frac{1}{(1 - A_9/A_{10})} \int_{A_9/A_{10}}^{1.0} \frac{d(A/A_{10})}{d(L/D_{eq})} \, d(A/A_{10})$
L	Length, ft(m)
M	Mach number
M_s	Started Mach number
P	Pressure, $lb_f/ft^2(Nt/m^2)$
PS	Power setting
q	Dynamic pressure, $lb_f/ft^2(Nt/m^2)$
r/D	Ratio of inlet lip radius to inlet highlite diameter
R_e	Reynolds number
T	Temperature, $^oR(^oK)$

SYMBOLS AND NOMENCLATURE (continued)

V	Velocity, ft/sec(m/sec)
W	Air flow, lb_m/sec(kg/sec)
	Weight, lb_m(kg)
	Width, ft(m)
W_{COR}	Corrected airflow - $\frac{W\sqrt{\theta}}{\delta}$, lb_m/sec(kg/sec)
α	Nozzle convergence angle
δ	Pressure ratio - P/2116.2
ϵ	Subsonic duct loss coefficient
γ	Ratio of specific heats
Θ	Temperature ratio - T/518.688
Θ_{DIV}	Divergence half angle
Θ_N	Wedge half angle (2D nozzle)

Θ_P	Plug half angle (round nozzle)
Θ_R	Radial tail orientation

Subscripts

AB	Aftbody
AC	Capture area
ADD	Additive
AMB	Ambient
BASE, B	Base flow region
BD	Bypass door
BLC	Bleed
BYP	Bypass
CD	Convergent-Divergent

CON	Convergent
D	Design
E	Exit
EFF	Effective
ENG	Engine
f	Flap
GEO	Geometric
HI	Hilite
lip	Inlet lip
MAX	Maximum
MIN	Minimum
MOM	Momentum
PRI	Primary

SYMBOLS AND NOMENCLATURE (continued)

REF	Reference
SEC	Secondary
SPILL	Spill
T	Throat
	Total
0	Local conditions for inlet, ambient conditions for nozzle
1	Inlet entrance
2	Compressor face
8	Nozzle throat
9	Nozzle exit

INTRODUCTION

During the preliminary design phase of aircraft development, it is necessary to evaluate many potential engine/airframe combinations to determine the best solution to a given set of mission requirements. The evaluation process must be thorough enough not to eliminate, at an early point in the preliminary design process, any configurations that might ultimately prove to be viable candidates if time were available to study them in detail. At the same time, speed in evaluating the configurations is also important because it permits many more configurations to be analyzed on the basis of actual data rather than subjective judgment or experience. In addition, manpower and money are often limited, especially in the typical preliminary design study group. This means that calculation procedures employed during these studies must be simple to use and require a minimum of input data preparation and setup time. Also, output data must be easily understood and the results presented in a format that is readily usable in comparing competing configurations.

The need for a practical first order propulsion installation method has been long recognized. Aircraft manufacturers have developed computerized methods for their own in-house analysis, but these are not generally available to the public. These in-house analytical methods are generally separate programs; thus, the total installation penalties are not normally visible until numerous types of installation routines are run. It was the purpose of this contract to develop a supervisory computer program which ties together these routines (either presently existing or to be developed) to assess the total installation penalty. These routines would include the capability of determining:

- engine performance
- engine weight and dimensions
- inlet/nozzle internal performance and drag
- nacelle drag
- inlet and nacelle weight

The estimation of engine performance is calculated by the NASA LeRC cycle analyzer entitled NAVY NASA Engine Program (NNEP) (see Reference 1).

The program WATE-2 (see Reference 2) provides a method to determine bare engine weight and dimensions based on the characteristics (airflow size, pressure ratio, etc.) of each engine component.

Inlet and nozzle internal performance and drag is determined using a modified version of PIPSI (see Reference 3). This installation routine utilizes inlet and nozzle performance maps of specific configurations. These performance maps are stored in a computer library. If an installation requires an inlet and/or nozzle which differs in physical or operational characteristics from those within the library, a derivative procedure is able to provide modified performance maps to reflect the changes of the required installation.

The Naval Weapons Center (NWC) inlet analysis program (see Reference 4) is used to determine internal and external performance for supersonic axisymmetric and two-dimensional fixed geometry inlets. This program, in general, predicts inlet performance at maximum airflow conditions, however, inlet total pressure recovery and inlet additive drag are determined as a function of terminal normal shock position during subcritical operation of a two-dimensional inlet.

A method (see Reference 5) was developed to analytically predict internal performance and drag for pitot inlets.

For podded installations, methods for determining nacelle drag and weight were developed.

Methods for predicting weight for pitot, axisymmetric and two-dimensional inlets were also developed.

1.0 PROGRAM DESCRIPTION

The following sections briefly describe the subprograms of the installation package.

1.1 NAVY NASA ENGINE PROGRAM (NNEP)

The Naval Air Development Center and the NASA Lewis Research Center have jointly developed a computer code (NNEP, see Reference 1) for thermodynamic cycle analysis of turbine engines. Through the use of stacked component maps and multiple flowpaths this code has the capability of simulating variable cycle engines with variable component geometry. It is also capable of design and off-design (matching) calculations and can optimize variables such as nozzle areas to minimize specific fuel consumption. It is a derivative of the Navy code NEPCOMP. A diagram of its subroutine connectivity is shown in Figure 1. A user guide for NNEP has been included in Vol. 2 of this report.

1.2 WATE-2

Industry, in general, has acquired an adequate computer capability to evaluate the thermodynamic performance of these diverse engine concepts, however, an accurate method of estimating engine weight and dimensions has not previously been available. An earlier weight predicting method (see Reference 6) that has been available to the general industry, predicts engine weight by statistical correlations of major cycle characteristics such as: airflow, bypass ratio, overall pressure ratio, etc. This method is probably capable of rough estimates for conventional engines; however, it is not applicable to nonconventional engines and could not predict weight within $\pm$10% as would be required in typical preliminary design studies.

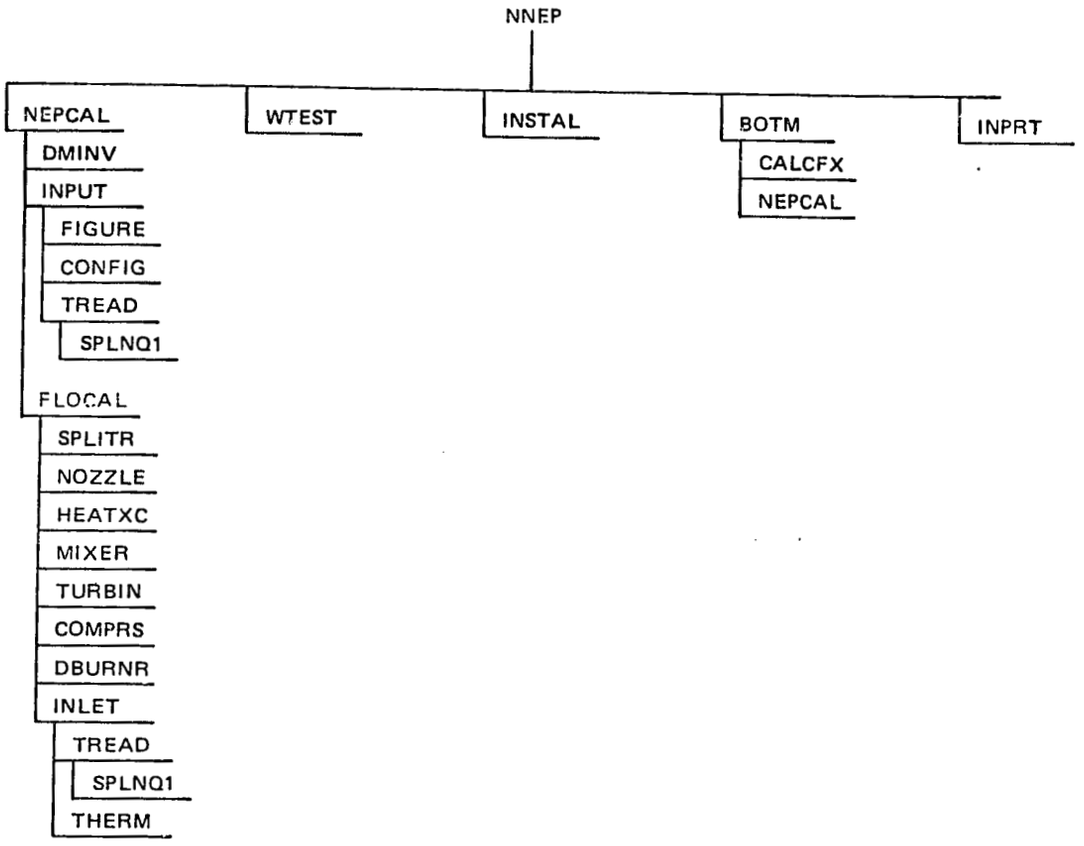

Figure 1. NNEP Connectivity Flow

A computerized program, WATE-2 (see Reference 2), was created to provide a more flexible and more accurate method based on correlations of component weight and physical characteristics, such as compressor airflow size, pressure ratio, hub-tip ratio, etc. This type of approach was more capable of estimating nonconventional engines, since the weight of each individual component was accounted for. As shown in Reference 2, no adequate correlations could be found and therefore a method based on mechanical preliminary design was chosen. This method uses stress levels, maximum temperature, material, geometry, stage loading, hub-tip ratio an shaft mechanical overspeed to determine component weight and dimensions.

The accuracy of the method is generally better than $\pm$10%, usually about $\pm$5%. The accuracy was verified by applying the method to 9 different engines, some of which were in the original data base and one small gas turbine engine. Engines used in the validation were selected by NASA after completion of the program.

Figure 2 diagrams the WATE-2 subroutine connectivity. A user guide for WATE-2 has been included in Vol. 2 of this report.

1.3 INLET AND NOZZLE INSTALLATION METHODS (INSTAL)

INSTAL is a computerized method for calculating installed propulsion system performance using computer-stored files of inlet and nozzle/aftbody characteristics in conjunction with the uninstalled engine data determined by NNEP. The inlet and nozzle/aftbody characteristics used in this procedure are obtained from a library of maps representing specific configurations.

The development of the installation program took full advantage of the existing version of the Performance of Installed Propulsion Systems - Interactive (PIPSI) procedure developed for the Air Force Flight Dynamics Laboratory (AFFDL) under Contract AFFDL-TR-78-91 (Reference 3) and the

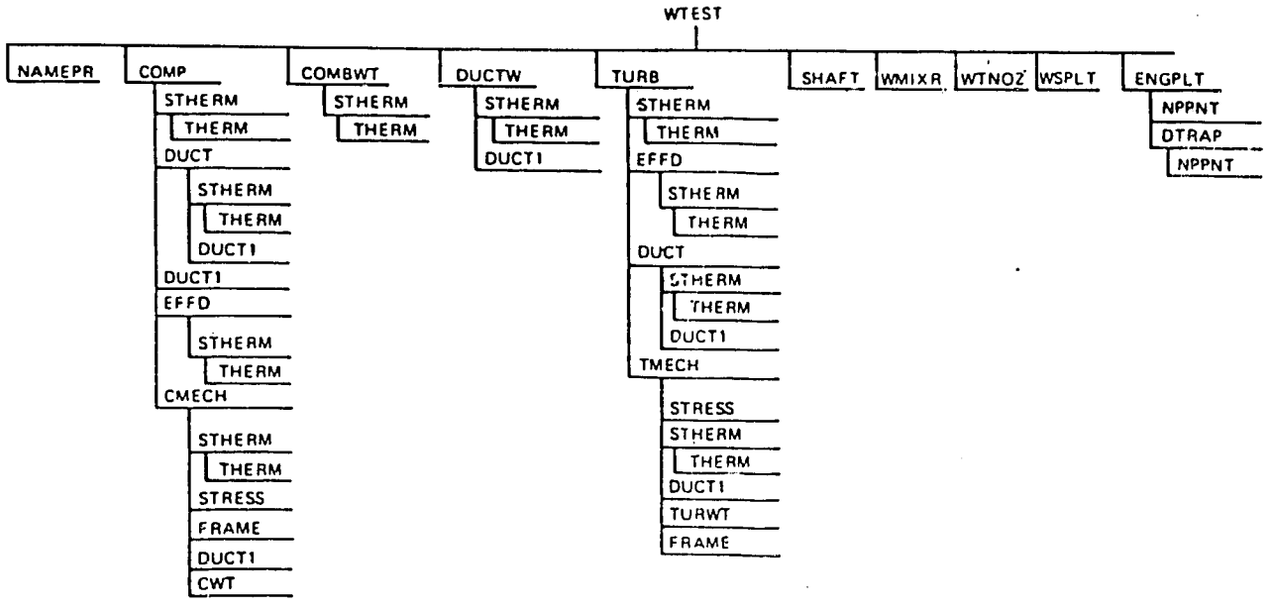

Figure 2 WATE2 Connectivity

Propulsion Installation and Table Assembly Program (PITAP) procedure developed for AFFDL under Contract F33615-72-C-1580 (Reference 5). The installation utilizes inlet and nozzle/aftbody performance characteristics obtained from a computerized file. This computerized file contains maps of standardized format which provide the internal losses and drag characteristics for a variety of specific inlet and nozzle/aftbody configurations. These configurations are designed to cover a wide spectrum of Mach numbers from subsonic to Mach 3.5.

The computer library of inlet and nozzle/aftbody characteristics enables the user to find in the available files an inlet or nozzle/aftbody configuration that is, in most cases, a fairly close match to the configuration under investigation. Inlet maps for a total of 19 configurations and nozzle/aftbody maps for 9 configurations are available for use with the installation procedure. The configurations to which these maps correspond are described in Section 2.3.1.1 of this report. The complete documentation of input maps is provided in Volume III.

A procedure exists which allows the program user to make trade studies between bypass and spillage airflow. The purpose of this procedure is to provide the user with maximum visibility of the effects on performance of various design options that may be available for handling excess inlet airflow. The bypass vs. spillage trade study analysis procedure is discussed in Section 2.3.1 of this report.

Figure 3 shows the installation routines connectivity diagram.

1.4 DERIVATIVE PROCEDURE

The purpose of the derivative procedure (see Reference 3) is to provide a first-order analytical and empirical method which determines the effects on the performance of an inlet and/or nozzle when the design parameters are altered. This procedure operates on the library of stored inlet and nozzle performance maps; it represents the performance characteristics of the perturbed configuration by generating new input maps. Figure 4 shows the derivative procedures subroutine connectivity diagram.

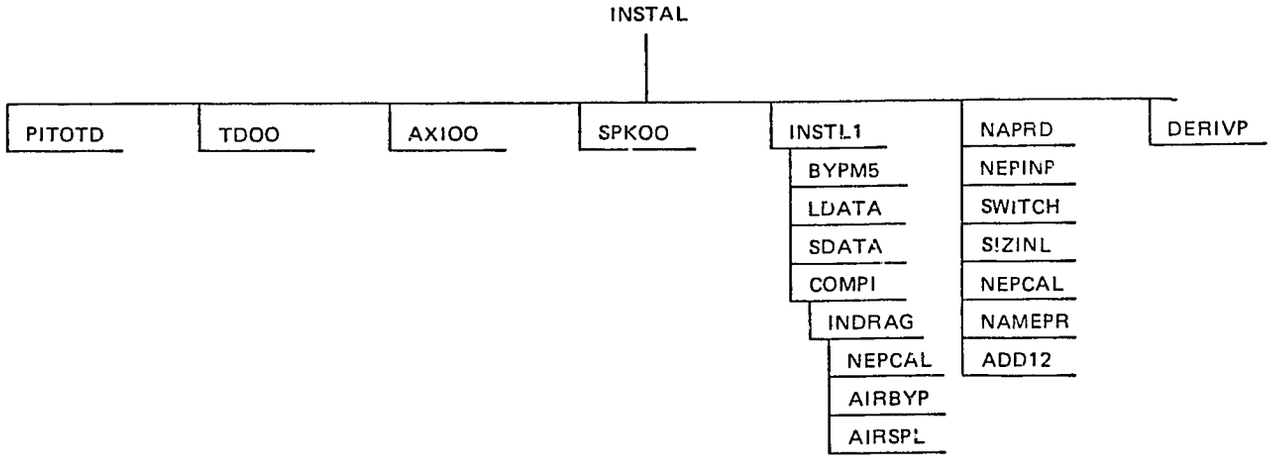

Figure 3 Instaliation Connectivity Diagram

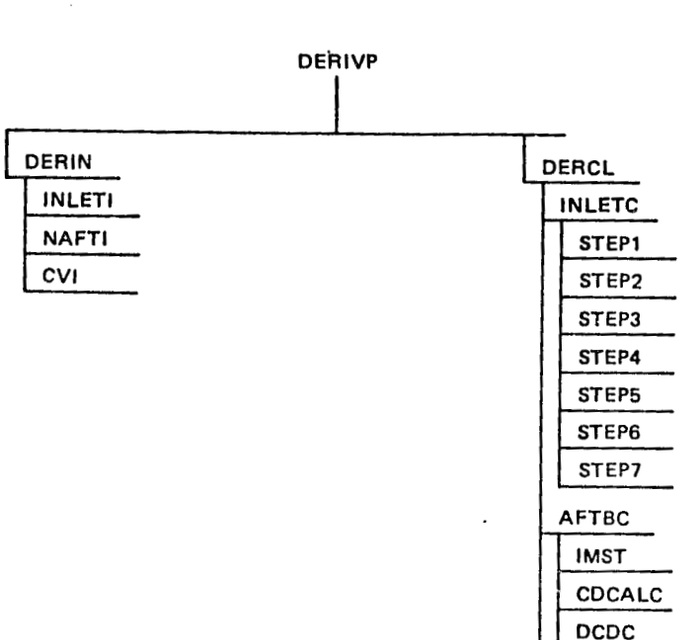

Figure 4 Derivative Procedure Connectivity Diagram

1.5 NAVAL WEAPONS CENTER INLET DESIGN AND ANALYSIS PROGRAM

McDonnell Aircraft Company (MCAIR) has completed a program (see Reference 4) for the Naval Weapons Center (NWC) under Contract No. N000123-72-C-0335 to automate procedures for the design and analysis of two-dimensional and axisymmetric inlets. These automated procedures are currently operational on the NWC UNIVAC 1108 system and the MCAIR CDC 6600 system. Under this contract with NASA LeRC, NAS3-21238, this routine was converted to be compatible with the IBM 360/67 TSS Computer System and the NNEP code.

The computer program's design and analysis procedures for fixed geometry two-dimensional and axisymmetric inlets cover the supersonic flight regime up to approximately Mach 5.

Analytical and empirical techniques are used in the procedures to calculate inlet flow field and performance parameters, including airflow, total pressure recovery, and drag. For the two-dimensional inlets, the methods are applicable both to external or mixed compression inlets which utilize external compression surfaces composed of single, double, or triple ramps, or single ramps followed by isentropic compression surfaces. The procedures include the capability for analyzing configurations with various sideplate and cowl shapes and lip radii.

For the axisymmetric inlets, the methods are applicable both to external and/or mixed compression inlets which utilize compression surfaces composed of single, double, or triple cones, or single cones followed by isentropic compression surfaces. The inlets which have a single cone followed by an isentropic compression surface will be referred to as spike inlets in this report. Pitot inlets are not addressed by the program.

Diagrams of its subroutine connectivity are shown in Figures 5 through 7.

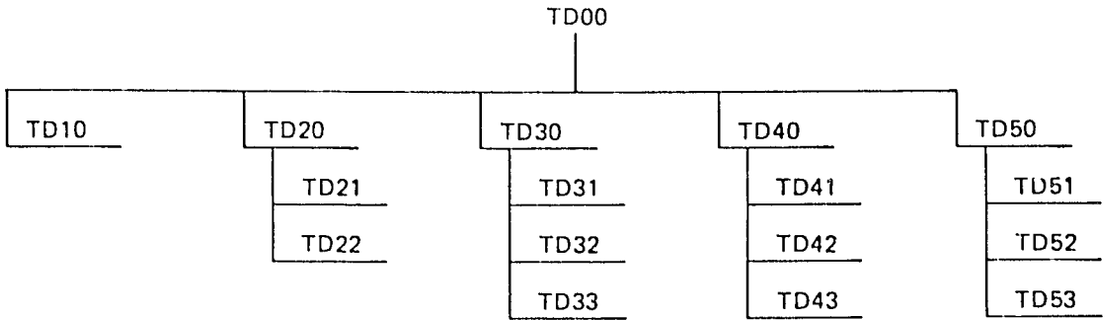

	Function
TD00	Controls transfers to Level 2 of structure
TD10	Takes in general input information
TD20	Sets up M_o and α loops for single ramp cases, controls transfers to TD 21 and 22
TD21	Analyzes critical and subcritical operation of a single ramp inlet
TD22	Analyzes supercritical operation of a single ramp inlet which has an external compression surface followed by a converging-diverging duct.
TD30	Sets up M_o and α loops for double ramp cases, controls transfers to TD 31, 32, and 33
TD31	Designs a double ramp external compression surface inlet and analyzes critical and subcritical operation of same
TD32	Analyzes critical and subcritical operation of a double ramp inlet
TD33	Analyzes supercritical operation of a double ramp inlet which has an external compression surface followed by a converging-diverging duct.
TD40	Sets up M_o and α loops for triple ramp cases, controls transfers to TD 41, 42, and 43
TD41	Designs a triple ramp external compression surface inlet and analyzes critical and subcritical operation of same
TD42	Analyzes critical and subcritical operation of a triple ramp inlet
TD43	Analyzes supercritical operation of a triple ramp inlet which has an external compression surface followed by a converging-diverging duct.
TD50	Sets up M_o and α loops for isentropic wedge (4 ramp) cases, controls transfers to TDs 51, 52, and 53
TD51	Designs an isentropic wedge external compression surface inlet, approximates this inlet as a 4 ramp inlet and analyzes critical and subcritical operation of same
TD52	Analyzes critical and subcritical operation of a 4 ramp inlet
TD53	Analyzes supercritical operation of a four ramp inlet which has an external compression surface followed by a converging-diverging duct.

Figure 5 Two-Dimensional Design Program Connectivity Diagram

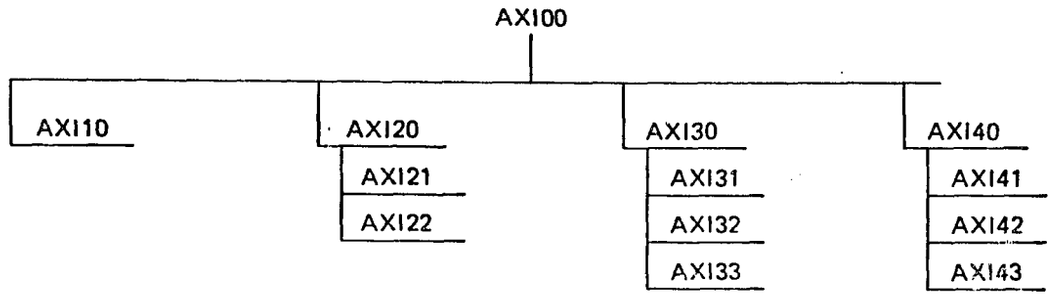

Function

AXI00 Controls transfers to Level 2 of structure

AXI10 Takes in general input information

AXI20 Sets up M_o loops for single cone cases, controls transfers to AXIs 21 and 22

AXI21 Analyzes critical operation of single cone inlet

AXI22 Analyzes supercritical operation of a single cone inlet which has an external compression surface followed by a converging-diverging duct.

AXI30 Sets up M_o loops for double cone cases, controls transfers to AXIs 31, 32, and 33

AXI31 Designs a double cone external compression surface inlet and analyzes critical operation of same

AXI32 Analyzes critical operation of a double cone inlet

AXI33 Analyzes supercritical operation of a double cone inlet which has an external compression surface followed by a converging-diverging duct.

AXI40 Set up M_o loops for triple cone cases, controls transfers to AXIs 41, 42, and 43

AXI41 Designs a triple cone external compression surface inlet and analyzes critical operation of same

AXI42 Analyzes critical operation of a triple cone inlet

AXI43 Analyzes supercritical operation of a triple cone inlet which has an external compression surface followed by a converging-diverging duct.

Figure 6 *Axisymmetric Design Subroutine Connectivity Structure*

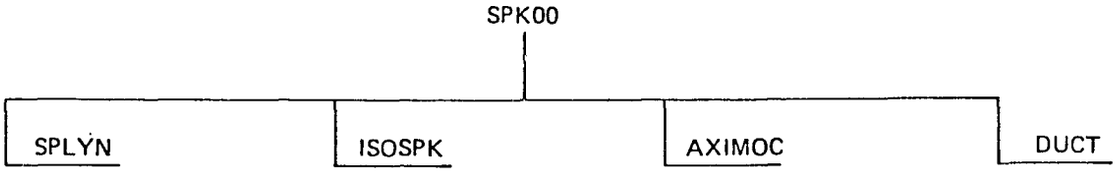

	Function
SPK00	Takes in general input information, controls transfers to Level 2 of structure
SPLYN	Takes the coordinate arrays defining the external compression surface and fits them to a curve fit
ISOSPK	Uses conical flow theory and method of characteristics computations to design an isentropic spike contour given focal point, free stream Mach number and flow deflections
AXIMOC	Uses method of characteristics computations to determine the flow field adjacent to the external compression surface of an axisymmetric spike inlet and analyzes critical operation of same
DUCT	Analyzes supercritical operation of a axisymmetric spike inlet which has an external compression surface followed by a converging-diverging duct.

Figure 7 Axisymmetric Spike Design Connectivity Structure

1.6 PITOT INLET ANALYSIS AND DESIGN

A theoretically-based computer procedure (see Reference 5) was developed to supplement the NWC program to provide inlet recovery, drag and major dimensions for pitot inlets. The method is applicable to two types of pitot inlet applications: (1) subsonic CTOL or V/STOL aircraft and (2) transonic and supersonic aircraft for flight at Mach numbers up to 2.0. The major dimensions that are determined are overall length, highlite area, throat area, lip contraction ratio, subsonic diffuser length, area ratio, and maximum diameter. The database of Section 1.3 also includes pitot inlet performance.

The diffuser total pressure losses for subsonic pitot inlet is determined from correlations of diffuser and lip losses ($\Delta P_T/q_1$ or P_{T2}/P_{T1}) as a function of inlet geometric variables and throat Mach number. These correlations have been developed from test data for a variety of pitot inlet configurations covering a wide range of geometric variables.

The drag and recovery prediction procedures have been computerized to provide a systematic way to obtain predicted performance as a function of inlet geometric variables.

For transonic and supersonic pitot inlet performance predictions, the effects of shock-generated losses are combined with the diffuser and lip losses to obtain predictions of overall recovery. Drag correlations for pitot inlets have been extended to Mach 2.0 to provide drag predictions.

A diagram of its subroutine connectivity is shown in Figure 8.

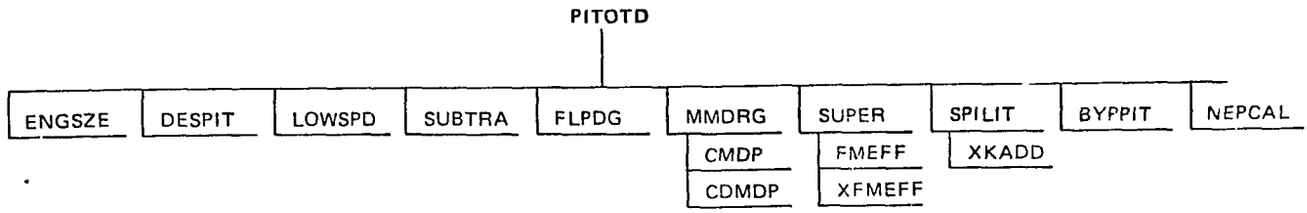

Figure 8 PITOT Connectivity Diagram

1.7 NACELLE AND INLET WEIGHT

Boeing Military Airplane Development Weight Technology Staff engineers have developed weight prediction methods for nacelles and inlets. These methods are currently being used in support of conceptual design, configuration development and technology assessment studies.

During conceptual design and/or configuration development, nacelle and/or inlet detail design data are not available. Only general airplane design parameters are known at this stage of airplane development: mission requirements, general arrangement drawing (a three view), basic engine dimensions and location (podded-wing or body mounted, body buried, etc.), engine airflow and sea level static thrust and inlet and nozzle type. These weight prediction methods are well suited when there is limited design information available. They will typically produce results within $\pm$ 10% of the actual weight of inlets and nacelles.

1.8 NACELLE DRAG

Nacelle drag is calculated for podded installations. During subsonic operation, skin friction drag and form drag will be caculated; during supersonic operation, skin friction drag and wave drag will be calculated.

Friction drag is the integral of the shearing stresses taken over the exposed surface (wetted area) of the vehicle. In practice, the friction drag is dependent on the amount of exposed surface, the average skin friction coefficient and the surface roughness. The major portion of subsonic minimum parasite drag can be attributed to skin friction. The component of parasite drag often referred to as form drag or "profile" drag results from the aircraft overall shape or profile which is submitted to the free stream. The form drag presented in this section is designed to be applied at subsonic speeds only. Wave drag is the zero lift pressure drag resulting from the formation of shock systems associated with the supersonic flow of compressible fluid around an object of finite thickness.

2.0 METHOD OF SOLUTION

The following sections describe the methods used to assess the various aspects of the installed performance of a propulsion system. The areas to be addressed are:

- o engine performance
- o engine weight and dimensions
- o inlet/nozzle internal performance and drag
- o nacelle drag for a podded installation
- o inlet and nacelle weight

The computer routines which determine these installation losses are tied together by the supervisory program, NNEP.

2.1 NAVY NASA ENGINE PROGRAM (NNEP)

The NASA-Lewis Research Center (NASA LeRC) utilizes the computer code, NNEP (see Reference 1) for thermodynamic cycle analysis of turbine engines. Through selected engine component combinations this program has the capablity of:

- o simulating any turbine engine
- o simulating variable component performance
- o changing airflow paths while operating
- o optimizing variable-geometry settings to minimize specific fuel consumption or maximize thrust

NNEP is used as the supervisory program which calls all installation subprograms:

WTEST:	engine weight and dimensions
INSTAL:	inlet and nozzle performance
	inlet and nacelle weight
	nacelle drag

Consult Reference 1 for a detailed description of the method of solution.

2.2 WATE-2

A method has been developed to estimate engine weight and major envelope dimensions of large axial flow aircraft jet engines and small gas turbine engines. The computerized method, called WATE-2 (Weight Analysis of Turbine Engines), determines the weight of each major component in he engine, such as compressors, burners, turbines and frames. A preliminary design approach is used where stress level, maximum temperature, material, geometry, stage loading, hub-tip ratio, and shaft mechanical overspeed are used to determine the component weight.

For podded installations, the engine dimensions that WATE-2 predicts are used to determine a nacelle configuration. The weight and drag of this nacelle (see sections 2.3.5 and 2.3.6) then can be determined.

Consult Reference 2 for a detailed description of the method of solution.

2.3 INSTALLATION

A computer program entitled, "Performance of Installed Propulsion System - Interactive" (PIPSI) (see Reference 3), was designed to:

- o provide a rapid process of calculating installed propulsion system performance data while including realistic effects of inlet and nozzle losses due to drag and internal performance.
- o assure the accuracy and suitability of the installation procedure for use in preliminary design studies
- o reflect the effects of throttle sensitive changes in inlet and nozzle/afthody losses.

The reference version of PIPSI utilizes a computer stored library of inlet and nozzle performance characteristics in conjunction with an intermediate file of uninstalled engine data as input. The basic structure of the main

calculation procedures of the PIPSI computer program is shown by the flow charts of Figures 9 and 10. Figure 9 shows how the inlet procedure handles the functions of sizing the inlet, matching the inlet input data with the engine airflow demand, and obtaining the matched inlet performance parameters from the inlet data tables. Engine corrected airflow demand is the matching parameter between engine data and inlet data. Figure 10 shows the nozzle/aftbody procedure. Nozzle total-to-ambient pressure ratio is used as the matching parameter for matching nozzle performance data to engine data.

Under this contract, the PIPSI installation procedure was modified to run in conjunction with NNEP; no intermediate file of uninstalled engine performance data is generated.

After the desired inlet and nozzle are selected, each flight condition that is to be installed must be run through NNEP twice. In the initial pass, all &D inputs are identical to those of the basic form of NNEP with the exception of a new variable INST. This parameter must be set to zero. This first pass is needed to determine the corrected airflow that the engine requires. The installation routine will then determine the pressure recovery that the desired inlet must operate at in order to supply engine demand. With INST = 1, the second pass through NNEP will use this inlet recovery along with the proper value of C_{F_G}, determined from the gross thrust coefficient map to determine engine performance. Each s[illegible]d portion of the installation routine:

- o inlet drag
- o nozzle drag
- o inlet and/or nacelle weight
- o nacelle drag

will then be executed.

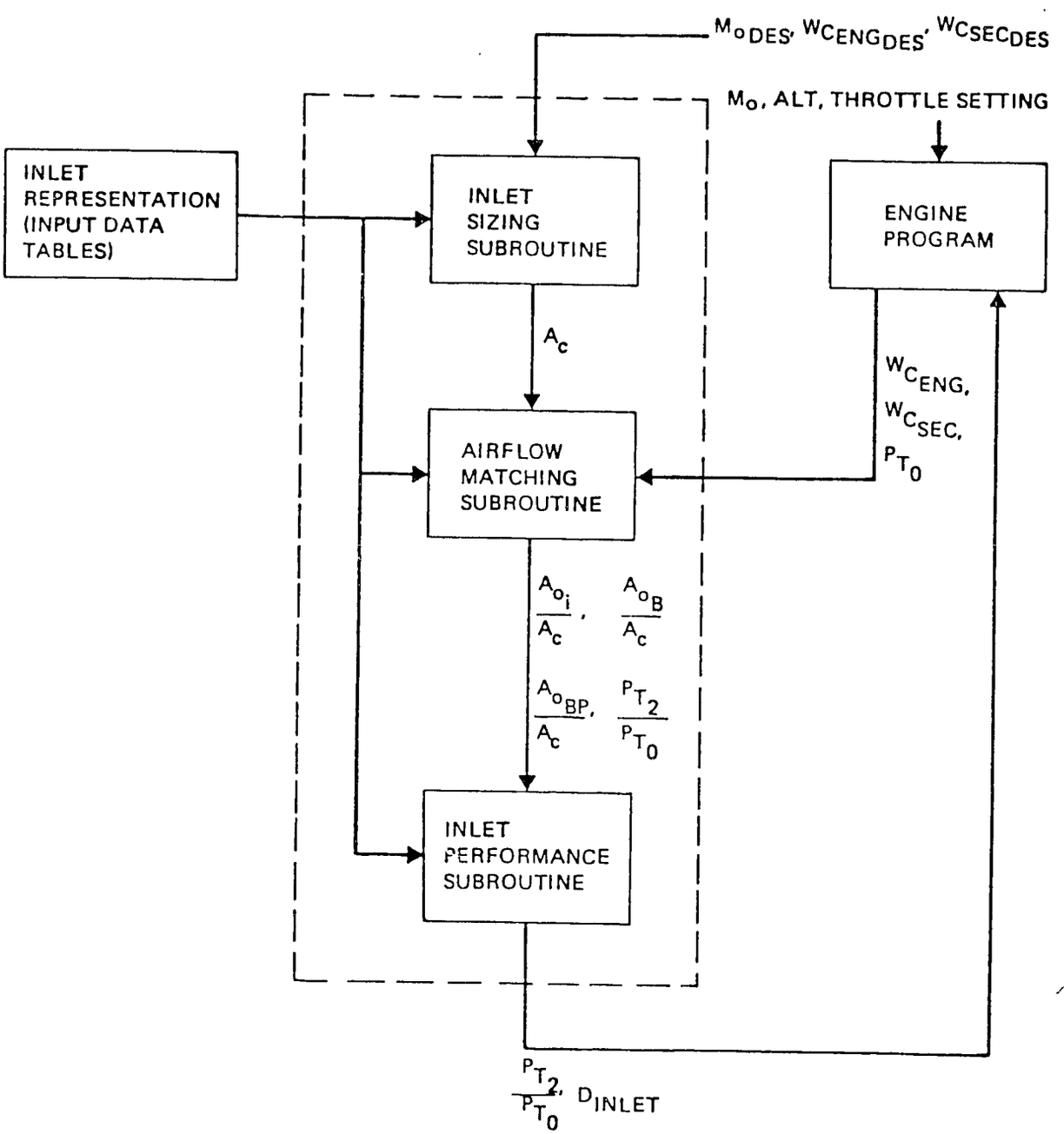

Figure 9 Inlet Procedure

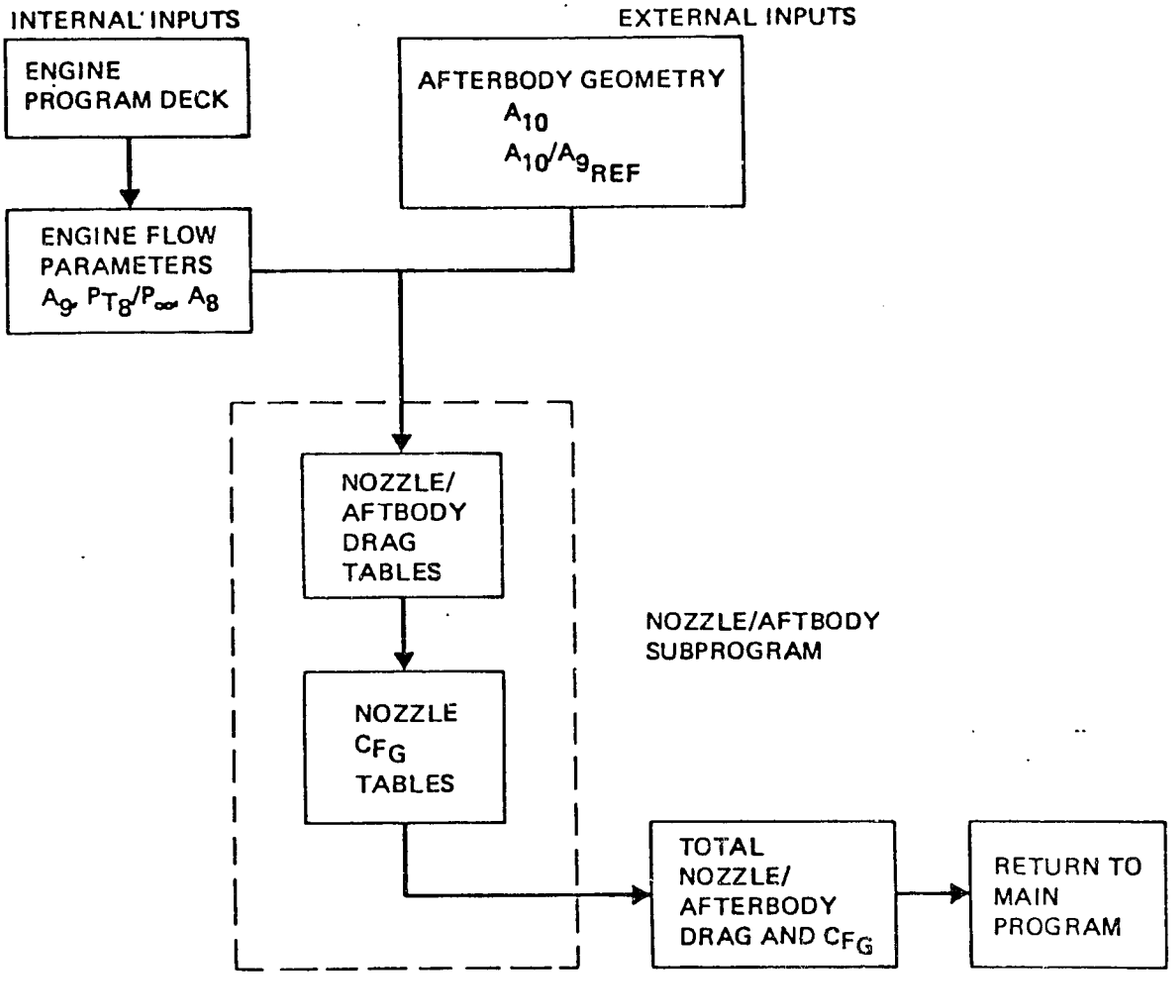

Figure 10 Nozzle/Aftbody Procedure

Pitot inlets are included in the inlet map data base. However, if the pitot inlet analytic design routine is utilized, the inlet pressure recovery and drags are determined analytically (see Section 2.3.1.2.1) at each flight condition. Maps of inlet performance data are not used. The NWC inlet analysis routine for supersonic axisymmetric and two-dimensional inlets also does not require performance maps. This program, in general, predicts inlet performance at maximum airflow conditions, however, inlet total pressure recovery and inlet additive drag are determined as a function of terminal normal shock position during subcritical operation of a two-dimensional inlet.

2.3.1 INLET PERFORMANCE ESTIMATION

The inlet performance subprogram of the INSTAL procedure involves considerably more procedural steps than the nozzle/aftbody drag and gross thrust coefficient subprograms. This is due to the fact that each aspect of the inlet system that contributes to the total inlet drag must be calculated separately. The drag due to spillage, bleed, and bypass must be determined as a function of mass flow ratio, adding to the complexity of the computer program.

Inlet performance maps are input data to the inlet subprogram. This subprogram sizes the inlet capture area (if desired) and converts the inlet performance maps into total pressure recovery and inlet drags that are matched to the corrected airflow demand of the engine.

The sizing routine permits the inlet to be sized for operation at a desired inlet mass flow ratio and recovery using the engine airflow demand. If desired, a specified capture area can also be input. The capability of inputing or sizing a new capture area for any throttle setting of any flight conditions exists to permit better matching between engine demand and inlet supply.

The inlet input requires fourteen tables of input data which describe the performance characteristics of the inlet. Engineering data obtained from

wind tunnel tests and theoretical calculations are used to obtain the inlet performance characteristics. The format for the inlet data is shown in Figure 11. The relationship between local and flight Mach numbers may be input by the user if this information exists. Otherwise, the relationship will be one-to-one as shown in the data base (Vol. 3).

The inlet procedure recognizes three modes of inlet operation: low-speed, external compression, and mixed compression. The low-speed mode is used only at very low Mach numbers, e.g., takeoff conditions, when only high engine power settings are likely to be of interest and inlet drag is negligible. The external-compression mode is used over the remaining Mach number regime for external-compression inlets. It is also used for the remaining subsonic regime and supersonic Mach numbers less than the starting Mach number for mixed-compression inlets. The mixed-compression mode is used at or above the starting Mach number for mixed-compression inlets.

a) External-Compression Inlets. The INSTAL calculation of recovery and drag for an external-compression inlet is illustrated in Figure 12. Table 1 is used to represent the effect of the airplane flow field on the local Mach number seen by the inlet. Table 2A gives the basic recovery/mass-flow-ratio characteristics of the inlet. The minimum Mach number for which data is input in Table 2A is taken by the program to be $M_{o_{min}}$, below which only the lowspeed mode is used.

   In the low-speed mode, recovery is read directly out of Table 2B as a function of local Mach number only, and inlet drag is neglected.

   If the local Mach number exceeds $M_{o_{min}}$, the recovery and mass flow ratio are determined using Table 2A, Table 7 (which gives the scheduled bypass flow, if any, as a function of engine mass flow ratio), and the engine corrected airflow demand.

   INSTAL iterates to solve simultaneously for the matchpoint recovery

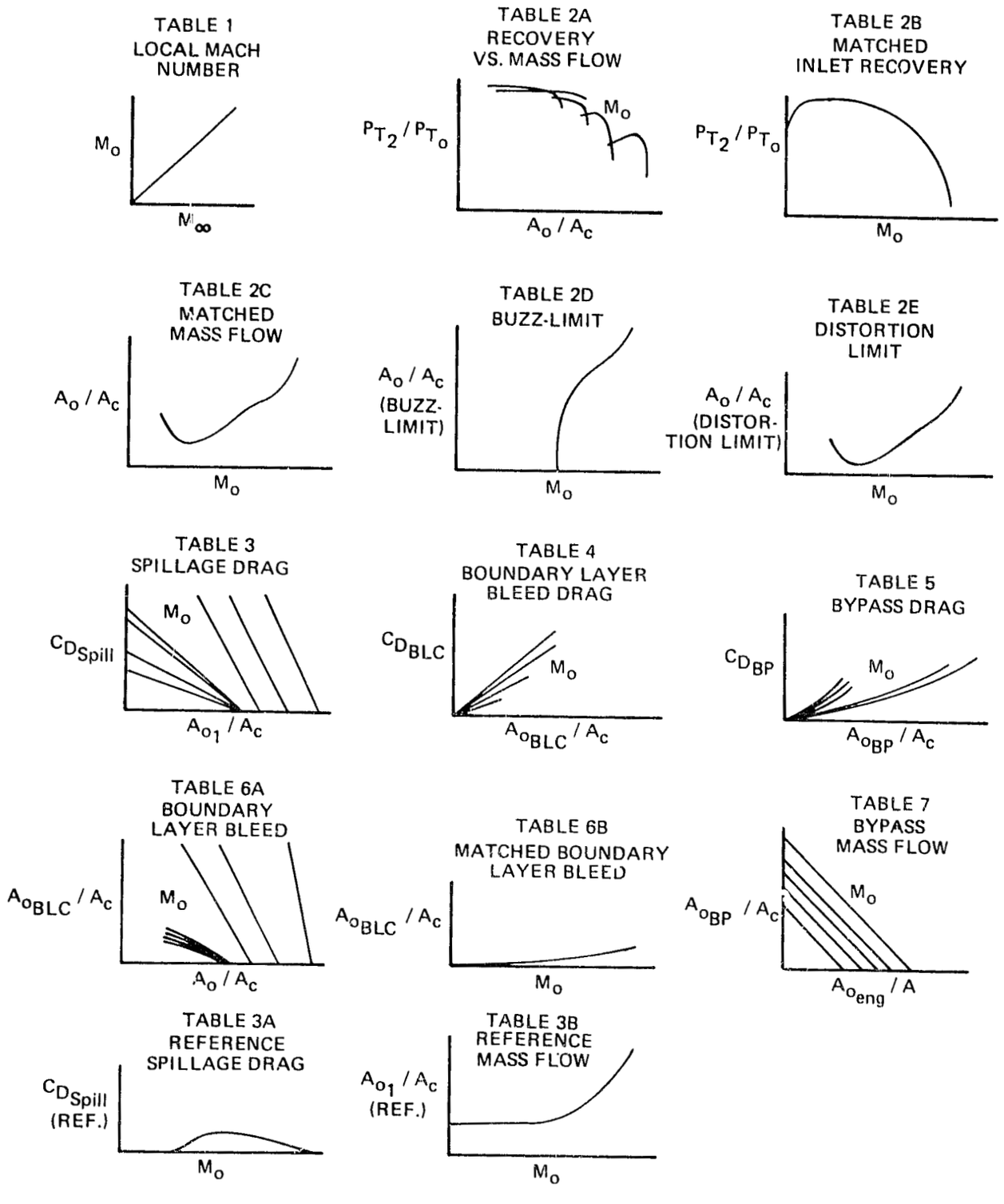

Figure 11 Format for Inlet Performance Maps.

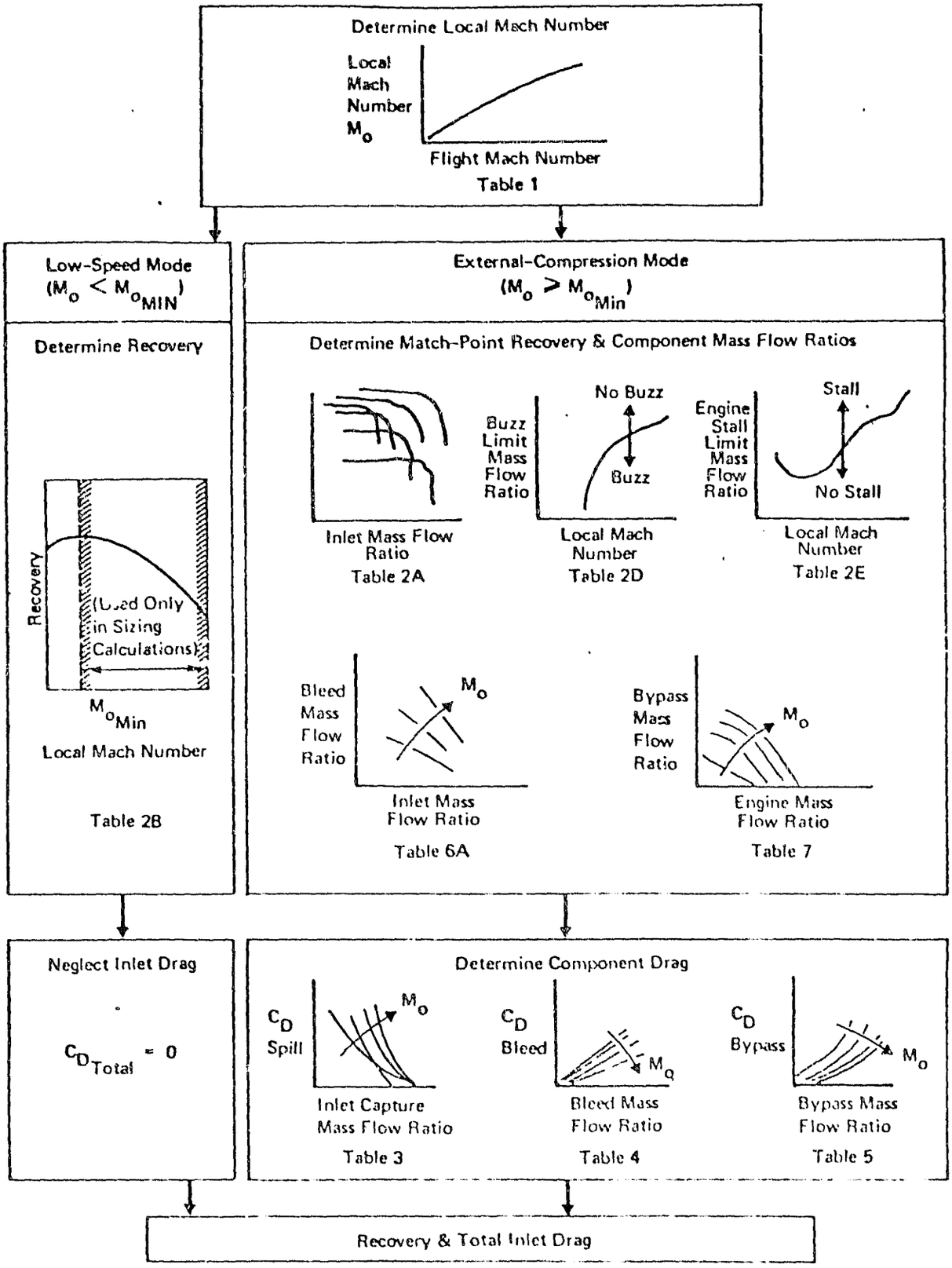

Figure 12 PIPSI Performance Calculation for an External-Compression Inlet

and inlet mass flow ratio, as well as the engine mass flow ratio and scheduled bypass flow. If the indicated buzz (Table 2D) or distortion (Table 2E) limits are exceeded, an appropriate warning message will appear, but no fatal error will result. The bleed mass flow associated with the calculated inlet mass flow ratio is determined from Table 6A.

After the required mass flow ratios are determined, spillage, bleed, and bypass drags are found from Tables 3, 4, and 5, respectively. Spillage drag is the incremental change in additive drag and pressure drag on the airplane due to inlet operations at mass flow ratios less than a reference mass flow ratio. The bleed and bypass drags include door drags as well as momentum loss of the airflow.

b) Mixed-Compression Inlets. The performance calculation for a mixed-compression inlet is illustrated in Figure 13. Below the starting Mach number, M_S, the low-speed mode and external compression mode are used in the same way as in the case of an external-compression inlet. The mixed-compression mode, used at or above M_S, is based on the assumption that a closed-loop bypass system is available to remove all excess air. Thus, except for the case of excessive engine airflow demand, the inlet mass flow ratio, bleed flow, and recovery may all be scheduled as a function of local Mach number only; the bypass system compensates for changes in engine airflow demand.

If the corrected airflow delivered by the inlet is inadequate to meet the engine demand at the scheduled recovery, the program will permit the inlet to operate at an excessive supercritical margin. The recovery will be lowered sufficiently to match the engine corrected airflow demand, and an appropriate message will warn the user of an undersized inlet.

Inlet spillage, bleed, and bypass drag are found using Tables 3, 4, and 5, as in the external-compression mode. The data in these tables for Mach numbers equal to or greater than M_S apply only for started inlet operation.

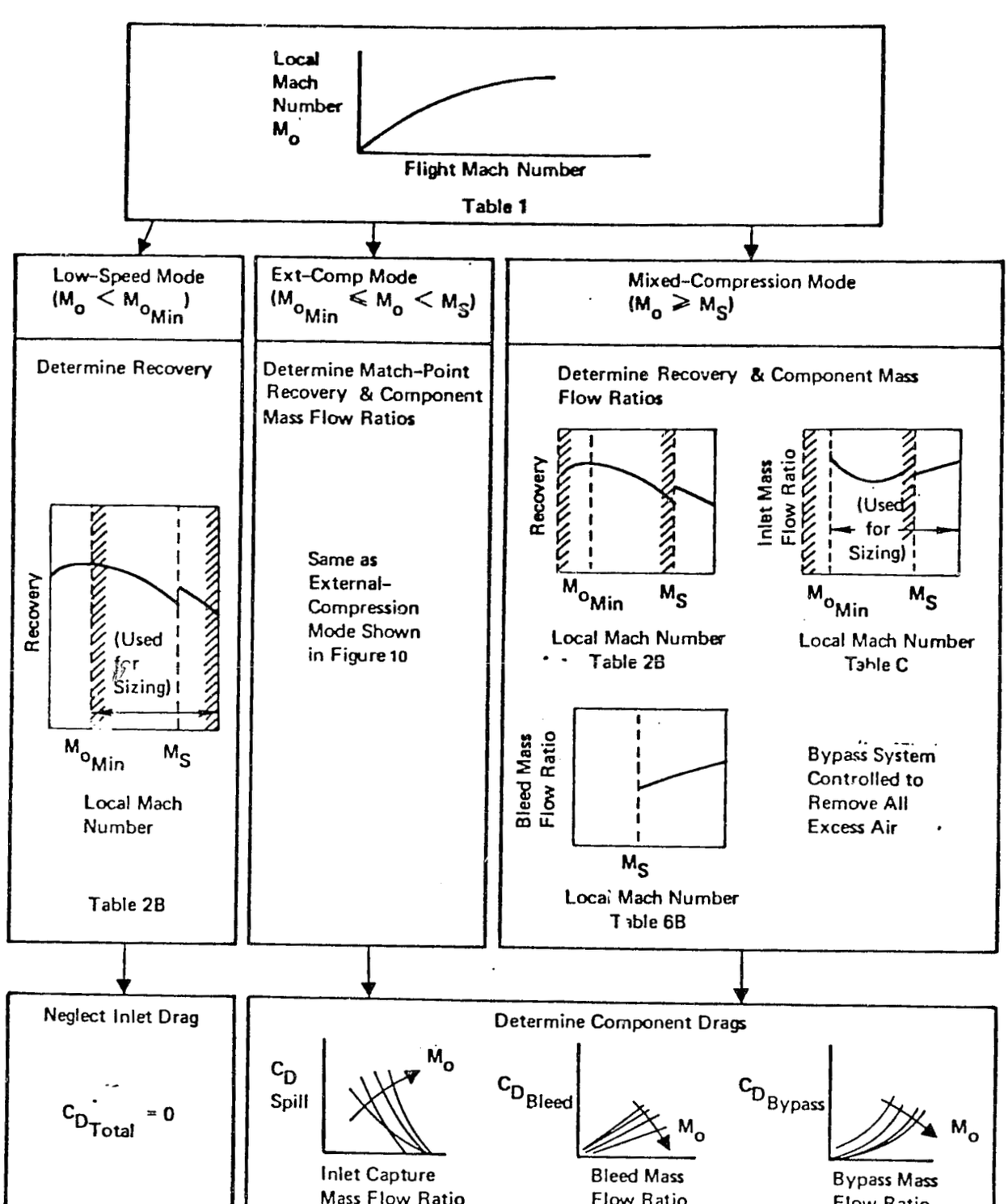

Figure 13 PIPSI Performance Calculation for a Mixed-Compression Inlet

Inlet Sizing

For sizing calculations, Table 2C of recommended inlet airflow variations A_o/A_C vs. M_o and Table 2B of recommended inlet total pressure recovery vs. M_o are used to determine the required capture area variation with Mach number. These parameters are used in the following equations to calculate capture area, A_C:

$$A_c, \text{in.}^2 = \frac{A_{o\,ENG}}{(A_o/A_c)_{MATCHED}} = \frac{\left(\frac{W\sqrt{\theta}}{\delta}\right)\left(\frac{P_{T_2}}{P_{T_o}}\right)_{MATCHED}\left(\frac{A}{A^*}\right)_o}{.343\,(A_o/A_c)_{MATCHED}}$$

Inlet Reference Conditions

For purposes of aero-propulsion thrust/drag bookkeeping, a reference mass flow ratio is employed. This reference mass flow ratio is shown in Table 3B of Figure 11. It represents the inlet mass flow ratio, A_{o_I}/A_C, at which the spillage drag is defined as zero. This reference provides the zero drag reference base for the input spillage drag variations vs. A_{o_I}/A_C at each Mach number input as Table 3. The reference mass flow ratio is selected to be a mass flow ratio at or near the point of maximum inlet flow areas ratio at each M_o. At this point, no further throttle-dependent inlet airflow variations would be expected. Therefore, at this mass flow ratio it is logical to include the drag of the spilled airflow in the airplane drag polar. The inlet drag reference mass flow ratio concept is illustrated in Figure 14.

For users who prefer to use a mass flow ratio of 1.0, an option is included in the computer program to add the incremental reference spillage drag to the spillage drag input data of Table 3, thereby creating a reference mass flow ratio equal to 1.0.

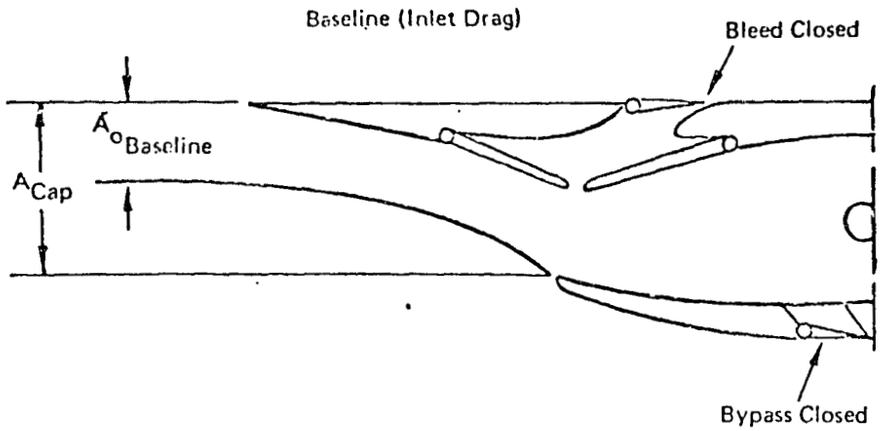

The inlet baseline reference condition for spillage drag is defined at each Mach number as shown below. This condition was chosen because:

a) it corresponds to an accurate reference and measurable condition for the real inlet,

b) it corresponds to a condition when inlet spillage drag is minimum (i.,e., minimum lip separation and therefore less error in scaling),

c) it is near the operating condition of the inlet (airplane reference model therefore contains major inlet interference effects).

Figure 14 Definition of Inlet Reference Mass Flow Ratio

Bypass vs. Spillage Trade Calculation

A calculation procedure (see flow diagram of Figure 15) has been developed and programmed that provides the capability to automatically perform trade studies between bypass and spillage airflow. The purpose of this procedure is to provide the program user with maximum visibility of the effects of various design options that may be available for handling excess inlet airflow.

The trade study procedure provides the user with the option to select any of the following modes for disposing of excess airflow:

Mode	
1	All excess airflow spilled
2	All excess airflow bypassed above a specified Mach number
3	Scheduled bypass with remainder of excess airflow spilled
4	Optimum combination of bypass and spillage for minimum drag
5	Optimum combination of bypass and spillage for minimum installed SFC (includes effect of bypass on total pressure recovery)

For visibility, an optional printout can be specified by the user that will display the complete results of the spillage/bypass trade studies.

2.3.1.1 INLET PERFORMANCE MAP LIBRARY

The purpose of the library of inlet maps is to provide a readily-available source of inlet performance characteristics that can be utilized by the installation computer program. When calculations are to be performed, the library computer file representing the inlet data is searched for the requested inlet using namelist inputs.

The inlet performance characteristics are stored in the form of tables of standardized format (see Figure 11). This format was selected to provide a standardized framework in which either experimental data or the results

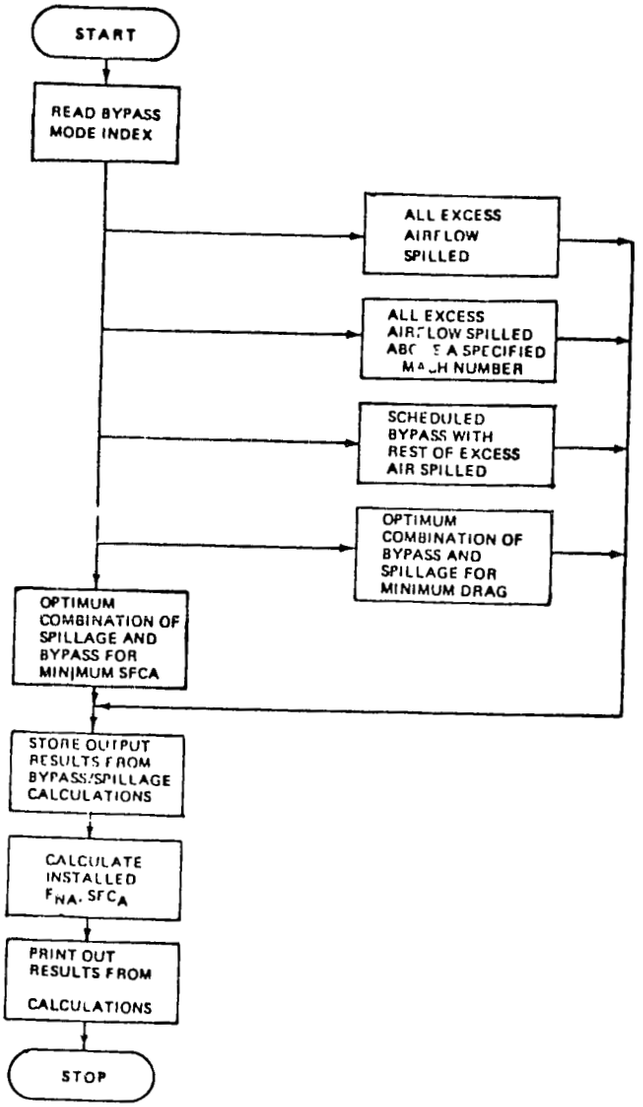

Figure 15 General Flow Chart for Bypass Vs. Spillage Trade Studies

of analytical calculations can be used. The input format for the data remains constant, but the data that goes into the tables can come from various sources depending on the amount of time available for preparing the data and/or the amount of experimental data available. Because of the fact that data in the input tables can be changed, it is possible to improve the accuracy of the installed propulsion system performance calculations as more detailed data become available.

The matrix of inlet configurations for which performance characteristics are available is shown in Figure 16. Performance characteristics are available for a total of 19 separate inlet configurations. These configurations include a variety of inlet types: chin, pitot, two-dimensional and axisymmetric external compression, and two-dimensional and axisymmetric mixed compression. The design Mach number range covered by the configurations is 0.5 to 3.5.

The inlet configurations that are represented by the library of performance characteristics have been selected by considering the following factors:

1. At each design Mach number, the configuration must be typical of an inlet that could reasonably be used at that Mach number. Design Mach number affects such design features as variable geometry, number of compression ramps, boundary layer bleed system design, and mixed vs. external compression scheme. The way typical inlet design features vary as design Mach number is increased is illustrated in Figure 17. In general, the trend is toward more inlet complexity and more variable geometry as design Mach number increased, assuming a high level of total pressure recovery is to be maintained.

2. Experimental data were available for several inlet configurations that could be used to provide well-substantiated inlet performance maps. It has been an objective of the program to use experimental data whenever it is available and the

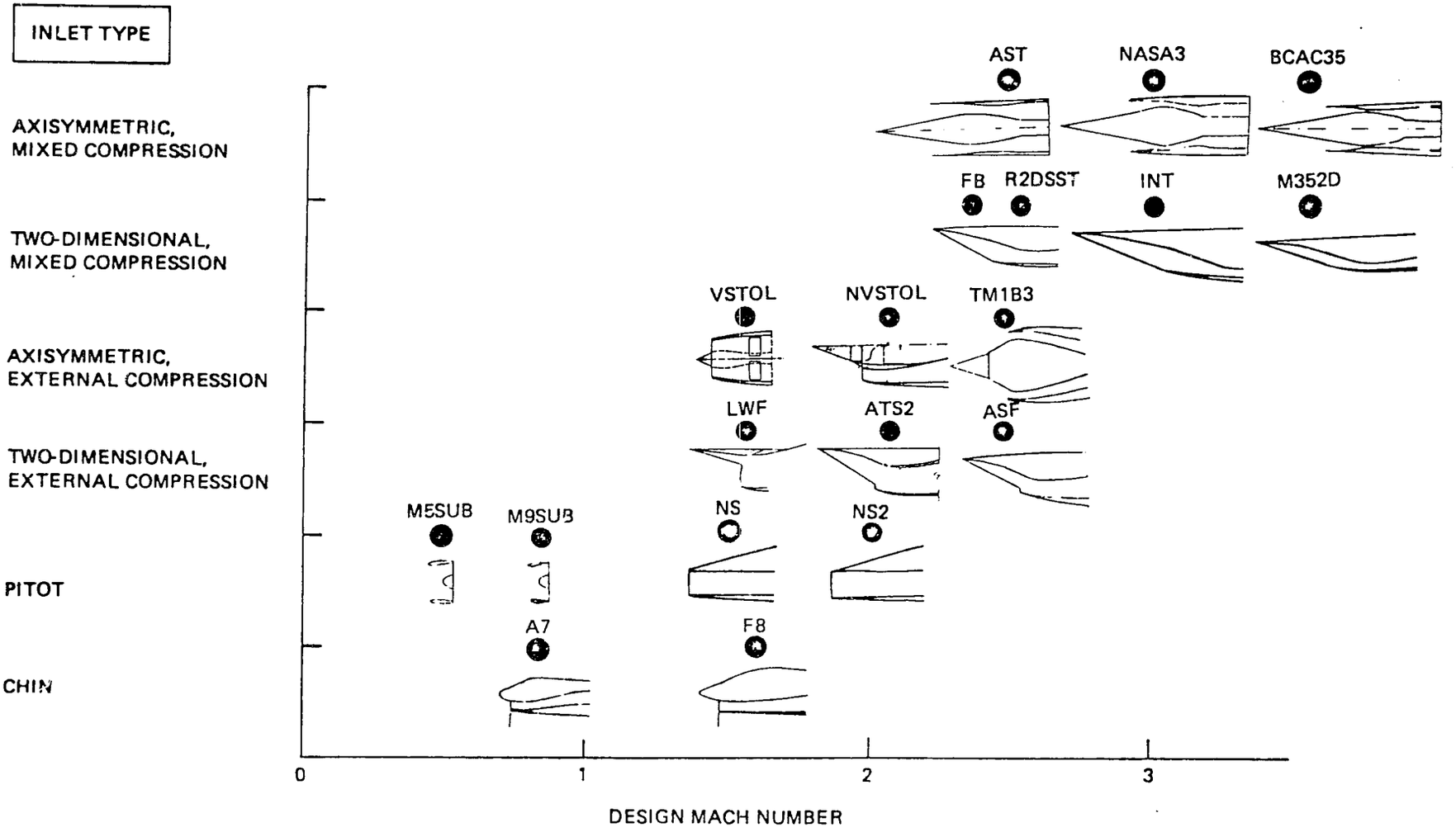

Figure 16 Matrix of Inlet Maps

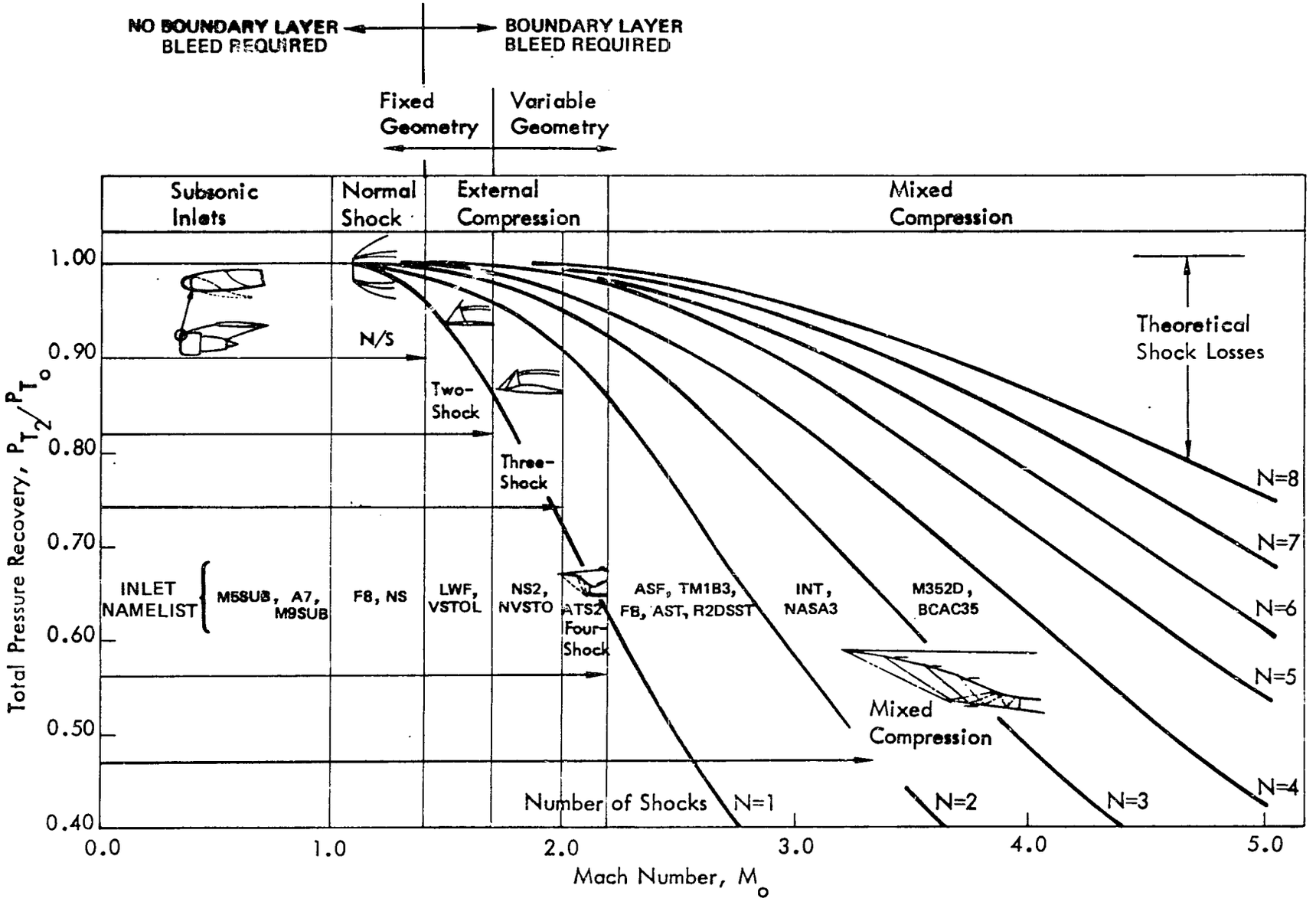

Figure 17. Representative Spectrum of Inlets

configuration is suitable (or typical) for the intended application. Examples of some of the useful sources of data that have been utilized in developing the inlet performance characteristics are: Tailor-Mate tests (Reference 7), F-15 inlet tests (Reference 8), Boeing LWF tests (Reference 9), XB-70 tests (Reference 10), NAR F-100 inlet tests (Reference 11), and Boeing subsonic inlet tests (Reference 12).

3. Several sets of inlet performance characteristics were available from the Air Force Contract F33615-72-C-1580 (Reference 5). These data were used for Configurations NS2, LWF, ASF, VSTOL, FB, and INT, largely unchanged, except for some revisions in the data table formats.

4. Inlet data were available at Boeing for Configurations ATS2 and NVSTO. These inlets represent typical inlet configurations for the required design Mach numbers.

A summary chart is presented in Figure 18 which shows the inlet configuration namelist, a brief description of the inlet, and the source of the data and/or methods used to obtain the inlet performance characteristics. In addition to the information shown in Figure 18, each of the inlets is described in detail in Vol. III.

2.3.1.2 INLET DESIGN AND ANALYSIS METHODS

The capability of determining inlet performance through the use of a theoretically-based analysis procedure was required. The NWC inlet program (see Reference 4) was used for the design and analysis of two-dimensional and axisymmetric inlets operating in the supersonic flight regime. The analytical method of Reference 5 was modified to analyze pitot inlets of CTOL or V/STOL design.

INLET FILE NAME	INLET CONFIGURATIONS AND SOURCES OF DATA USED TO DEVELOP THE INLET MAPS
A7	A-7 type inlet; developed from published A-7 data and engineering analysis
F8	F-8 type inlet; developed from published F-8 inlet data and analysis
M5SUB	Subsonic inlet type; based on data and methods from Boeing subsonic inlet (i.e., 707,727, etc.)
M9SUB	Subsonic inlet type; based on data and methods used to develop Boeing 747-type inlets
NS	Normal shock inlet; based on data from Rockwell tests of F-100 airplane inlet
NS2	Normal shock-type inlet; based on data from Rockwell F-100 inlet, Boeing LWF inlet tests, and GD LWF inlet data
LWF	Fixed-Geometry, 2-shock inlet; based on data from Boeing LWF inlet tests
ATS2	Four-shock, variable ramp inlet; theoretical design based on analysis, optimized for M_O = 2.0
ASF	Four-shock, variable ramp inlet; based on data from NR inlet tests of IPS model
VSTOL	Fixed-Geometry, single cone inlet; based on analytical design for a M_O = 1.6 VTOL
NVSTOL	Three-Shock, half-round inlet with variable-diameter centerbody; analytical design for a supersonic Navy VTOL configuration
TM1B3	Three-shock, half-round inlet with variable second cone angle; GD tailor-mate tests
FB	Mixed-compression; analytical design documented in AFFDL-TR-72-147-vol IV
INT	Mixed compression; based on XB-70 type configuration and data
M352D	Mixed compression; based on NASA AMES configuration and tests of a mach 3.5, 2-D inlet
AST	Mixed compression axisymmetric; based on a Boeing analytical study of an AST inlet for NASA AMES
NASA3	Mixed compression axisymmetric; based on data from NASA AMES tests of M_O = 3.0 inlet
BCAC35	Mixed compression axisymmetric; based on results of Boeing analytical studies for a NASA AMES mach 3.5 inlet
R2DSST	Mixed compression 2-D; based on results of Boeing/Rockwell studies for a SST inlet

Figure 18 Sources of Data for Inlet Maps

2.3.1.2.1 PITOT INLET ANALYSIS METHOD

The inputs required for this method are described in the users manual, section 3.2.4.4.

Inlet capture area may either be inputed or calculated for any flight condition. If capture area is not input, the flight condition inputs are run through NNEP to determine the engine demand connected airflow, W_{COR_2}. The inlet recovery used for this first pass through NNEP is a user input (see users manual, section 3.2.1.1).

Using the inputed maximum effective throat mach number, $MT_{EFF_{MAX}}$, the following procedure determines the maximum Mach number at the inlet entrance, $M_{AC_{MAX}}$:

(see figure 19.)
$$A_T/A^* = \frac{\left[1. + .2\left(M_{T_{EFF_{MAX}}}\right)^2\right]^3}{1.728 M_{T_{EFF_{MAX}}}}$$

Figure 20 is required to determine the maximum geometric throat Mach number, $M_{T_{GEO_{MAX}}}$ as a function of $M_{T_{EFF_{MAX}}}$, lip bluntness ratio (r/D), and flight Mach number (M).

The ratio of effective throat area to geometric throat area, $A_{T_{EFF}}/A_{T_{GEO}}$ is determined using the equation for the isentropic area ratio (figure 19):

$$\frac{A_{T_{EFF}}}{A_{T_{GEO}}} = \frac{(A/A^*)_{EFF}}{(A/A^*)_{GEO}}$$

A simplifying assumption is made that the pressure recovery from the inlet hilite to the inlet throat, $P_{T_T}/P_{T_{AC}}$, equals $A_{T_{EFF}}/A_{T_{GEO}}$. This assumption is based on the following rationale:

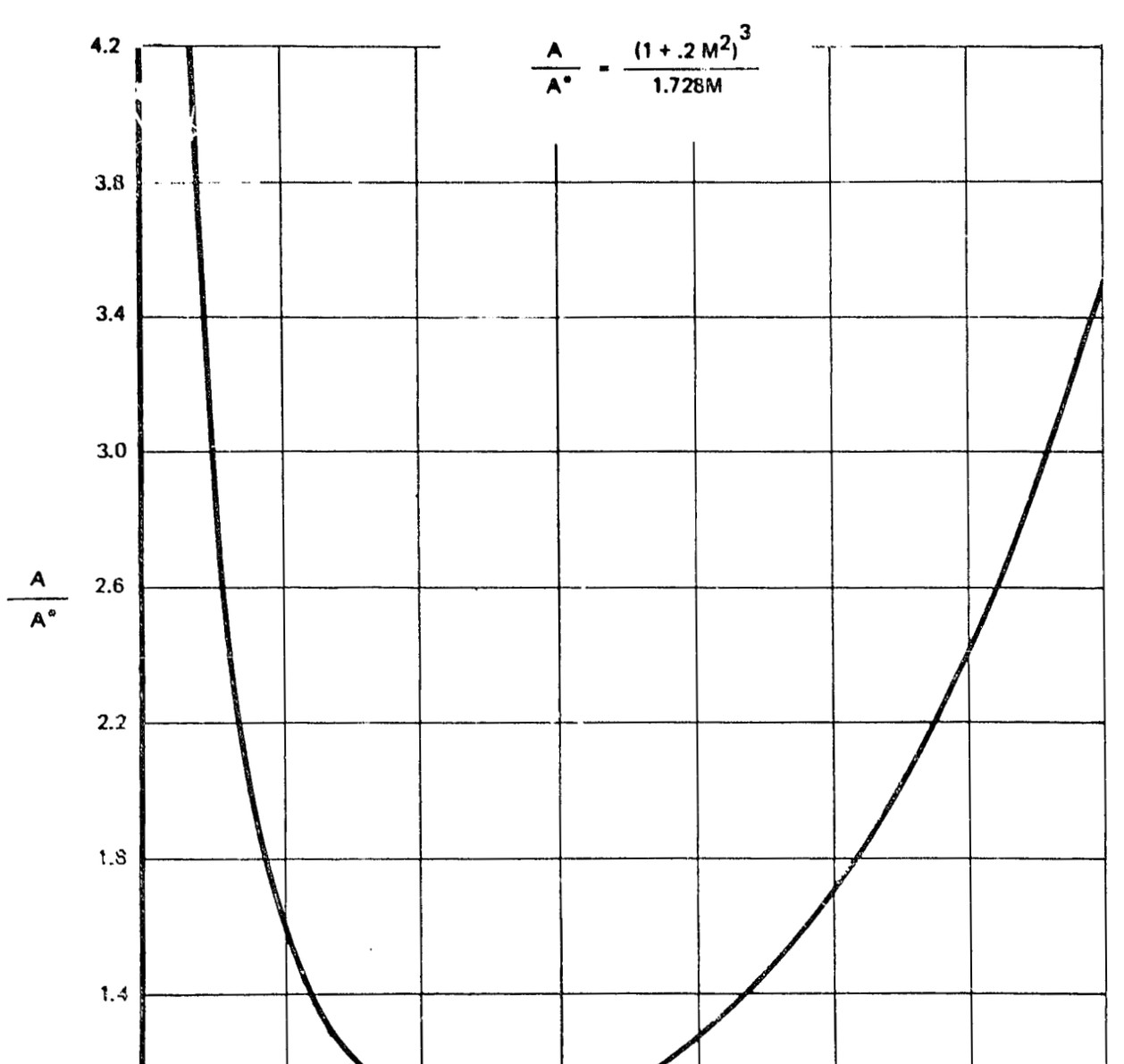

Figure 19 : ISENTROPIC AREA RATIO

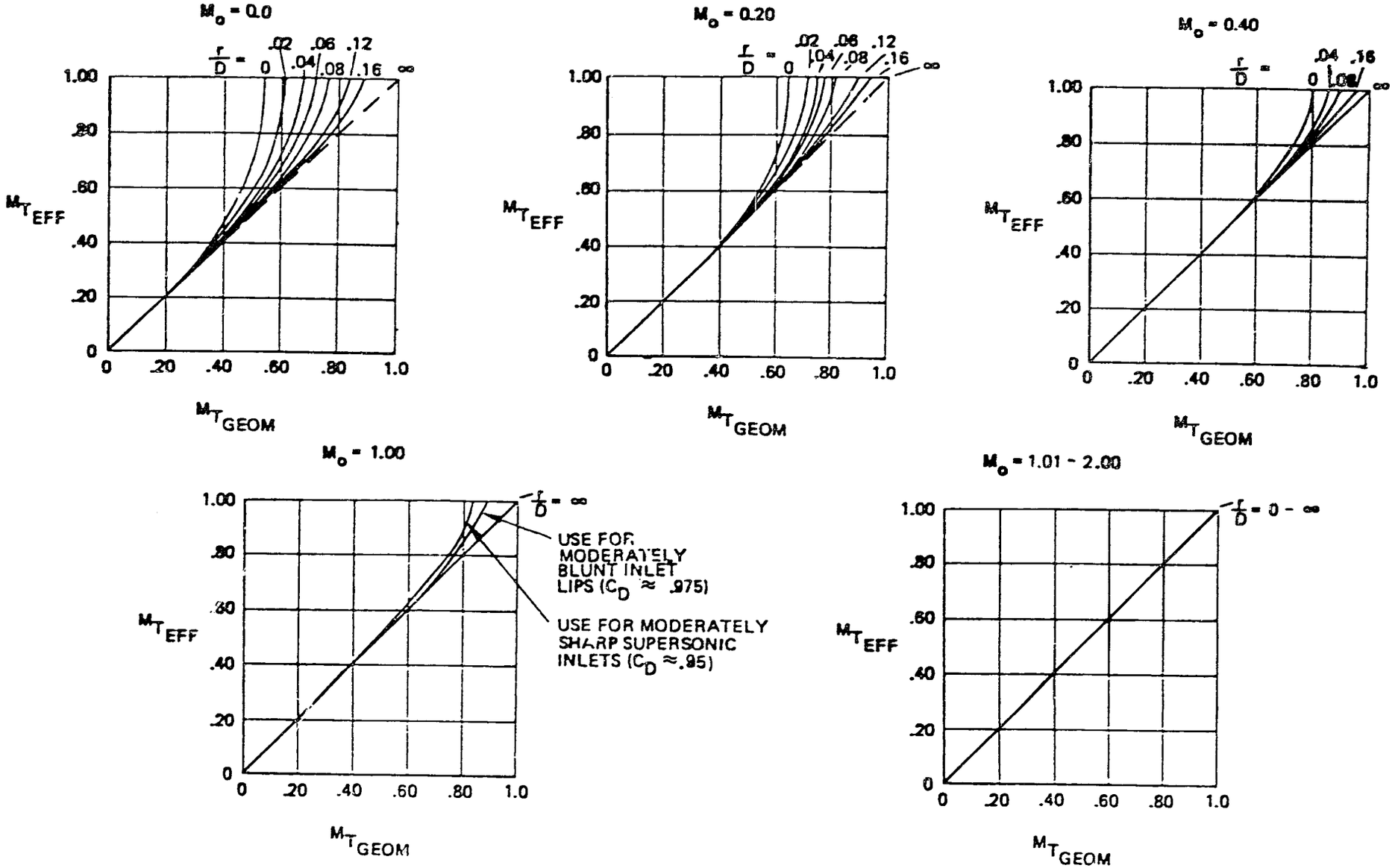

Figure 20: EFFECTIVE INLET THROAT MACH NUMBER

If $A_1=A_2$ but there is a loss in total pressure between point 1 and 2, then the Mach number at point 2 will be higher than that at point 1, because of the effective reduction in area ratio, $(A/A^*)_2$, since $(A^*)_2$ has increased. The present method assumes that the reduction in $(A/A^*)_2$ is equivalent to that obtained by reducing A_2 and keeping A*constant between points 1 and 2. Thus, there is a direct relationship between $A_{2_{EFF}}$ and A_1 which is related to the lip loss. This relationship can be expressed as:

$$\frac{P_{T_T}}{P_{T_1}} = \frac{A_{2_{EFF}}}{A_2}$$

and since $A_2 = A_1$, and $A_2 = A_T$

$$\frac{P_{T_T}}{P_{T_1}} = \frac{A_{T_{EFF}}}{A_{T_{GEO}}}$$

$M_{AC_{MAX}}$ is then determined from the isentropic area ratio at the capture area (figure 19). $A_C/A^* = \left(A_T/A^* \left(\frac{r_{HI}}{r_T}\right)^2\right) \Big/ \left(\frac{P_{T_T}}{P_{T_{AC}}}\right)$

Next, the effective throat Mach number, $M_{T_{EFF}}$, is determined. If the flight Mach number is supersonic, the Mach number behind and the pressure recovery across the normal shock are determined using the normal shock relations:

$$\frac{P_{T_{AC}}}{P_{T_0}} = \left[\frac{(\gamma+1)M^2}{(\gamma-1)M^2+2}\right]^{\frac{\gamma}{\gamma-1}} \left[\frac{\gamma+1}{2\gamma M^2-(\gamma-1)}\right]^{\frac{1}{\gamma-1}}$$

$$M_2 = \sqrt{\frac{(\gamma-1)M^2+2}{2\gamma M^2-(\gamma-1)}}$$

where M = free stream Mach number

If M_2 (for supersonic flight conditions) or (for subsonic flight conditions) is greater than $M_{AC_{MAX}}$ then $M_{T_{EFF}} = M_{T_{EFF_{MAX}}}$. If M_2 or M is less than or equal to $M_{AC_{MAX}}$ then $M_{T_{EFF}}$ must be determined through an interation. The recovery from the inlet hilite to the inlet throat, $P_{T_T}/P_{T_{AC}}$ is assumed to be .995. The isentropic area ratio at

the inlet hilite is determined

$$(A/A^*)_{AC} = \frac{(1 + .2M^2)^3}{1.728M^2}$$

A_T/A^* is then calculated from the isentropic area ratio at the throat:

$$A_T/A^* = \frac{A_{AC}/A^* \dfrac{P_{T_T}}{P_{T_{AC}}}}{r/D^2}$$

$P_{T_T}/P_{T_{AC}}$ is then calculated using

$$\frac{P_{T_T}}{P_{T_{AC}}} = \frac{\left(1 + .2\left(M_{T_{EFF}}\right)^2\right)^3}{\left(1 + .2\left(M_{T_{GEO}}\right)^2\right)^3} \qquad \frac{M_{T_{GEO}}}{M_{T_{EFF}}}$$

The calculated recovery is then compared to the guessed recovery. If they differ, a new assumed recovery is determined by averaging the old guessed value with the calculated value. When the guessed recovery equals the calculated recovery, the inlet total recovery is determined.

The subsonic diffuser duct loss coefficient, $\epsilon = P_T/q_1$, is obtained from input data showing the variation of versus the effective throat Mach number. Figure 21 shows the data that is programmed; this can be changed to suit the application. ϵ is then used to calculate the total pressure recovery of the subsonic diffuser (see figure 22).

$$\frac{P_{T_2}}{P_{T_T}} = 1 - \epsilon\left(1 - \frac{1}{(1 + .2\,(M_{T_{EFF}})^2)^{3.5}}\right)$$

The overall total pressure recovery is then calculated

$$\frac{P_{T_2}}{P_{T_0}} = \frac{P_{T_2}}{P_{T_1}} \frac{P_{T_T}}{P_{T_{AC}}} \frac{P_{T_{AC}}}{P_{T_0}}$$

where $\dfrac{P_{T_{AC}}}{P_{T_0}} = 1$ for subsonic flight.

(1) Ref: PG 117
NA 68-655
Vol X
(2) Subsonic Entrance Profile
(3) Diffuser $L/h_t = 9$
(4) Thin Boundary Layer

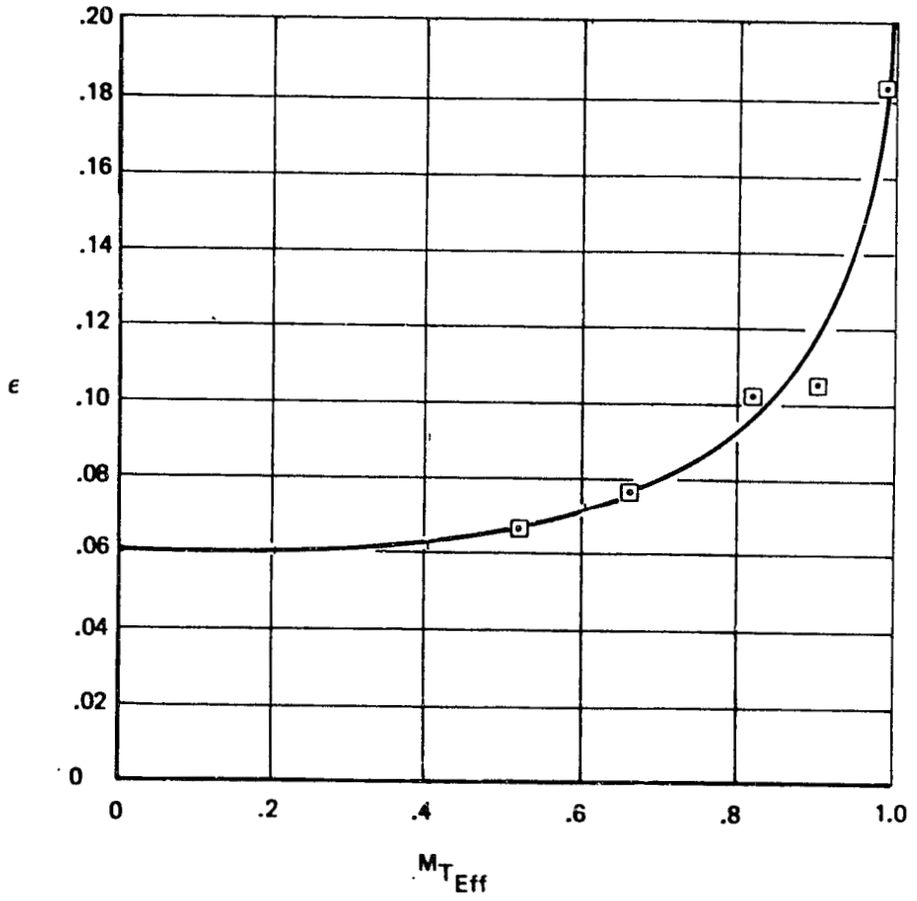

Figure 21: DIFFUSER LOSS COEFFICIENT

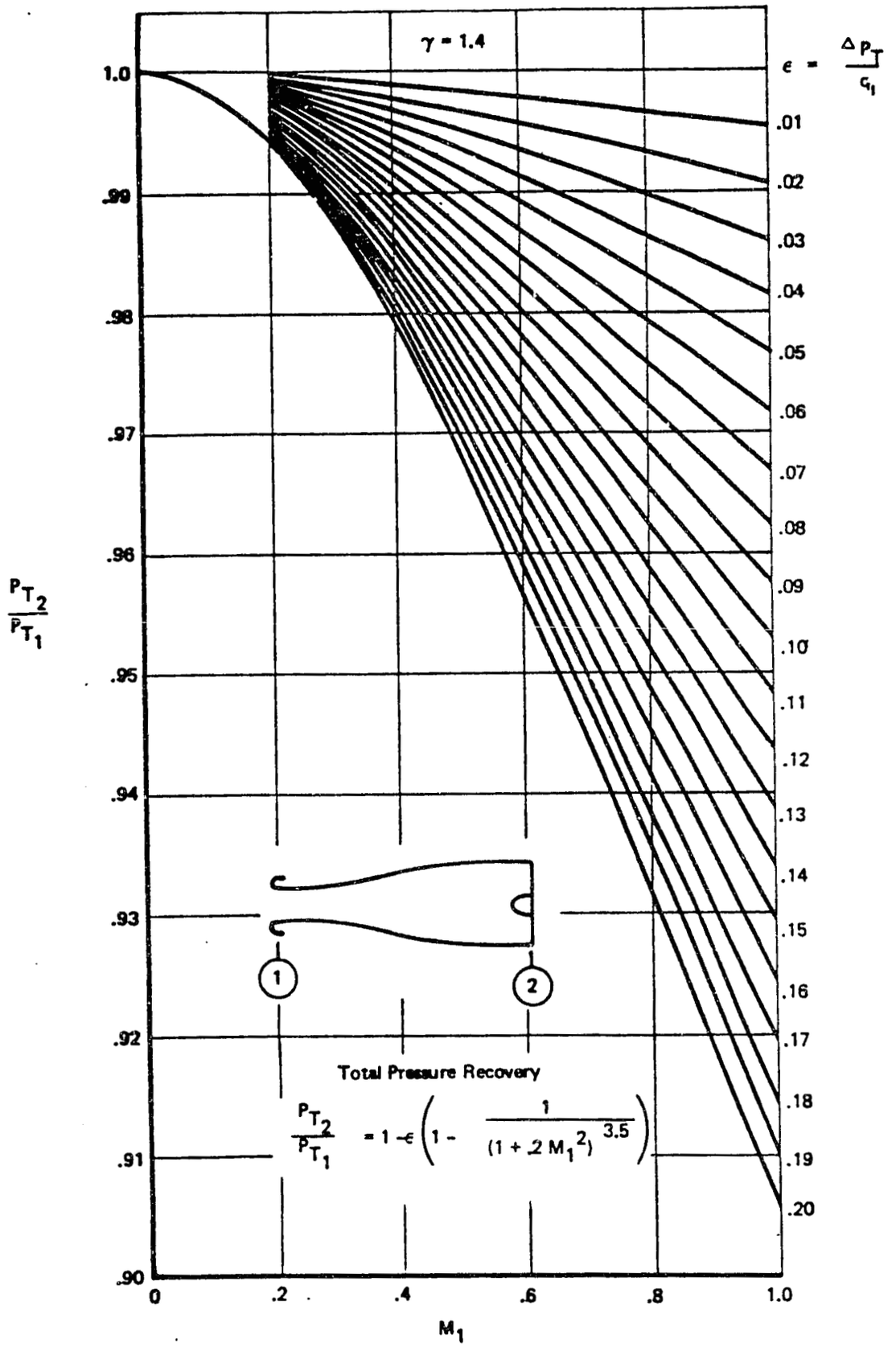

Figure 22: SUBSONIC DIFFUSER LOSS FACTORS

Using figure 23 and the geometric throat Mach number, the geometric throat corrected airflow parameter $W_T\sqrt{\theta_T}/\delta_T A_{T_{GEOM}}$ is determined. Likewise, the effective throat corrected airflow parameter $W_T\sqrt{\theta_T}/\delta_T A_{T_{EFF}}$ is determined as a function of the effective throat Mach number. The effective throat area, $A_{T_{EFF}}$, and the geometric throat area, $A_{T_{GEO}}$, are determined from:

$$A_{T_{EFF}} = \frac{W_{COR_2}\frac{P_{T_2}}{P_{T_T}}}{\frac{W_T\sqrt{\theta_T}}{\delta_T A_{T_{EFF}}}} \qquad A_{T_{GEO}} = \frac{W_{COR_2}\frac{P_{T_2}}{P_{T_T}}}{\frac{W_T\sqrt{\theta_T}}{\delta_T A_{T_{GEO}}}}$$

Capture area is calculated from

$$A_C = A_{T_{GEO}}\left(\frac{r_{HI}}{r_T}\right)^2$$

The maximum airflow the inlet can pass, m_{MAX}, is determined using the inputed $M_{T_{EFF_{MAX}}}$ and the calculated capture area, A_C.

$$m_{MAX} = \frac{32.174 M_{T_{EFF_{MAX}}}}{\left(1 + .2\left(M_{T_{EFF_{MAX}}}\right)^2\right)^3} P_{T_T}\sqrt{\frac{1.4}{1716.23}\frac{1}{T_{T_T}}} A_{T_{EFF}}$$

where

$$P_{T_T} = \frac{P_{T_T}}{P_{T_I}}\frac{P_{T_I}}{P_{T_0}} P_{T_0}$$

T_{T_T} = throat total temperature.

In this pitot analysis it is assumed that there is no boundary layer control bleed system. The amount of bypassed air will be determined through an iterative process to determine what split between bypassed and

$$\frac{W\sqrt{\theta}}{A\delta} = .592 \left[\frac{M}{(1 + .2\,M^2)^3}\right]$$

W = Lb/Sec
A = In^2
$\theta = T_T/T_{Std}$
$\delta = P_T/P_{Std}$

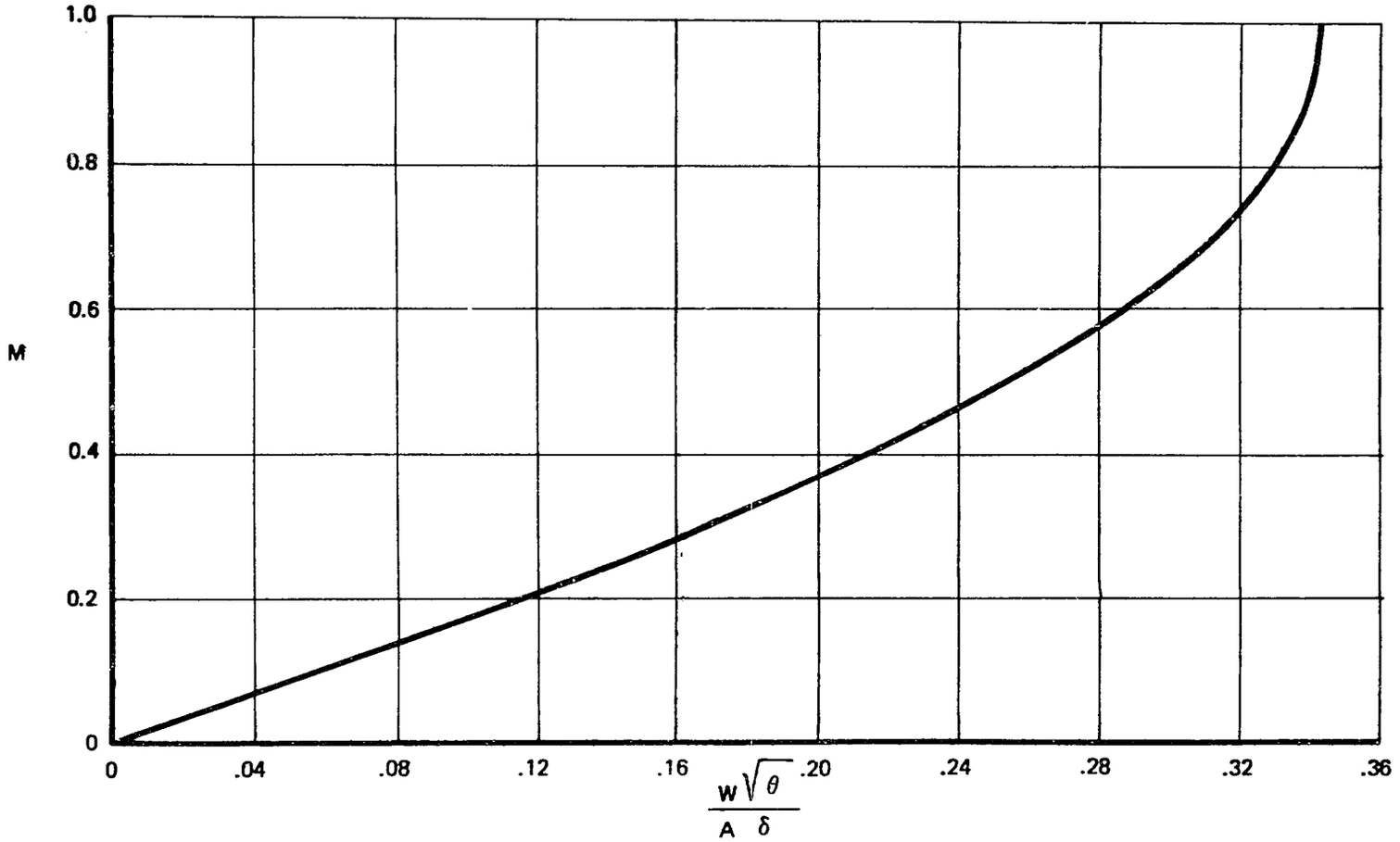

Figure 23: CORRECTED AIRFLOW PARAMETER

spilled air yield minimum inlet drag. This iterative process will also have an impact on inlet pressure recovery.

If inlet capture area is input, the inlet recovery will be determined as a function of flight speed.

- o Lowspeed. MN 0.4
- o Subsonic & Transonic 0.4 MN 1.0
- o Supersonic MN 1.0

During lowspeed operation, the primary total pressure loss generating mechanisms are sharp lip losses and subsonic diffuser losses. The methods used to calculate sharp lip losses accounts for lip bluntness, effect of takeoff door area, and inlet flow velocity. The subsonic diffuser losses are calculated by using an input variation of duct loss coefficient, ε, as a function of inlet throat Mach number. The sharp lip losses are combined with the subsonic diffuser losses to obtain the overall inlet total pressure recovery.

The determination of the inlet pressure recovery during lowspeed operation is an iterative process. Initially, both the hilite to throat recovery, $P_{T_T}/P_{T_{AC}}$, and the total inlet recovery, P_{T_2}/P_{T_0} are assumed to be 0.95.

The ratio of the free stream tube area of engine demand air to the inlet capture area, A_{0_E}/A_C, is determined:

$$A_{0_E}/A_C = .02023\ A/A^* \frac{P_{T_2}}{P_{T_0}} W_{COR_2}$$

where A/A* = the isentropic area ratio for free stream conditions.
The amount of bypass air for this iteration is added to engine demand to determine inlet supply (zero bleed air):

$$A_0/A_C = A_{0_{BYP}}/A_C + A_{0_E}/A_C$$

After determining the corrected airflow parameter at the throat (which includes takeoff door area, A_{TO}), the $M_{T_{GEO}}$ is determined using figure 23. Figure 20 is required to determine $M_{T_{EFF}}$. The recovery from inlet hilite to inlet throat is determined using $M_{T_{GEO}}$ and $M_{T_{EFF}}$.

$$\frac{P_{T_T}}{P_{T_{AC}}} = \frac{(A/A^*)_{T_{EFF}}}{(A/A^*)_{T_{GEO}}}$$

This calculated recovery is compared to the guessed recovery. If different, a new guess is determined by averaging the old guessed value with the calculated value. When these values do agree, the subsonic diffuser duct loss coefficient ϵ, is determined from figure 21 (as before, this data may be changed to suite the application). Then

$$\frac{P_{T_2}}{P_{T_1}} = 1 - \epsilon\left(1 - \frac{1}{(1+.2m_{T_{EFF}}^2)^{3.5}}\right)$$

The guessed total presure recovery is compared to the calculated value. If the values do not equal, the average of these two determines the new guessed total pressure recovery. When convergence is reached the maximum airflow the inlet can pass at this flight condition is determined using $M_{T_{EFF_{MAX}}}$ and A_C as before.

The determination of inlet pressure recovery for subsonic and transonic flight speeds is identical to that of the lowspeed method with takeoff door area equal to zero. For supersonic flight speeds, the pressure loss across the normal shock is accounted for.

Bypass Drag

To calculate the drag of bypass air, it is necessary to know the geometry and location of the bypass exit nozzle, the amount of bypass airflow, and the total pressure recovery of bypass air at the nozzle exit.

The pressure recovery of the bypass system is assumed to vary linearly from a value of 100% of inlet recovery (bypass doors closed) to 70% of inlet recovery (bypass doors fully open). This is portrayed in figure 24.

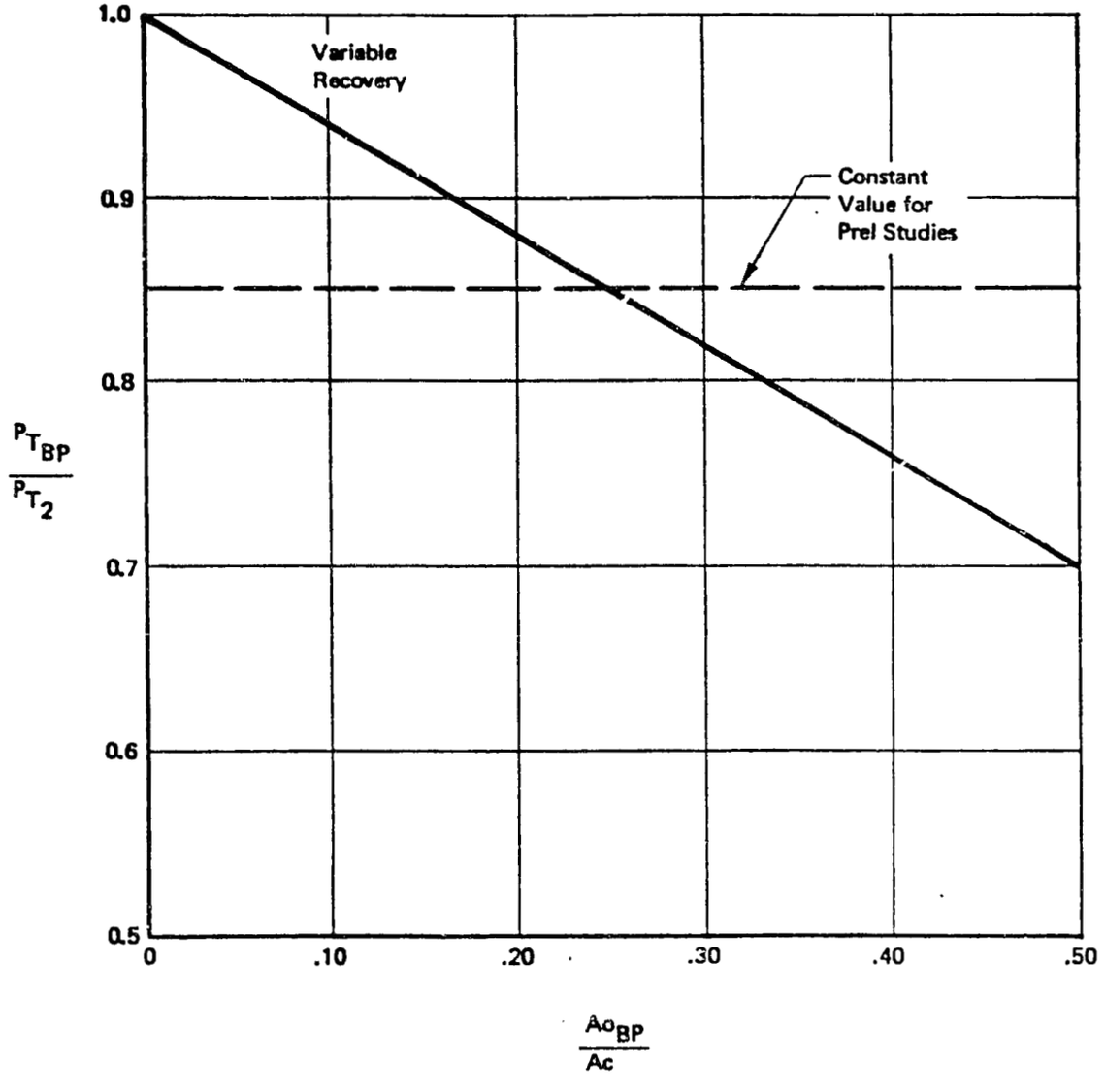

Figure 24 BYPASS AIRFLOW TOTAL PRESSURE RECOVERY

Bypass drag is composed of two parts: momentum drag and flap (or exit) drag. Momentum drag depends on the exit angle and total pressure recovery of the discharged air, type of nozzle through which the air is exited and free-stream Mach number. Flap drag depends on door angle, door aspect ratio and free-stream Mach number.

Momentum Drag

For a convergent bypass nozzle, a choked flow condition must be checked for. The minimum free stream Mach number, M_{MIN}, at which the available total pressure recovery of the bypassed air, P_{T_E}/P_{T_0}, will be able to choke the bypass nozzle is determined by:

$$M_{MIN} = \sqrt{\frac{6}{\left(\frac{P_{T_E}}{P_{T_0}}\right)^{.286}} - 5}$$

For a choked convergent bypass nozzle, both the exit Mach number and the exit static pressure ratio are 1. It's throat area, $A_{T_{CON}}$, is:

$$A_{T_{CON}} = \left(\frac{A_{O_{BYP}}}{A_C} A_C\right) \Big/ \left((A/A^*)_{A_C} \frac{P_{T_E}}{P_{T_0}}\right)$$

For an unchoked convergent bypass nozzle, the exit Mach number, M_E, is determined by:

$$M_E = 5\sqrt{\frac{1}{\left(\frac{P_E}{P_{T_E}}\right)^{.286}} - 1}$$

where:

$$\frac{P_E}{P_{T_E}} = \frac{P_0}{P_{T_0}} \frac{P_{T_0}}{P_{T_E}}$$

Its throat area, $A_{T_{CON}}$, is:

$$A_{T_{CON}} = \frac{\frac{A_{O_{BYP}}}{A_C} A_C}{(A/A^*)_{A_C}} P_{T_E/P_{T_0}}$$

where $(A/A^*)_E$ = the isentropic area ratio at the bypass nozzle exit.

For a convergent-divergent bypass nozzle, a test is first performed to determine whether the nozzle throat is choked. As in the case of the convergent nozzle calculation, M_{MIN} is calculated and compared with the free stream Mach number. If the nozzle throat is determined to be unchoked, excessive drag will result and the configuration should be re-examined. If this happens, the computer program terminates this case and proceeds to the next case.

For a choked convergent-divergent bypass nozzle, the exit Mach number, is determined by:

$$M_E = \sqrt{5\left(\frac{1}{\left(\frac{P_E}{P_{T_E}}\right)^{.286}} - 1\right)}$$

where: $\frac{P_E}{P_{T_E}} = \frac{P_0}{P_{T_0}} \frac{P_{T_0}}{P_{T_E}}$

It's throat area, $A_{T_{CD}}$, is: $A_{T_{CD}} = \frac{\frac{A_{0_{BYP}}}{A_C} A_C}{(A/A^*)_{A_C}} \frac{P_{T_E}}{P_{T_0}}$

Using the isentropic area ratio at the bypass nozzle exit, $(A/A^*)_E$, the nozzle exit area is determined

$$A_{E_{CD}} = A_{T_{CD}} (A/A^*)_E$$

The flap drag routine must be called to determine the nozzle exit flap angle.

Flap Drag

Flap drag is calculated by integrating the predicted pressure coefficients acting on the exit doors in the flight direction. To accomplish this, tables of average pressure coefficients for doors of various aspect ratios (W/h) from .75 to 4.0 are used as input data to obtain the pressure

coefficients. These tables can be found in figure 25. A correction is used to account for the fact that the doors are usually operating in a region of turbulent boundary layer.

For a convergent bypass nozzle, the ratio of nozzle exit area to inlet capture area, A_E/A_C, is determined by:

$$\frac{A_E}{A_C} = \frac{A_{T_{CON}}}{A_C N_{BD} C_{FLOW}}$$

where: N_{BD} = number of bypassed nozzles

C_{FLOW} = flow coefficient (0.95)

For a convergent-divergent bypass nozzle, the ratio of nozzle exit area to inlet capture area, A_E/A_C, is determined by

$$\frac{A_E}{A_C} = \frac{A_{E_{CD}}}{A_C N_{BD} C_{FLOW}}$$

The nozzle door flap angle, $\theta_{FL_{ACT}}$, is determined from:

$$\theta_{FL_{ACT}} = \tan^{-1} \frac{A_E/A_C}{A_{FL}}$$

where $A_{FL} = \frac{Wh}{A_C}$

W = Bypass door width

h = Bypass door height

Using $\theta_{FL_{ACT}}$ and the free stream Mach number, the effective nozzle door flap angle, $\theta_{FL_{EFF}}$, is obtained from figure 26. This plot shows what effect turbulent boundary layer has on nozzle door flap angle.

The average pressure coefficient, C_p, over the surface of the nozzle door flap is obtained from figure 25 as a function of $\theta_{FL_{EFF}}$, freestream Mach number and AR(W/h). With Cp, the flap drag coefficient $C_{D_{FLP}}$ is calculated by: $C_{D_{FLP}} = C_p \, SIN(\theta_{FL_{ACT}}) \, A_{FL} \, N_{BD}$

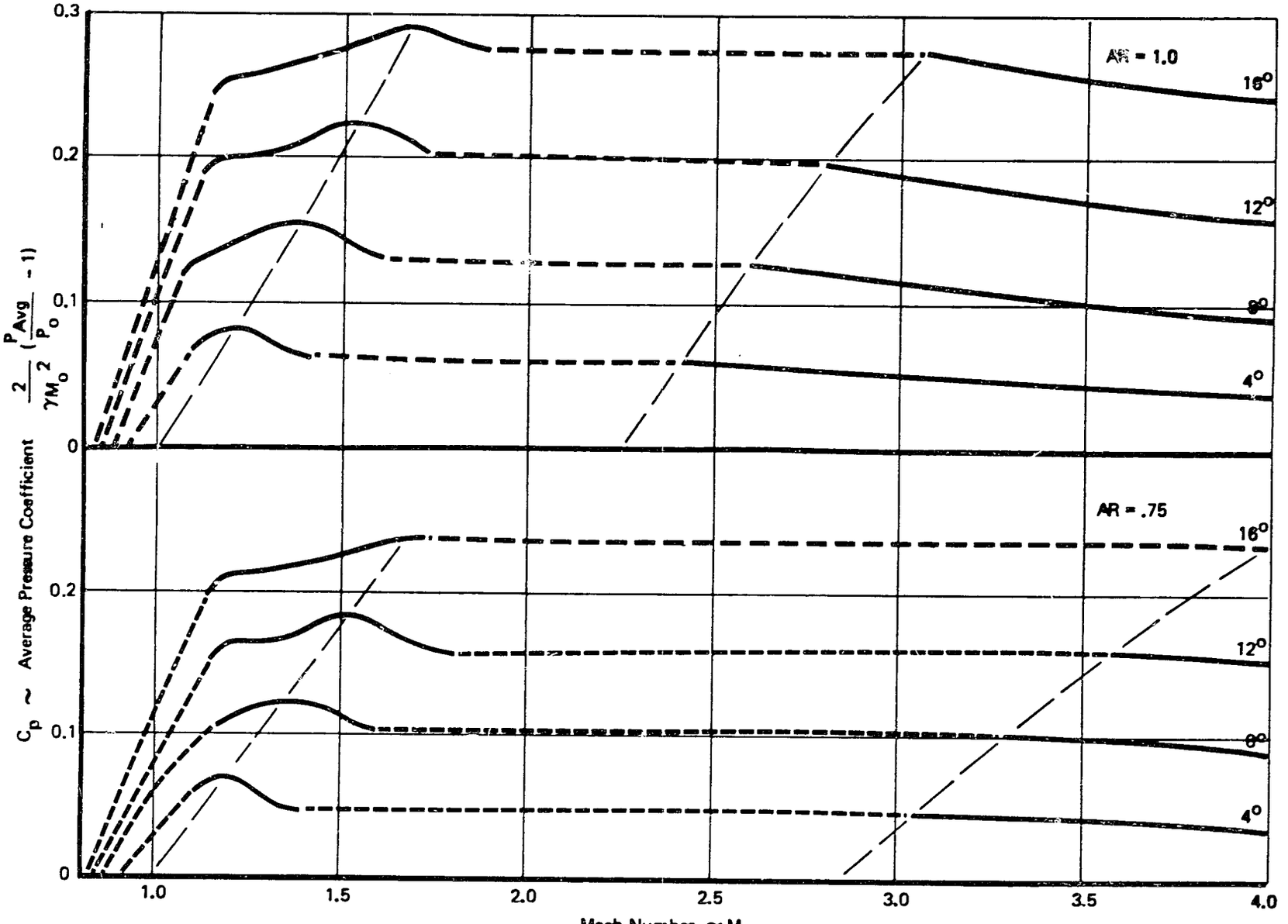

Figure 25: BYPASS DOOR PRESSURE COEFFICIENTS

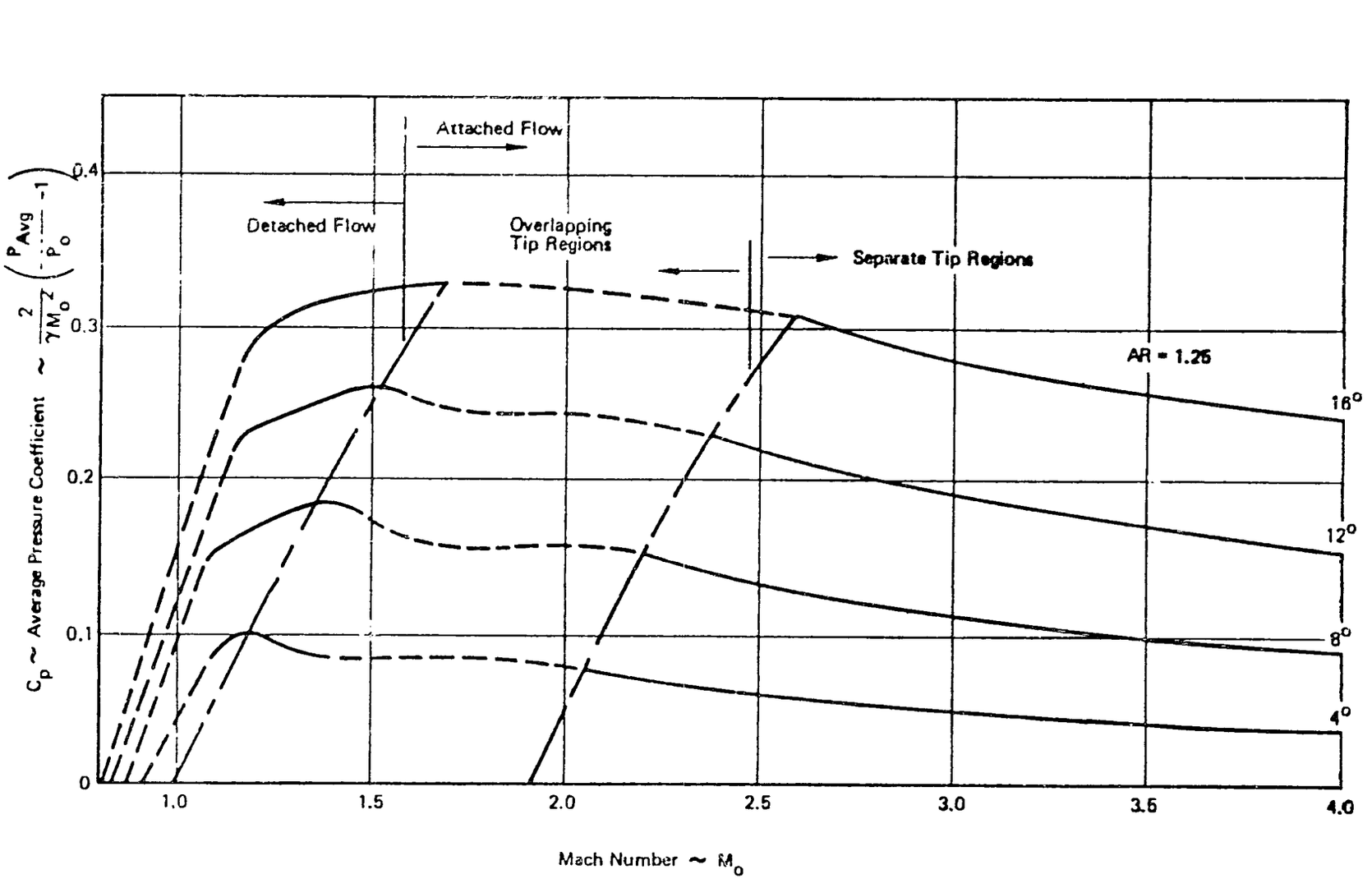

Figure 25: BYPASS DOOR PRESSURE COEFFICIENTS (Cont)

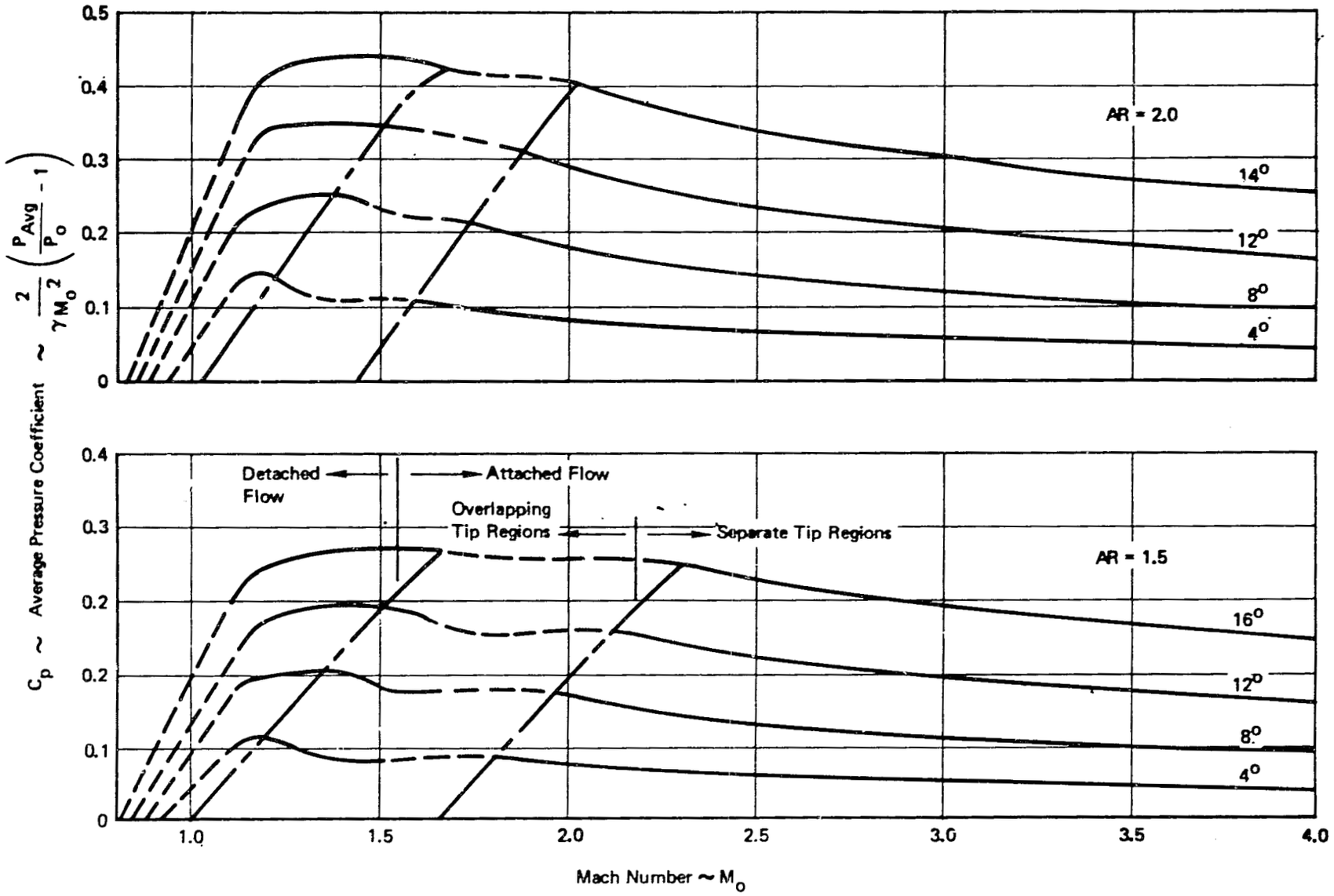

Figure 25. BYPASS DOOR PRESSURE COEFFICIENTS (Cont)

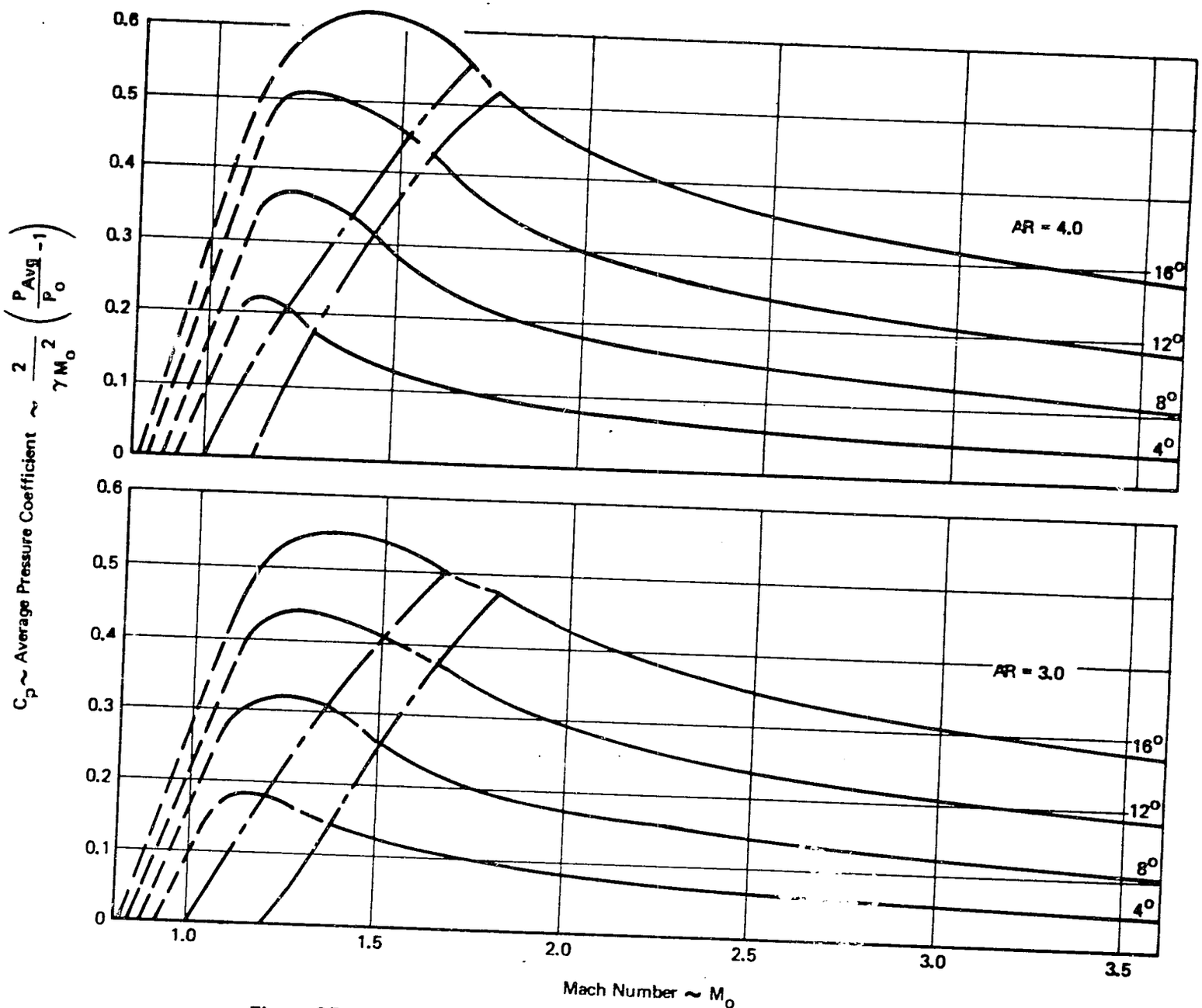

Figure 25: BYPASS DOOR PRESSURE COEFFICIENTS (Concluded)

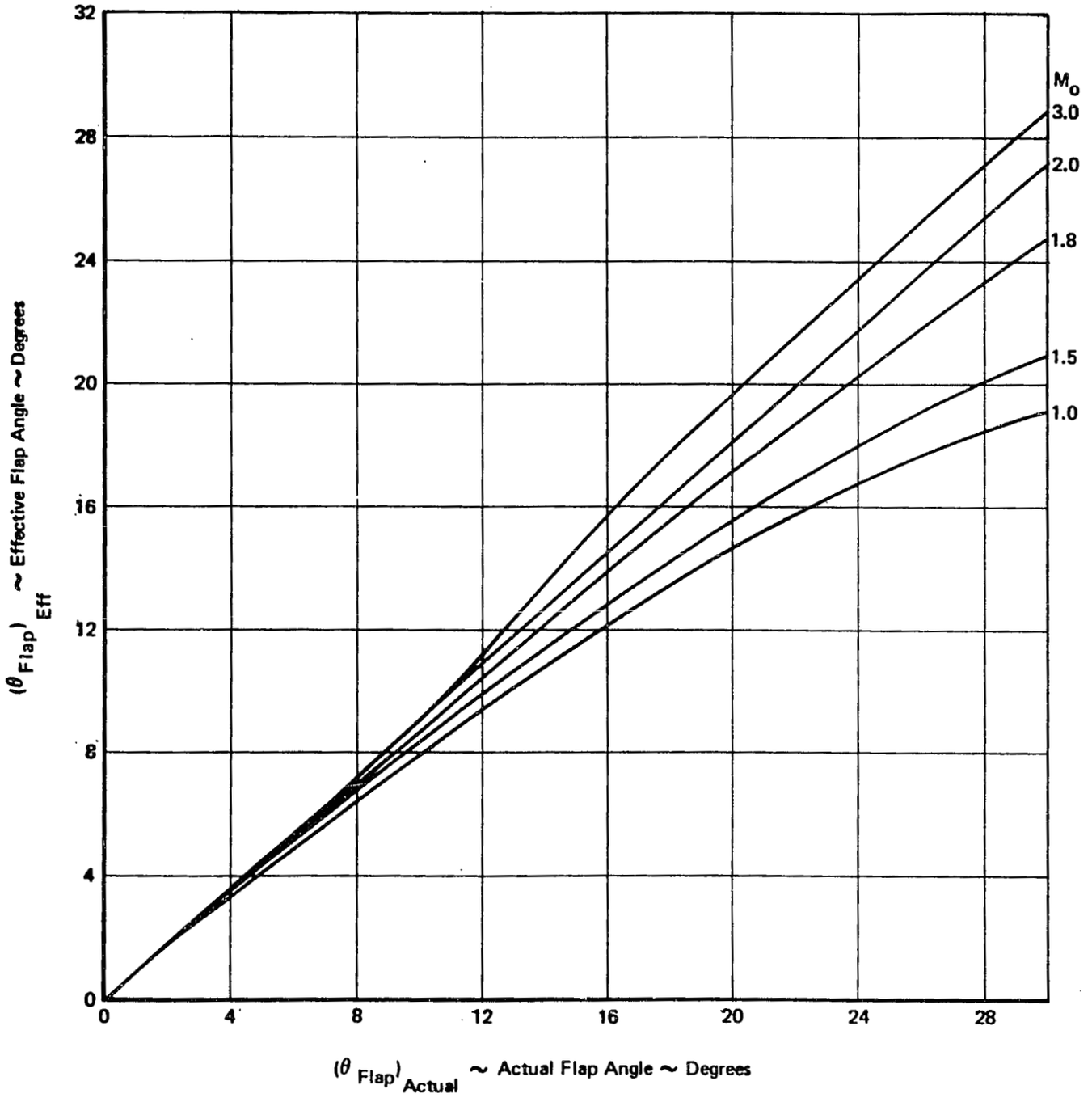

Figure 26 : EFFECT OF TURBULENT BOUNDARY LAYER ON BYPASS FLAP ANGLE

Knowing the nozzle door flap angle the momentum drag can be calculated as a fraction of the freestream momentum of the bypassed air, $\frac{D}{\frac{W_a V_0}{g}}$

For a choked convergent bypass nozzle:

$$\frac{D}{\frac{W_a V_0}{g}} = 1 - \frac{\cos(\Theta FL_{ACT})}{M} \sqrt{\frac{2+.4m^2}{2.4}} \left(1.715 - \frac{1}{\frac{P_{T_E}}{P_{T_0}} \frac{2+.4m^2}{2.4}^{3.5}} \right)$$

For an unchoked convergent bypass nozzle:

$$\frac{D}{\frac{W_a V_0}{g}} = 1 - \cos(\Theta FL_{ACT}) \sqrt{\left(\frac{1}{.2M^2} + 1\right)\left(1 - \frac{1}{(1+.2m^2)^{\left(\frac{P_{T_E}}{P_{T_0}}\right)^{.286}}}\right)}$$

For a choked convergent divergent bypass nozzle:

$$\frac{D}{\frac{W_a V_0}{g}} = 1 - \cos(\Theta FL_{ACT}) \sqrt{\left(\frac{1}{.2M^2} + 1\right)\left(1 - \frac{1}{(1+.2m^2)^{\left(\frac{P_{T_E}}{P_{T_0}}\right)^{.286}}}\right)}$$

Converting this into a momentum drag coefficient:

$$C_{D_{mom}} = 2 \frac{A_{o_{BYP}}}{A_c} \frac{D}{\frac{W_a V_0}{g}}$$

The total bypass drag is the summation of flap and momentum drag:

$$C_{D_{BYP}} = C_{D_{mom}} + C_{D_{FLP}}$$

Spillage Drag

Spillage drag is calculated from the following equation:

$$C_{D_{SPL}} = K_{ADD} C_{D_{ADD}}$$

It is defined as the incremental change in total airplane drag due to spilling excess air ahead of the inlet. However, it is usually measured as an increment ($\Delta C_{D_{SPL}}$) from the drag level obtained for the full

airplane configuration with the inlet operation at a baseline mass flow ratio. When the inlet is operating at this baseline mass flow ratio, the $\Delta C_{D_{SPL}}$ is zero. The spillage drag at the baseline mass flow ratio is included in the airplane aerodynamic drag. The baseline mass flow ratio is specified for each inlet configuration as a function of freestream Mach number. It is normally selected at mass flow ratios where spillage effects will be a minimum, for realistic operating airflow conditions. This baseline mass flow is normally taken to be critical mass flow ratio. At supersonic speeds, critical inlet operation means that the normal shock is at or inside the cowl lip. For subsonic and detached shock wave conditions, the inlet captured stream tube area, A_0 , is equal to the physical flow area at the cowl. The establishment of the baseline mass flow ratio as described provides a basis for accounting of aero and propulsion forces. The throttle-dependent drag is thus included in the spillage drag (which is accounted for in installed net thrust) and the drags that are independent of throttle setting are included in the aerodynamic drag of the airplane.

$C_{D_{ADD}}$ is the theoretical additive drag of the inlet. It is computed by several different methods, depending on the configuration of the inlet, freestream Mach number, and shock geometry. The additive drag of an open-nose inlet is calculated as shown in figure 27. This equation can be used for both subsonic Mach numbers and supersonic Mach numbers where normal shock is standing ahead of the inlet.

The theoretical additive drag is multiplied by a correction factor, K_{ADD} , based on experimental data, to account for the configuration effects. These effects include the effect of cowl lip shape bluntness. These factors are obtained by comparing experimentally measured drag variation as a function of inlet mass flow ratio with the theoretically calculated drag variation. A catalog of K_{ADD} factors to be used is presented in figures 28-32.

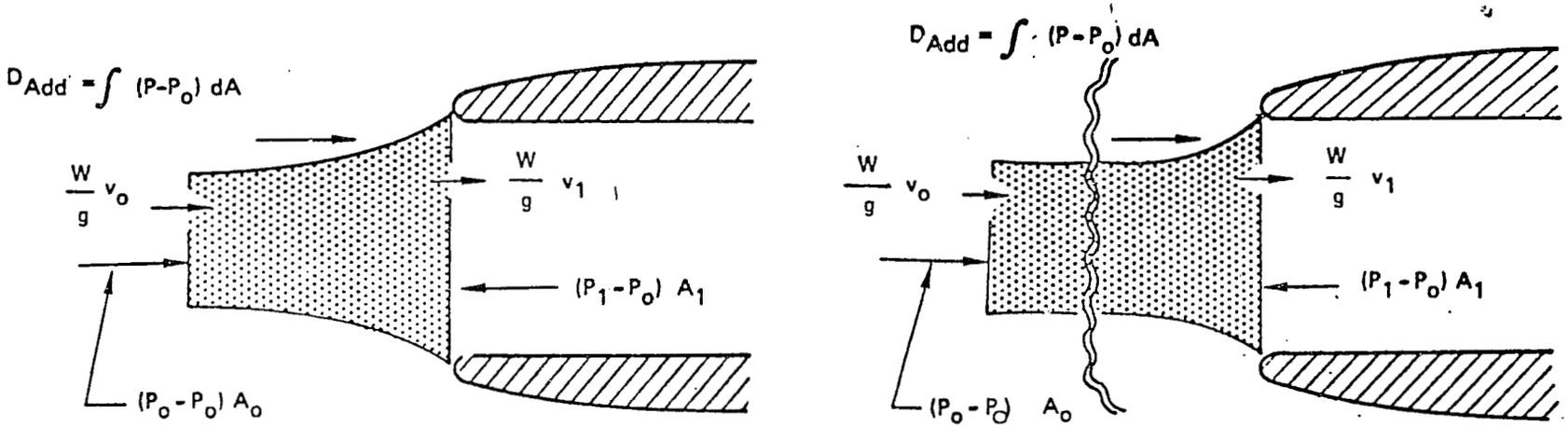

(A) Subsonic

(B) Supersonic

$$D_{Add} = \int (P - P_o)\, dA = \frac{W}{g} v_1 + (P_1 - P_o) A_1 - \frac{W}{g} v_o$$

Figure 27: ADDITIVE DRAG OF A PITOT INLET

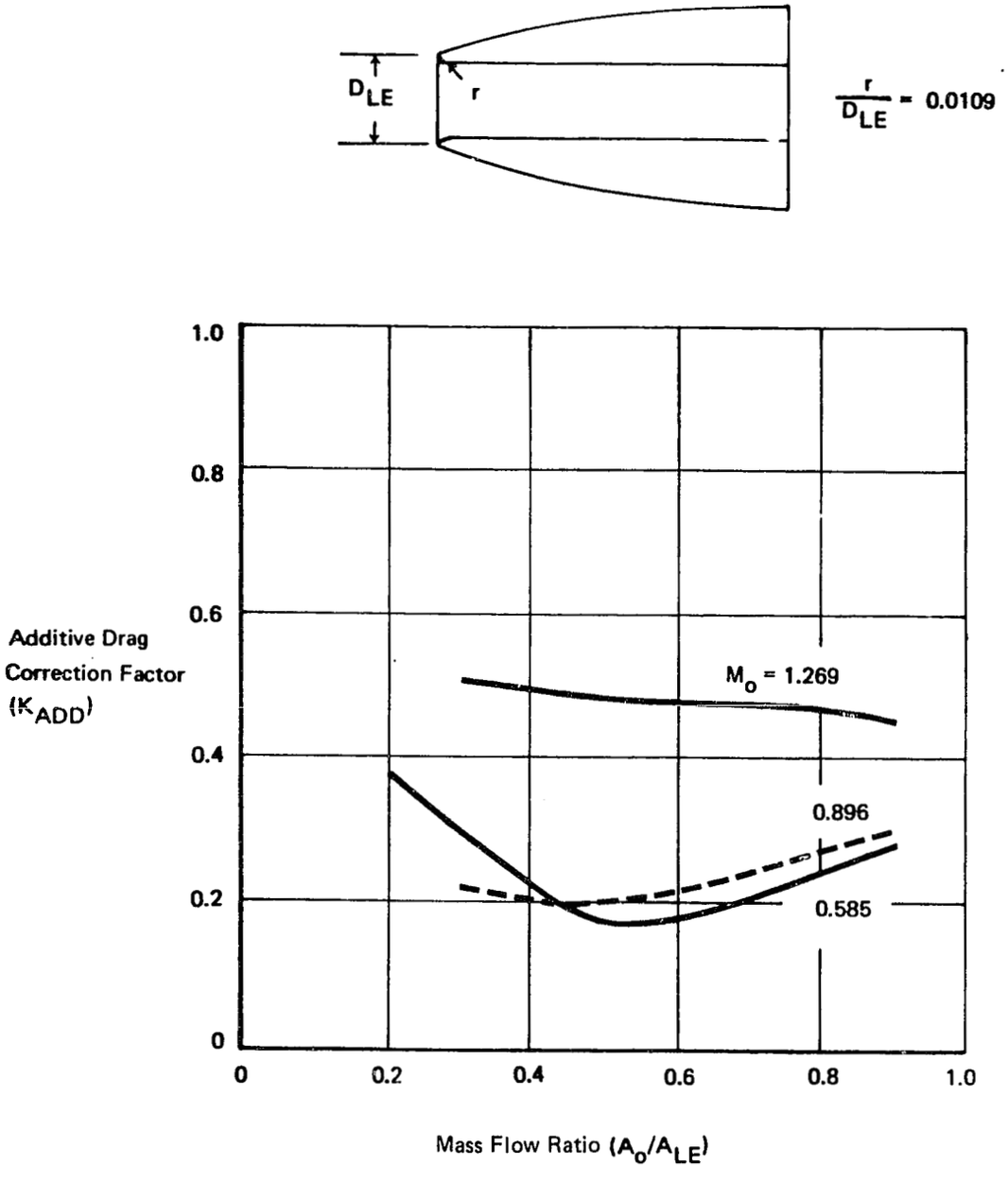

Figure 28 : K_{ADD} *FOR OPEN NOSE INLETS, CURVED COWL —* $r/D_{LE} = 0.0109$

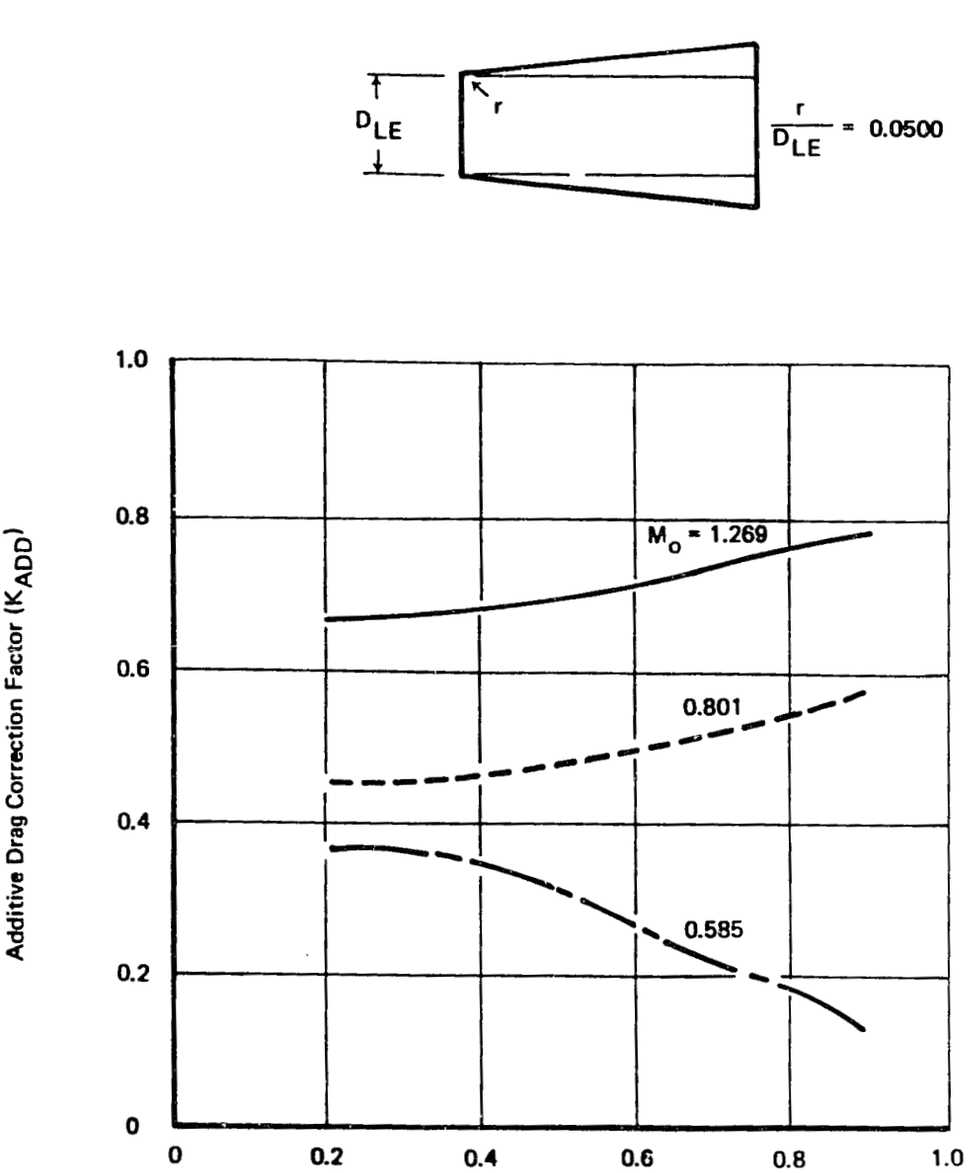

Figure 29 : K_{ADD} *FOR OPEN NOSE INLETS, STRAIGHT COWL —* $r/D_{LE} = 0.0500$.

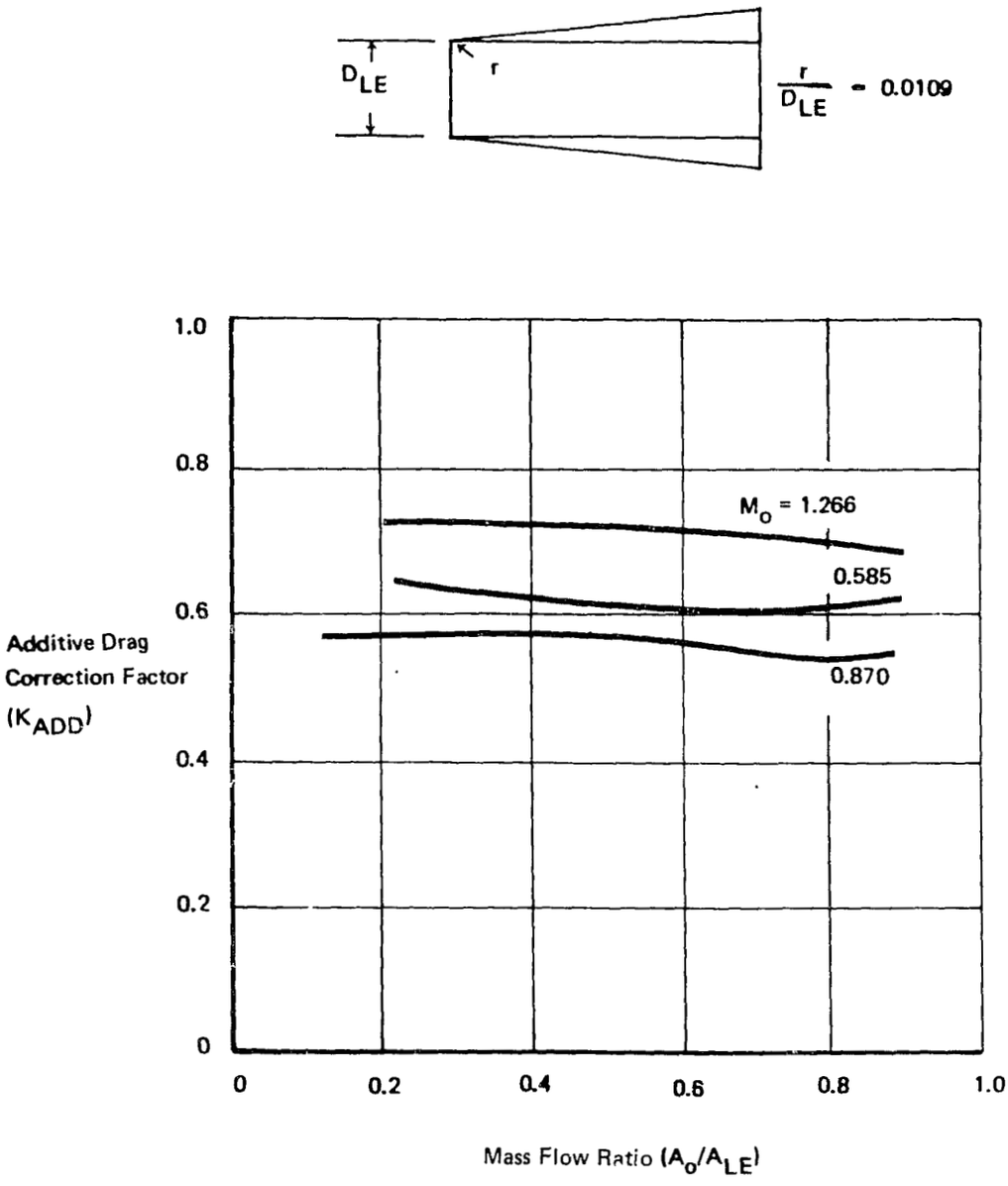

Figure 30 : K_{ADD} *FOR OPEN NOSE INLETS. STRAIGHT COWL –* $r/D_{LE} = 0.0109$.

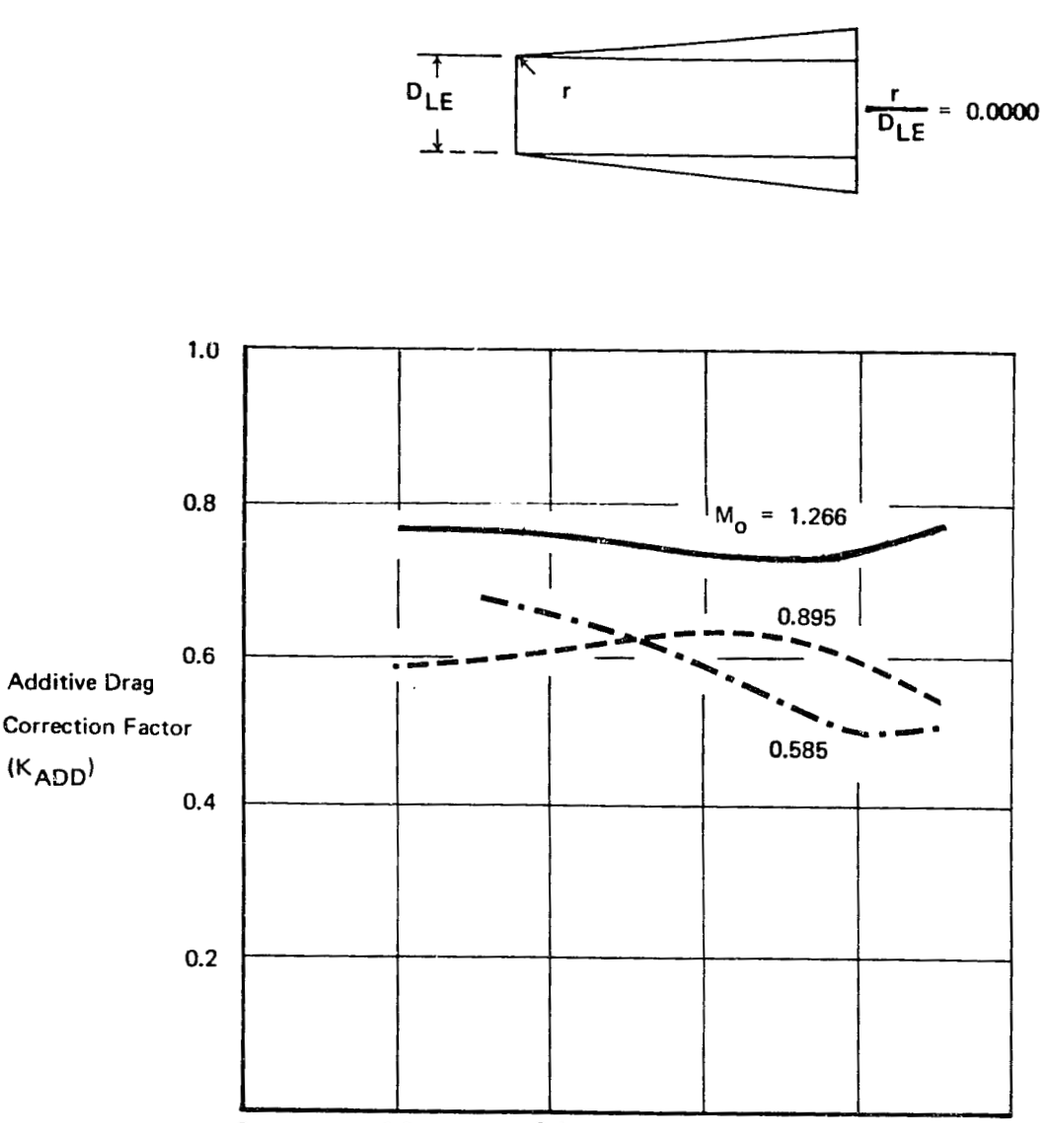

Figure 31 : K_{ADD} FOR OPEN NOSE INLETS. STRAIGHT COWL (r/D_{LE} = 0.000)

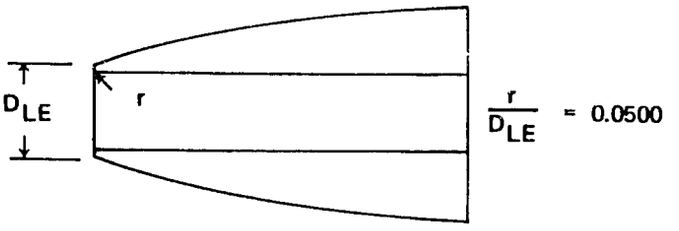

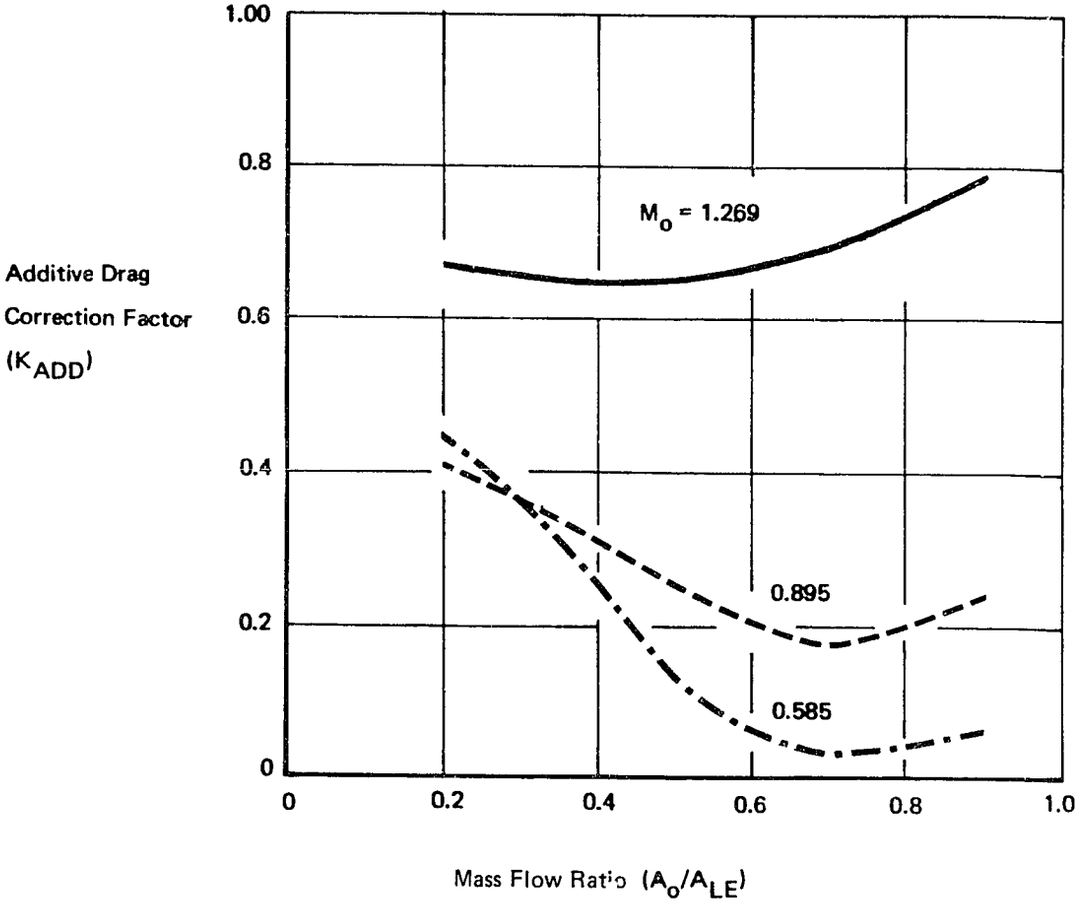

Figure 32 : K_{ADD} *FOR OPEN NOSE INLETS, CURVED COWL —* $r/D_{LE} = 0.0500$.

2.3.1.2.2 PITOT INLET DESIGN METHOD

A pitot inlet design method for both subsonic and supersonic application has been written. This routine is only used for those pitot inlets whose performance is determined by the analysis method of Section 2.3.1.2.1. and for those used installed with a "podded" or "isolated" nacelle.

For a subsonic design Mach number, the inlet entrance contour from the hilite to throat is considered a quarter ellipse. This contour is determined with an input of the ratio of the major to minor axes of this ellipse. The diffuser contour (inlet throat to fan face) is based on a defaulted dimensionless coordinates (see Figure 33) obtained from a "747 type" inlet and requires as a user input, the ratio of intake diffuser length to engine fan tip diameter. The external forebody contour is also based on dimensionless coordinates (see Figure 33) developed during the C5A and 747 programs. This requires the input of cowl forebody length (hilite to maximum diameter) and maximum nacelle diameter. The cowl forebody length is determined in two sections. The user inputs the ratio of the nacelle length (hilite to maximum nacelle diameter) to maximum nacelle diameter; the WATE-2 program will determine the length from engine face to the maximum engine (or nacelle) diameter. The user has the capability of adding "X" inches to the maximum nacelle diameter to allow for the nacelle outside dimensions. Figure 34 is an example of a typical output page for a CTOL type subsonic inlet.

This method is also used for the design of a VSTOL type inlet. Since the contraction ratio of the inlet varies around the inlet, two values of major to minor axis ratios are required (see Figure 35). This nacelle configuration was taken from Reference 13.

Additional output includes capture area, throat area, engine face area, overall length (hilite to maximum nacelle diameter), subsonic diffuser length (throat to engine fan face) and lip contraction ratio.

For a supersonic design Mach number, the ratio of nacelle length (hilite to maximum nacelle diameter) to maximum nacelle diameter is input. The

FOREBODY COWL

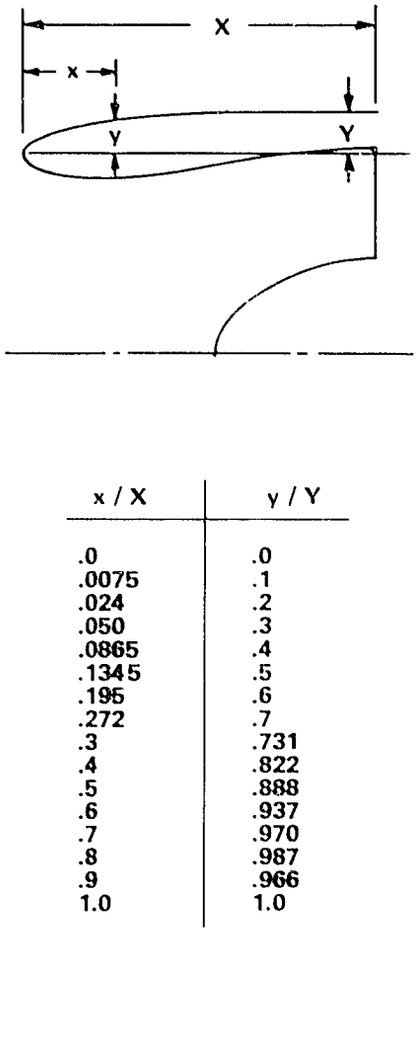

x / X	y / Y
.0	.0
.0075	.1
.024	.2
.050	.3
.0865	.4
.1345	.5
.195	.6
.272	.7
.3	.731
.4	.822
.5	.888
.6	.937
.7	.970
.8	.987
.9	.966
1.0	1.0

DIFFUSER

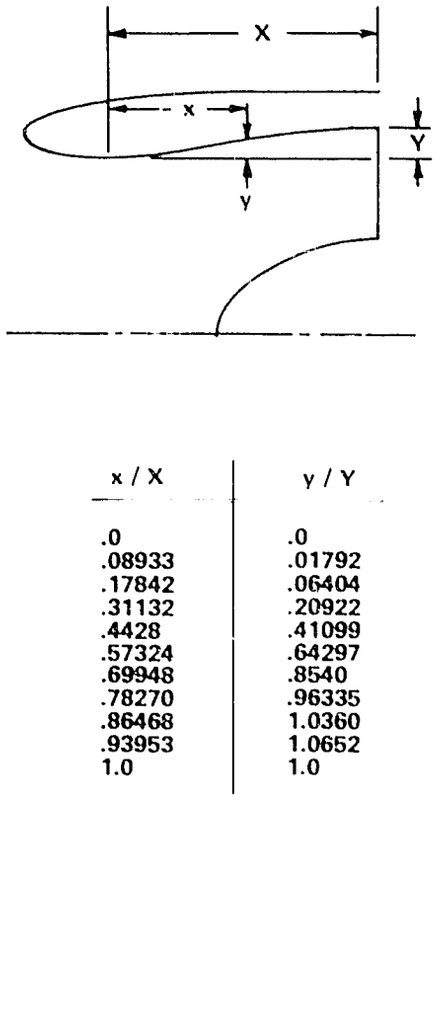

x / X	y / Y
.0	.0
.08933	.01792
.17842	.06404
.31132	.20922
.4428	.41099
.57324	.64297
.69948	.8540
.78270	.96335
.86468	1.0360
.93953	1.0652
1.0	1.0

Figure 33 CTOL Dimensionless Coordinates

PITOT INLET COORDINATES

X : DISTANCE FROM HILITE (INCHES)
R : DITSANCE FROM THE ENGINE CENTERLINE (INCHES)

INTERNAL INLET COORDINATES

HILITE TO THROAT

	HILITE							THROAT
X :	0.0	0.412	1.030	2.059	4.118	8.236	14.414	20.591
R :	41.182	39.543	38.610	37.592	36.240	34.593	33.325	32.946

THROAT TO ENGINE FACE

	THROAT										ENGINE FACE
:	20.591	22.905	25.213	28.656	32.062	35.417	38.711	40.867	42.991	44.930	46.496
:	32.946	33.055	33.337	34.223	35.455	36.872	38.160	38.828	39.272	39.450	39.052

EXTERNAL INLET COORDINATES

HILITE TO MAX NACELLE DIAMETER

	HILITE							
X :	0.0	0.349	1.116	2.325	4.022	6.254	9.067	12.647
R :	41.182	41.369	41.556	41.743	41.930	42.117	42.304	42.491

								MAX NACELLE DIAMETER
X :	13.949	18.598	23.248	27.898	32.547	37.197	41.846	46.496
R :	42.549	42.719	42.842	42.934	42.996	43.028	43.044	43.052

Figure 34 Typical Output Page CTOL Type Subsonic Inlet

68

****
* INLET DIMENSION SUMMERY *
****

HILITE AREA	THROAT AREA	HUB/TIP RATIO	ENGINE FACE AREA
5327.977 IN**2	3409.904 IN**2	0.400	4024.512 IN**2

OVERALL LENGTH (HILITE TO MAX NACELLE DIAMETER)	SUBSONIC DIFFUSER LENGTH
46.496 IN	25.905 IN

LIP CONTRACTION RATIO (HILITE TO THROAT)	AREA RATIO (ENGINE TO THROAT)
1.563	1.180

WETTED AREA

12496.109 IN**2

Figure 34 (cont.) Typical Output Page C1OL Type Subsonic Inlet

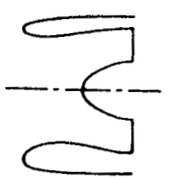

FOREBODY COWL

TOP

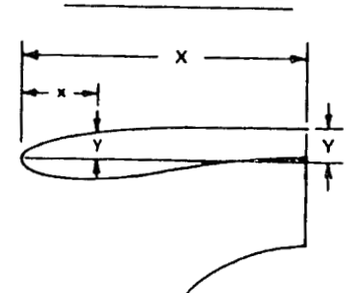

x / X	y / Y
.0	.0
.0059	.1447
.0124	.2162
.0234	.2833
.0416	.3674
.1	.5571
.2	.7411
.3	.8555
.4	.9394
.5	.9921
.6	1.025
.7	1.017
.8	1.014
.9	1.003
.95	1.0015
1.0	1.0

DIFFUSER

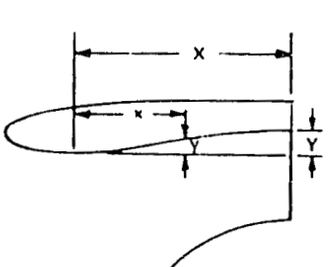

x / X	y / Y
.0	.0
.1	.0828
.2	.1983
.3	.3372
.4	.4884
.5	.6377
.6	.7580
.7	.8683
.8	.9481
.9	.9894
1.0	1.0

BOTTOM

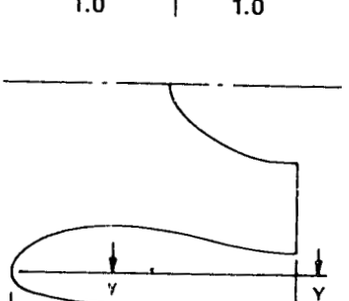

x / X	y / Y
.0	0.
.0067	.1792
.0210	.3502
.0387	.4619
.0553	.5452
.0767	.6103
.1	.6618
.2	.7908
.3	.8759
.4	.9216
.5	.9564
.6	.9644
.7	.9803
.8	.9852
.9	.9820
1.0	.9800

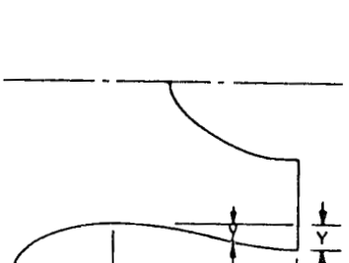

x / X	y / Y
.0	.0
.1	.0119
.2	.0163
.3	.1071
.4	.2181
.5	.3857
.6	.5588
.7	.7318
.8	.8592
.9	.9501
1.0	.9664

Figure 35 V/STOL Dimensionless Coordinates

program will calculate inlet half angle. Like the subsonic designed inlet, the inlet entrance contour from the hilite to throat is considered a quarter ellipse and requires an input of the ratio of the major to minor axes of this ellipse. Additional output will include capture area, throat area, hub to tip ratio, engine face area, and inlet wetted area.

2.3.1.2.3 NAVAL WEAPONS CENTER INLET DESIGN AND ANALYSIS PROGRAM

McDonnell Aircraft Companay (MCAIR) completed a program for the Naval Weapons Center under Contract No. N00123-72-C-0335 to automate procedures for the design and analysis of fixed geometry two-dimensional and axisymmetric inlets operating in the supersonic flight regime to approximately Mach 5.

Program options are provided to design inlets or to analyze an established inlet design and define the performance. The design options define the contours of the external compression surface at the inlet design Mach number. The analysis options define the inlet performance in terms of airflow, pressure recovery, and drag.

Two-Dimensional Inlets

The analysis and design procedures for two-dimensional inlets are applicable to inlets with external compression surfaces composed of 1, 2, or 3 ramps or an isentropic wedge. For off-design analysis of isentropic wedge inlets the external compression surface is approximated by a 4 ramp configuration.

The inlet design options provide for the design of the external compression surface for a given input design Mach number, wave focal point, cowl lip location, and capture height. Inlet designs with two ramps, three ramps, or an isentropic wedge contour may be generated. Additionally, the design option may be followed by an analysis option, in which case the external compression surface will be designed and the resulting inlet analyzed over input Mach number and angle of attack ranges.

The inlet analysis options provide for the analysis of a given inlet over input Mach number and angle-of-attack ranges. The inlet geometry descriptions requires the definition of the external compression surface together with the diffuser duct. The duct configurations together with the range of normal shock positions which can be analyzed are:

Duct Configuration	Normal Shock Position
No Duct	Normal shock at or forward of cowl lip
Diverging Duct	(Critical and subcritical inlet operation)
Converging-Diverging Duct	Normal shock forward of cowl lip or aft of inlet throat (Critical, subcritical and supercritical inlet operation)

The inlet analysis procedure is composed of the following steps:

1. External compression surface flow field is defined.

2. Inlet airflow, drag and recovery are computed for critical inlet operation

3. Supercritical inlet operation is analyzed for a converging-diverging duct if no more than one shock originating on the external compression surface is ingested.

The available computed parameters are summarized below:

Parameter	Type
Airflow	Inlet
	Sidespill
	Spill due to sidewall contraction
	Bleed and bypass.
Drag	Inlet additive (empirical data used for transonic mach numbers)
	Sidespill
	Spill due to sidewall contraction
	Bleed and bypass
	Cowl lip and wave
	Sideplate lip and wave
	Boundary layer diverter
Radius	Cowl lip
	Sideplate lip
Structural thickness	Duct wall
Total pressure Recovery	Oblique shock
	Terminal normal shock
	Subsonic diffuser

Axisymmetric Inlets

The axisymmetric inlet analysis and design procedures are divided into two programs, one applicable to inlets with external compression surfaces composed of 1, 2, or 3 cones, and one for inlets with an isentropic spike external compression surface.

The capability and structure of Program AXI00 used for design and analysis of multi-cone inlets, are discussed below.

The inlet design option provides for the design of the external compresson surface for a given input design Mach number, wave focal point, and cowl lip location. Inlet designs with two or three cones may be generated and may be combined with the analysis option to provide performance over a range of Mach numbers. The design option will not accomodate the converging-diverging (C-D) duct as an option but the performance of C-D ducts may be obtained with a subsequent analysis.

The inlet analysis options provide for the analysis of a given 1, 2 or 3 cone inlet over a range of Mach numbers. The inlet geometry description requires the definition of the external compression surface together with the duct. The analysis option is the only option which will give performance for a converging-diverging duct case. The duct configurations together with the range of normal shock positions which can be analyzed are:

Duct Configuration	Normal Shock Position
No Duct	Normal shock at cowl lip (Critical operation)
Diverging Duct (Subsonic Diffuser)	
Converging-Diverging Duct (Supersonic/Subsonic (Diffuser)	Normal shock at cowl lip or aft of inlet throat (Critical and supercritical operation)

The inlet analysis procedure is composed of the following steps:

1. External compression surface flow field is defined.

2. Inlet airflow, drag, and pressure recovery are computed for critical inlet operation using the mass averaged properties at the inlet cowl lip plane.

3. Supercritcal inlet operation is analyzed for a converging diverging duct if no more than one shock originating on the external compression surface is ingested.

The available computed parameters are summarized below:

Parameter	Type
Airflow	Inlet Bleed Inlet additive Bleed and bypass
Drag	Cowl lip and wave Boundary layer diverter Oblique shock - conical and planar
Total pressure recovery	Terminal normal shock Subsonic diffuser

Isentropic Spike Inlets

The capability and structure of Program SPK00 used for design and analysis of isentropic spike inlets, are duscussed below.
The inlet design option provides for the design of an isentropic spike external compression surface for a given input design Mach number,

isentropic turning, wave focal point, and cowl lip location. The design option may be combined with the analysis option to provide performance over a range of Mach numbers.

The inlet analysis option provides for the analysis of a given inlet over a range of Mach numbers. The inlet geometry description requires the definition of the external compression surface and the duct. The duct configurations together with the range of normal shock positions which can be analyzed are:

Duct Configuration	Normal Shock Position
No duct Diverging Duct (Subsonic Diffuser)	Normal shock at cowl lip (Critical operation)
Converging-Subsonic Duct (Supersonic/Subsonic Diffuser)	Normal shock at cowl lip or aft of inlet throat (Critical and supercritical operation)

The inlet analysis procedure is composed of the following steps:

1. External compression surface flow field is defined.

2. Inlet airflow, drag, and pressure recovery are computed for critical inlet operation, using the mass averaged properties at the inlet cowl lip plane.

3. Supercritical inlet operation is analyzed for a converging-diverging duct if the bow shock is not ingested.

The available computer parameters are summarized below:

Parameter	Type
Airflow	Inlet, bleed, and bypass Inlet additive Bleed and bypass
Drag	Cowl lip and waver Boundary layer diverter Bow shock
Total Pressure Recovery	Normal shock Subsonic diffuser

2.3.2 NOZZLE PERFORMANCE ESTIMATION

The purpose of the nozzle/aftbody drag and C_{F_G} input data and calculation subprograms is to calculate nozzle internal losses (ΔC_{F_G}) and nozzle/aftbody drag.

The PIPSI program of Reference 3, is only programmed to handle engine configurations which have one common nozzle:

- o turbojet
- o mixed flow turbofan

Since it is an overwhelming task to develop procedures to handle the numerous possibilities of nozzle configurations that NNEP is capable of processing, methods were developed to address these standard configurations in addition to the common nozzle configuration:

- o Split stream turbofan
- o Short fan duct
- o Coplanar nozzle exits

For a short fan ducted turbofan, the user must use the &D inputs of NNEP to input the C_{F_G} for each stream. For complete installation losses, the C_{F_G} input for the fan stream must account for scrubbing losses along the primary cowling. For a coplanar nozzle configuration, an axisymmetric nozzle from the configuration map library could be used for aftbody drag calculations. The fan stream and primary stream nozzle exit areas are added while the nozzle pressure ratios are mass weighed to give an equivalent nozzle exit area and an equivalent nozzle pressure ratio.

$$A_{9_{EFF}} = A_{9_{PRI}} + A_{19_{SEC}}$$

$$(P_9/P_{AMB})_{EFF} = \frac{P_{9_{PRI}}/P_{AMB} * W_{9_{PRI}} + P_{19_{SEC}}/P_{AMB} * W_{19_{SEC}}}{W_{9_{PRI}} + W_{19_{SEC}}}$$

2.3.2.1 NOZZLE/AFTBODY PERFORMANCE MAP LIBRARY

As was the case for the inlet maps, the purpose of the library of nozzle/aftbody maps is to provide a readily-available source of nozzle performance characteristics utilized by the installation computer program. This performance data is stored on permanent files for namelist retrieval. The nozzle/aftbody configurations include: axisymmetric convergent-divergent nozzles, (single and twin), two-dimensional convergent-divergent nozzles (single and twin), axisymmetric plug nozzles (single and twin), two-dimensional wedge nozzles (single and twin) and the ADEN nozzle. Convergent nozzles are included as special cases in the convergent-divergent axisymmetric nozzle database. The corresponding C_{F_G} table has a $A_g/A_8 = 1$ curve. The nozzle/aftbody files that are available are shown in Figure 36. These files and the configurations that are represented in the library of inlet and nozzle/aftbody maps are described in detail in Volume III.

C_V MAP	DRAG MAP	AXISYMMETRIC		2-DIMENSIONAL	C_V MAP	DRAG MAP
CV1	208N-TTY	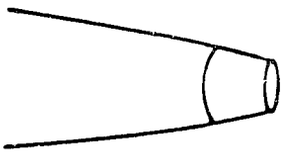	CONVERGENT-DIVERGENT	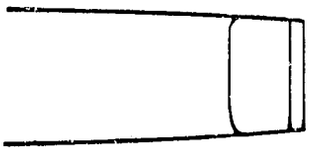	CV2D-CD	DCD2-D1
CV1	CD2R	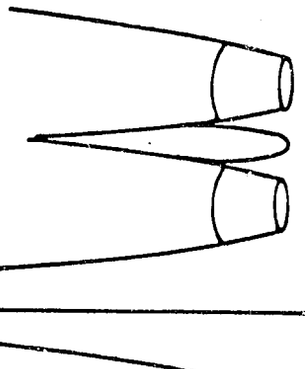		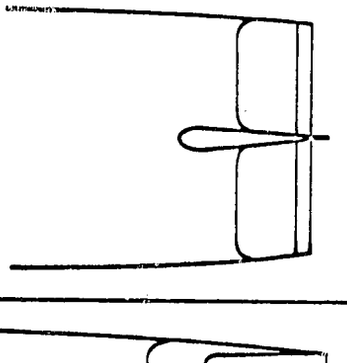	CV2D-CD	DCD2-D2
CVRP	DRP1	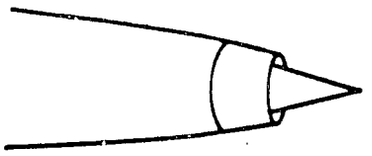	PLUG (WEDGE)	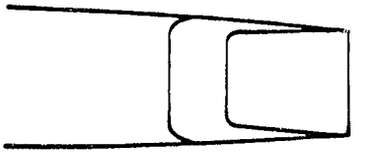	CV2D	SING-2D
CVRP	DRP2	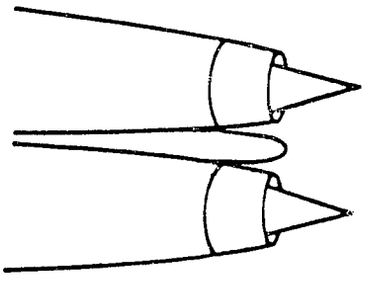		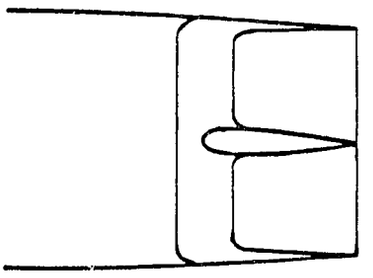	CV2D	ATS 2DM3
			SINGLE RAMP	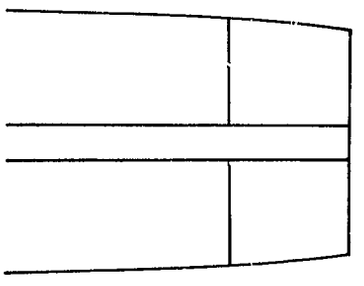	ADEN AB	ADEN CFG

Figure 36. Matrix of Nozzle/Aftbody Maps

C-2

2.3.2.2 NOZZLE/AFTBODY DRAG

The nozzle/aftbody drag (see Figure 37) is computed using performance maps which represent the aftbody drag characteristics, $C_{D_{AB}}$, for a fully expanded nozzle as a function of the ratio of maximum cross sectional area to nozzle exit area (A_{10}/A_9) and free-stream Mach number (M_o).

The definition of the nozzle aftbody drag coefficient, $C_{D_{A/B}}$, is defined differently for 2D and axisymmetric nozzles.

2D: $$C_{D_{A/B}} = \frac{D_{A/B}}{q(A_{10}-A_9)}$$

AXI: $$C_{D_{A/B}} = \frac{D_{A/B}}{qA_{10}}$$

In the long form output $C_{D_{A/B}}$ for 2D nozzles will be redefined in the form of the axisymmetric nozzles.

The nozzle/aftbody drag maps include throttle-dependent drag (that part of the nozzle/aftbody drag attributed to the propulsion system) and aerodynamic drag (that part of the nozzle/aftbody drag attributed to the airplane drag polar). To determine this drag split a reference condition must be established. The nozzle/aftbody drag increment to be included in propulsion system installed net thrust will be defined as zero when the nozzle is at a prescribed geometry (A_9 reference) and operating at a nozzle static pressure ratio, P_9/P_o, equal to 1.0 (fully-expanded). The nozzle/aftbody drag at this condition will be included in the aerodymanic drag. Incremental changes in nozzle aftbody drag due to changes in nozzle/aftbody geometry and/or nozzle static pressure ratio different from this condition will be included as propulsion system drag. This reference condition is illustrated in Figure 38 for a typical set of nozzle/aftbody drag data.

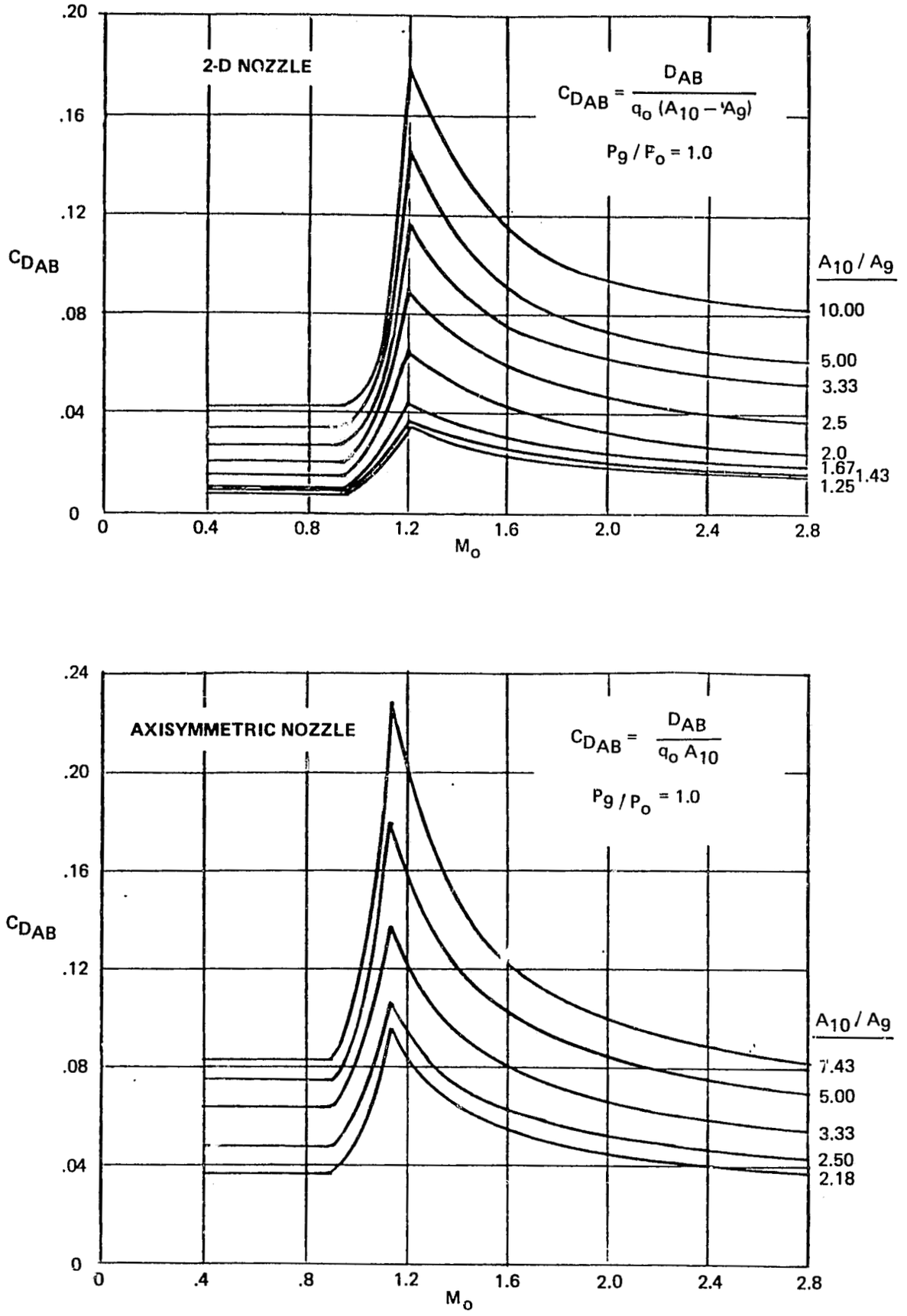

Figure 37 Data Format for Nozzle/Aftbody Drag Maps.

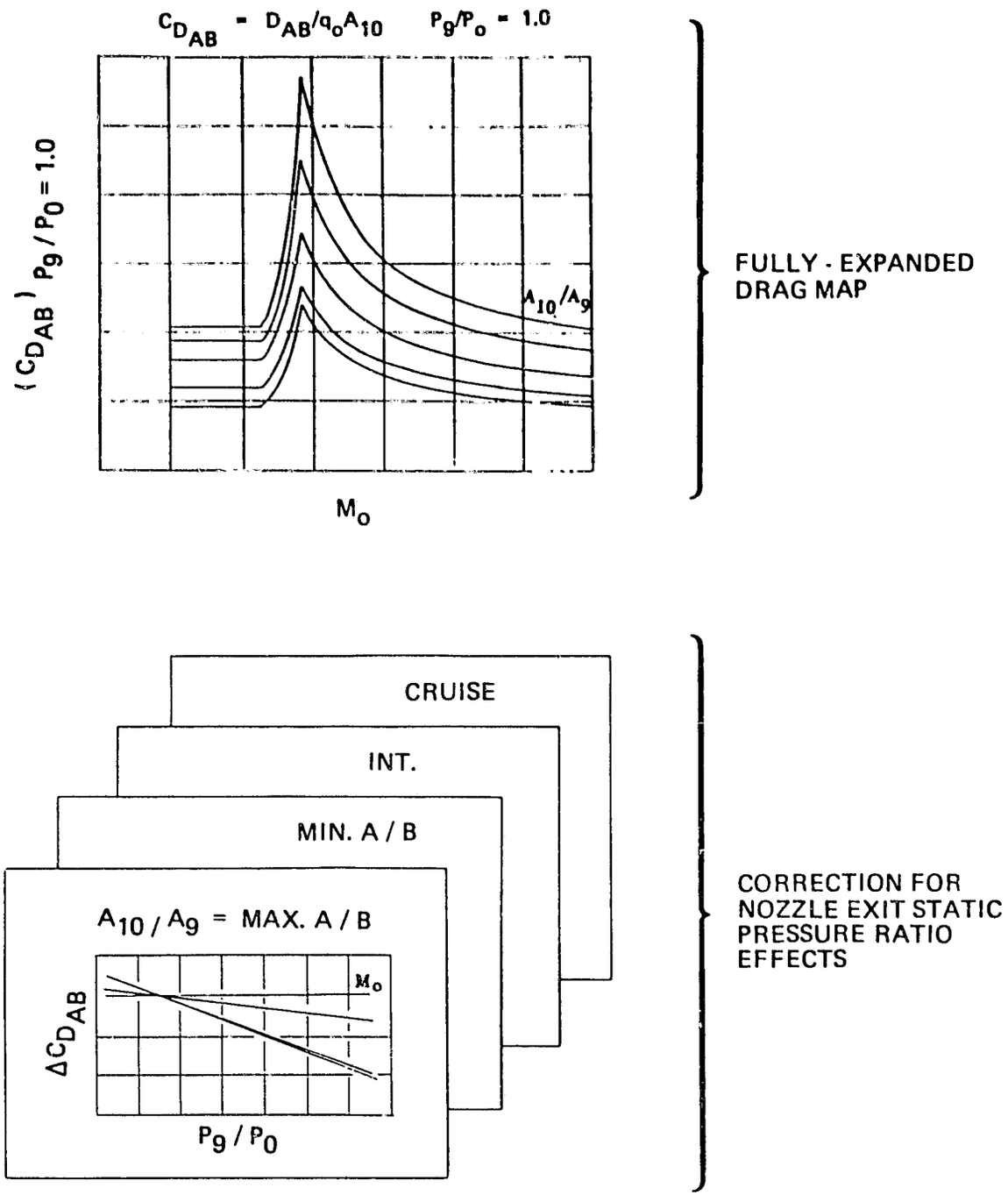

$$C_{D_{AB}} = (C_{D_{AB}})_{P_9/P_0 = 1.0} + (\Delta C_{D_{AB}})_{P_9/P_0, M_o, A_{10}/A_9}$$

Figure 38 Calculation Procedure for Effects of Nozzle Static Pressure Ratio on Drag

A procedure has been programmed that accounts for effects of varying nozzle exit static pressure ratio. This procedure determines an incremental drag coefficient, $\Delta C_{D_{AB}}$, to be added to the fully-expanded nozzle/aftbody drag coefficient. The incremental drag coefficient is a function of nozzle exit static pressure ratio (P_9/P_o) and free-stream Mach number, M_o, and is available for a range of nozzle/aftbody area ratios (A_{10}/A_9) from max A/B to subsonic cruise.

The incremental drag coefficient maps allow the user to input the pressure ratio effects data if it is available. If the user does not have such data available, a set of dummy maps are used that sets $\Delta C_{D_{AB}} = 0$ for all P_9/P_o, M_o, and A_{10}/A_9. A three-dimensional table look-up procedure is used to obtain the $C_{D_{AB}}$ values during the program operation. A maximum of four maps are used representing different nozzle/aftbody area ratios. The nozzle/aftbody drag procedure is illustrated in Figure 39.

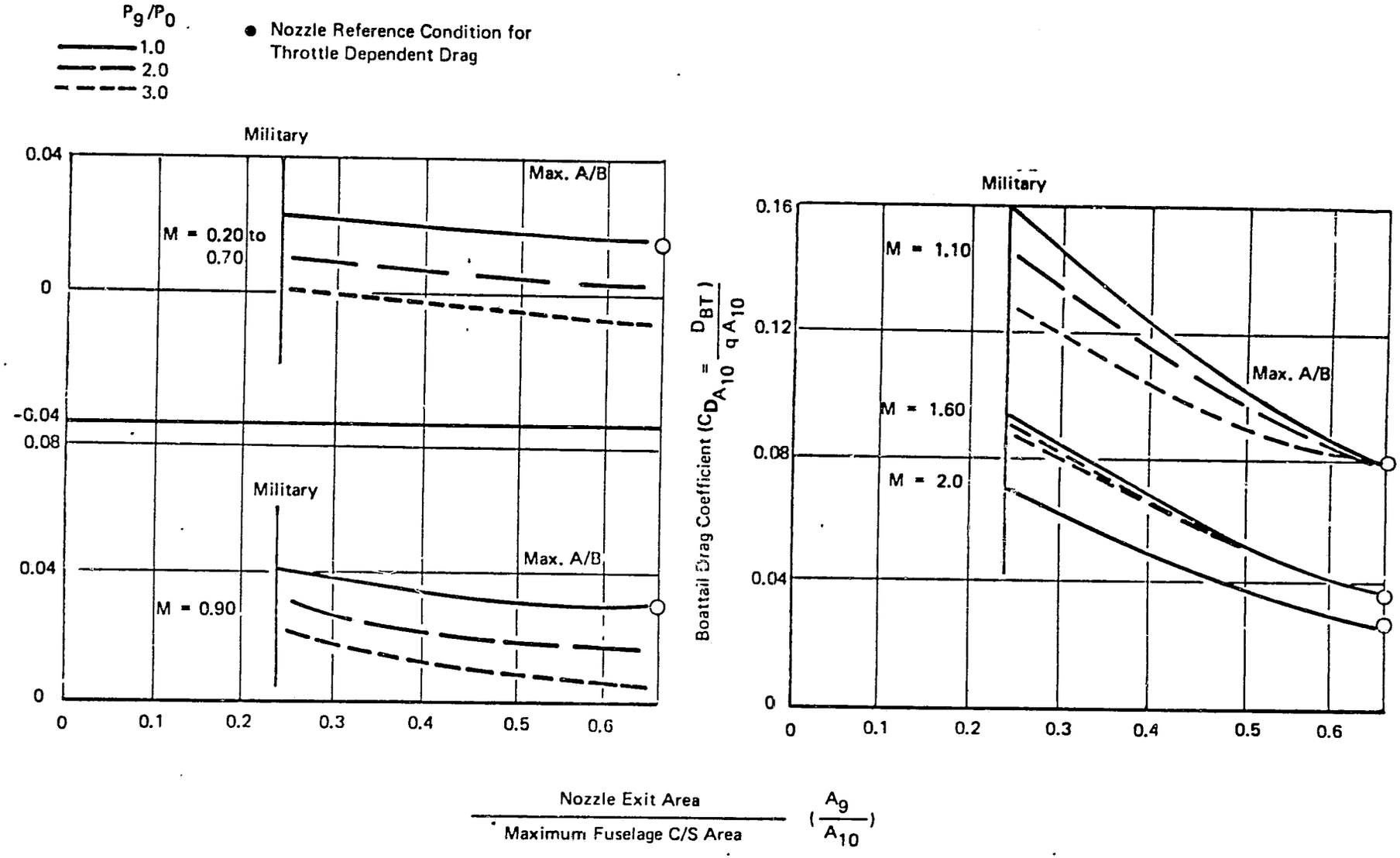

Figure 39 Typical Nozzle/Aftbody Drag Data

2.3.2.3 NOZZLE GROSS THRUST COEFFICIENT

The differences in the gross thrust coefficient map formats for axisymmetric and 2-D nozzles are shown in Figure 40. Axisymmetric nozzle C_{F_G}'s are presented as a function of nozzle total pressure ratio (P_{T_9}/P_{AMB}) and nozzle area ratio (A_9/A_8) Figure 40a. Two types of nozzle gross thrust coefficient maps are used for 2-D nozzles:

$$C_{F_G} = f(P_{T_8}/P_{T_{AMB}}, A_8)$$

$$C_{F_G} = f(P_{T_8}/P_{T_{AMB}}, PS)$$

where PS = power setting.

To utilize either type of 2D nozzle map, a &D input of the maximum (AJMAX) and minimum (AJMIN) nozzle exit areas encountered in a prescribed Mach/altitude placard is needed. When using the first type of map (figure 40b) the nozzle throat area experienced at a certain flight condition will be used to interpolate between AJMAX and AJMIN. For the second type of C_{F_G} map (figure 40c), a definition of power setting compatible with NNEP must be made:

$$PS = 2 - \frac{AJMAX\text{-}AREA}{AJMAX\text{-}AJMIN}$$

A maximum afterburning flight condition is equivalent to a power setting of 2; a maximum dry flight condition is equivalent to a power setting of 1. During an afterburning flight condition, values for both AJMAX (A_{8max}) and AJMIN A_{8min}) must be input. If the calculated power setting falls between 2 and 1, the C_{F_G} would be an interpolated value. The power setting would be set to 1 if the calculated power setting falls below 1. During a dry flight condition, AJMAX or AJMIN must be set to zero; power setting will be set equivalent to 1.

AXISYMMETRIC NOZZLE

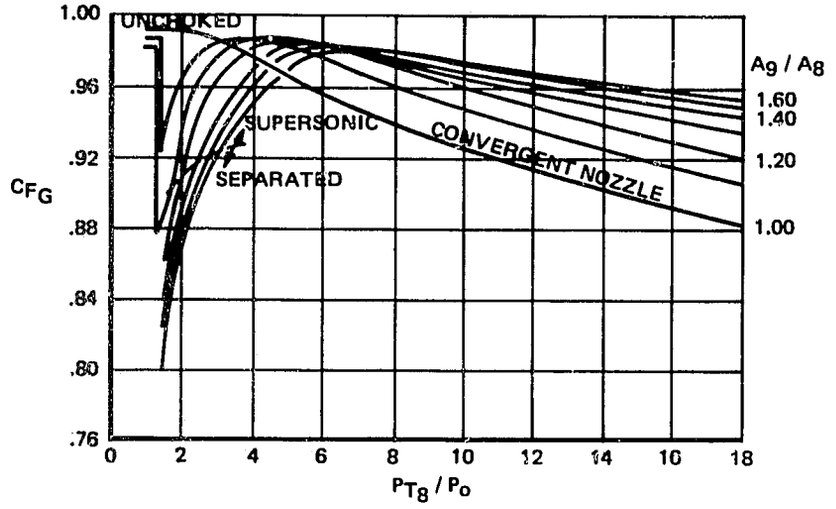

2 - D NOZZLE

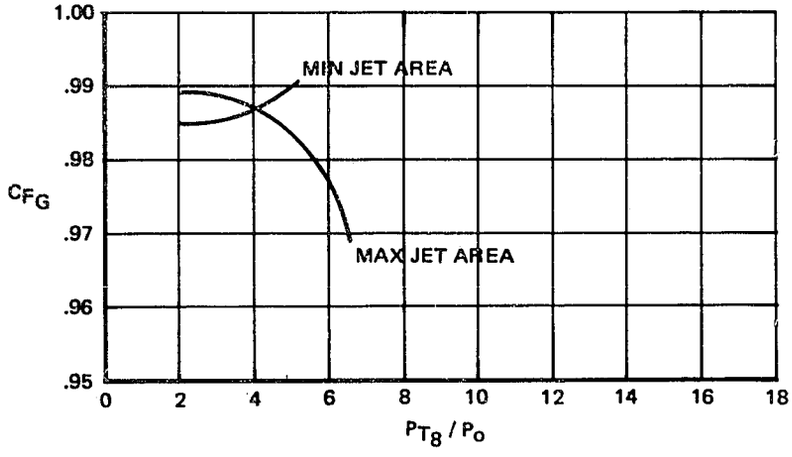

2 - D NOZZLE

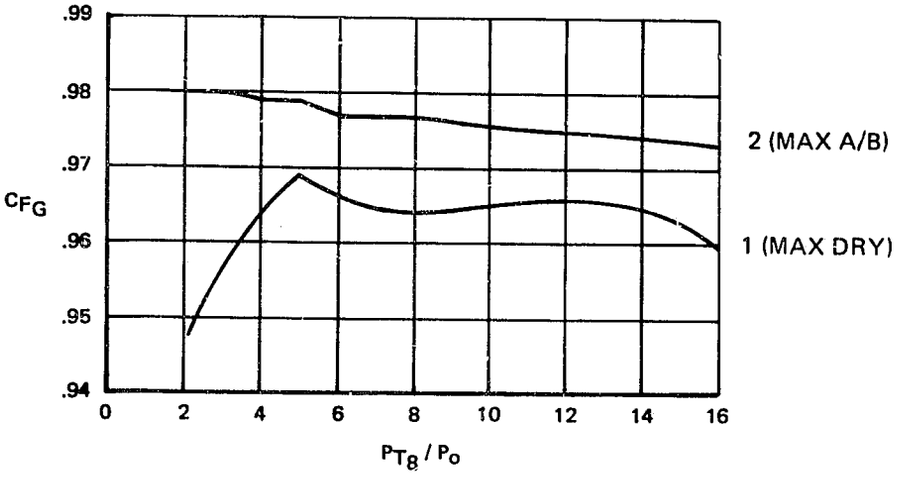

Figure 40 Nozzle Gross Thrust Coefficients

2.3.3 DERIVATIVE PROCEDURE

The use of inlet performance maps in mission analysis for preliminary design has simplified the task and provided for consistent, rapid results. The existing files of inlet performance maps do not cover all cases, however, and where the existing maps do not match the application, various approaches have been used to generate new maps. The user might modify the performance maps by hand to reflect changes, but no standard procedure is available, and the process would not be conducive to rapid response. Further, there would likely be a lack of consistency in map changes among many users. A common approach has been to use the maps as they exist and accept the possibility of reasonable errors. A rapid process which would produce modified performance maps that reflect the variables of the installation being considered, would allow maximum utilization of the advantages of the map installation analysis. The concept of a derivative processor fits this requirement. It will produce a new set of performance maps, reflecting the effects of the new installation.

Derivative Parameters

The first step in the development of the derivative procedure was the selection of the derivative parameters. These parameters are those that will be perturbed to produce a new set of performance characteristics from an existing (or "baseline") set of maps.

The criteria used to select the derivative parameters were:

(1) Variations in the parameter must have a significant effect on the content of the maps used to describe inlet or nozzle/aftbody performance. The derivative procedure should be used as part of an overall conceptual analysis procedure for calculating first-order propulsion system installation effects. The derivative parameters selected for the present procedure are those which have been clearly identified by test or analysis as having

"first-order" effects on installed performance. The derivative procedure should not be used for detailed design studies since the procedure may not be sensitive to the effects of small variations in some design variables.

(2) To the maximum extent possible, an attempt was made to define the derivative parameters in terms of geometric variables that can be easily related to the airplane configuration. This was done to help in evaluating the effects of configuration changes on installed performance.

(3) Derivative parameters had to represent trends that were strong enough to be clearly evident in spite of the scatter in test data obtained from typical inlet and nozzle tests.

Table I presents a list of the derivative parameters that have been selected for use in the derivative procedures. The definition of each of these parameters is included. Tables II & III present these same derivative parameters and the performance map variables that they affect, either directly or indirectly. Table IV, V and VI give the value of each derivative parameter for each data base inlet and nozzle/aftbody configuration.

TABLE I

INLET DERIVATIVE PARAMETERS AND THEIR DEFINITIONS

1. Aspect Ratio (AR)	- Applicable to two-dimensional inlets only
	- Defined as inlet width divided by inlet lip height (relative to tip position).
2. Sideplate Cutback (SPC)	- Applicable to two-dimensional inlets only
	- Defined as the percent of a full sideplate area that is removed to define a partial sideplate.
	The upper edge of a full sideplate extends from the ramp tip to the cowl lip.
3. First Ramp or Cone Angle	- Applicable to two-dimensional and axisymmetric inlets
	- Defined as surface ramp angle, in degrees, relative to horizontal reference line for two-dimensional inlets
	- Defined as cone surface angle, in degrees, relative to inlet centerline for axisymmetric inlets (cone half-angle)

TABLE I (Continued)

4. Design Mach Number (M_o Design)	- Applicable to all inlets - Defined as the maximum Mach number at which the inlet is designed to operate
5. Cowl Lip Bluntness	- Applicable to all inlets - Defined as the inlet lip surface radius divided by the lip height.
6. Takeoff Door Area	- Applicable to all inlets - Defined as the total door area for the takeoff auxiliary air system divided by the inlet capture area
7. External Cowl Angle	- Applicable to all inlets - Defined as external cowl surface angle, in degrees, relative to inlet horizontal reference line
8. Exit Nozzle Type for Bleed	- Applicable to two-dimensional and axisymmetric inlets - Defines whether bleed exit nozzle is convergent or convergent-divergent
9. Exit Nozzle Angle for Bleed	- Applicable to two-dimensional and axisymmetric inlets - Defined as bleed exit nozzle angle, in degrees, relative to inlet horizontal reference line

TABLE 1 (Continued)

10. Exit Flap Aspect Ratio for Bleed (AR_F)	- Applicable to two-dimensional and axisymmetric inlets - Defined as flap width divided by flap length
11. Exit Flap Area for Bleed (A_F/A_C)	- Applicable to two-dimensional and axisymmetric inlets - Defined as flap area divided by inlet capture area
12. Exit Nozzle Type for Bypass	- Applicable to all inlets - defines whether bypass exit nozzle is convergent or convergent-divergent
13. Exit Nozzle Angle for Bypass	- Applicable to all inlets - Defined as bypass exit nozzle angle, in degrees, relative to inlet horizontal reference line
14. Exit Flap Aspect Ratio for Bypass (AR_F)	- Applicable to all inlets - Defined as flap width divided by flap length
15. Exit Flap Area for Bypass (A_F/A_C)	- Applicable to all inlets - Defined as flap area divided by inlet capture area

TABLE I (Continued)

16. Subsonic Diffuser Area Ratio (A_2/A_1)
- Applicable to all inlets
- Defined as exit area (compressor face) divided by entrance area (throat)

17. Subsonic Diffuser Total Wall Angle
- Applicable to all inlets
- Defined as the total equivalent wall divergence angle, from entrance to exit

18. Subsonic Diffuser Loss Coefficient (ϵ)
- Applicable to all inlets
- Defined by the equation

$$P_{T_2}/P_{T_1} = 1.0 - \epsilon \left[1 - \frac{1}{(1 + 0.2M^2)^{3.5}} \right]$$

19. Throat to Capture Area Ratio (A_T/A_C)
- Applicable to Pitot inlets only
- Defined as the fixed throat area divided by the inlet capture area

NOZZLE/AFTBODY DRAG DERIVATIVE PARAMETERS AND THEIR DEFINITION

20. Nozzle/Aftbody Area Distribution
- Applicable to all nozzle/aftbodies. Defined by the cross-sectional area distribution as a function of station from A_{10} (ref. area) to A_9 (nozzle exit area). Characterized by the parameter IMS_T

21. Radial Tail Orientation
- Applicable to all nozzle/aftbodies with tails. Defined by the angular orientation of the tail relative to the vertical position.

TABLE 1 (Continued)

22. Fore-and-aft Tail Location	-	Applicable to all nozzle/aftbodies with tails. Defined by the location of the aft point of the tail/aftbody junction relative to the aftbody length ($X_{A_{10}} - X_{A_9}$)

NOZZLE C_{F_G} DERIVATIVE PARAMETERS AND THEIR DEFINITION

23. Base Area	-	Applicable to all nozzle/aftbodies with base area. Defined by the ratio of the base area, A_{BASE} to the aftbody reference area, A_{10}
24. Plug Half Angle	-	Applicable to round plug nozzles. Defined as the half-angle of the plug centerbody measured relative to the plug axial centerline.
25. Ramp Half Angle	-	Applicable to two-dimensional wedge nozzles. Defined by the wedge half-angle relative to the wedge centerline.
26. Aspect Ratio (W_9/H_9)	-	Applicable to two-dimensional nozzles, both C-D and wedge types. Defined by the ratio of nozzle width to height at the nozzle exit station.
27. Divergence Half-Angle (Θ_{DIV})	-	Applicable to convergent-divergent round and 2-D nozzles. Defined as the angle of the diverging section nozzle wall relative to the axial centerline of the nozzle.

TABLE II INLET DERIVATIVE PROCEDURE CROSS-REFERENCE

	DERIVATIVE PARAMETER	AFFECTED PERFORMANCE MAP VARIABLES						
		A_{OI}/A_C	$\frac{A_{O_{BLC}}}{A_C}$	A_O/A_C	P_{T_2}/P_{T_O}	$C_{D_{SPILL}}$	$C_{D_{BLC}}$	$C_{D_{BYP}}$
1	ASPECT RATIO (FOR 2-D INLETS)	●	●	●	●	●	●	●
2	SIDEPLATE CUTBACK (FOR 2-D INLETS)	●	●	●	●	●	●	●
3	FIRST RAMP (CONE) ANGLE	●	●	●	●	●	●	●
4	DESIGN MACH NUMBER	●	●	●	●	●	●	●
5	COWL LIP BLUNTNESS	●		●	●			●
6	TAKEOFF DOOR AREA	●		●	●			●
7	EXTERNAL COWL ANGLE					●		
8	EXIT NOZZLE TYPE FOR BLEED						●	
9	EXIT NOZZLE ANGLE FOR BLEED						●	
10	EXIT FLAP ASPECT RATIO FOR BLEED						●	
11	EXIT FLAP AREA FOR BLEED						●	
12	EXIT NOZZLE TYPE FOR BYPASS							●
13	EXIT NOZZLE ANGLE FOR BYPASS							●
14	EXIT FLAP ASPECT RATIO FOR BYPASS							●
15	EXIT FLAP AREA FOR BYPASS							●
16	SUBSONIC DIFFUSER AREA RATIO	●		●	●			●
17	SUBSONIC DIFFUSER TOTAL WALL ANGLE	●		●	●			●
18	SUBSONIC DIFFUSER LOSS COEFFICIENT	●		●	●			●
19	THROAT/CAPTURE AREA RATIO (FOR PITOT INLETS)	●		●				

TABLE III NOZZLE/AFTBODY DERIVATIVE PROCEDURE REFERENCE LIST

DERIVATIVE PARAMETER	AFFECTED PROGRAM AREAS	
	NOZZLE/AFTBODY DRAG CALCULATION	GROSS THRUST COEFFICIENT CALCULATION
AFT-END CLOSURE (INCLUDES EFFECT OF ASPECT RATIO, BOAT-TAIL ANGLE, TWIN NOZZLE SPACING	●	
RADIAL TAIL ORIENTATION	●	
FORE- AND -AFT TAIL LOCATION	●	
BASE AREA	●	
DIVERGENCE HALF-ANGLE (FOR AXI-SYMMETRIC AND 2-D C-D NOZZLES		●
AXISYMMETRIC PLUG HALF-ANGLE		●
ASPECT RATIO (FOR 2-D C-D AND 2-D WEDGE NOZZLES)		●
WEDGE HALF-ANGLE (FOR 2-D WEDGE NOZZLES)		●

Table IV Derivative Parameter Summary of Inlet Configurations

	DERIVATIVE PARAMETERS	DEFINITION	FILE NAME: A7	F8	M5SUB	M9SUB	NS	NS2	LWF	ATS2	ASF	VSTOL	NVSTO	TM183	FB	INT	M352D	AST	NASA3	RCAC35	R202ST
1	Inlet Aspect Ratio	$W_c\ h_c$	N/A	N/A	N/A	N/A	N/A	N/A	2.0	1.0	1.0	N/A	N/A	N/A	1.0	1.0	1.0	N'A	N'A	N A	.98
2	Sideplate Cutback	A_{cB}/A_{sp}	N/A	N/A	N/A	N/A	N/A	N/A	.75	.20	.25	N/A	N/A	N/A	0.0	0.0	0.0	N'A	N'A	N A	0.0
3	First Ramp Angle	Deg.	N/A	N/A	N/A	N/A	N/A	N/A	7.0	7.3	6.0	25.0	22.0	18.0	7.0	7.0	7 0	10.4	10 0	10 0	5.0
4	Design Mach Number	~	.80	1.60	.50	.80	1.50	1.60	1.60	2.0	2.5	1.60	2.0	2.5	2.5	3.0	3.5	2.35	3 0	3 5	2.6
5	Cowl Lip Bluntness	R_{lip}/h_c	.03	.02	.030	.022	.022	0.	.012	.012	.006	.02	.015	.015	0.	0.	0.	0.	0.	0	0
6	Takeoff Door Area	A_{to}/A_c	0.0	0.0	N/A	.028	.18	.22	.235	.20	.11	.462	.46	.25	.12	.50	.20	.20	20	20	.186
7	External Cowl Angle	Deg.	4.5	2.5	12.	17.	5.0	5.0	13.0	17.5	17.0	10.	19.	12.	12.	12.	15.0	1.0	0 0	3 0	5.7
8	Bleed Exit Nozzle Type	Conv. or C-D	N/A	N/A	N/A	N/A	N/A	N/A	Conv.	Conv.	Conv.	N/A	Conv.	Conv.	Conv.	Conv	Conv	Conv.	Conv	Conv	Conv
9	Bleed Exit Nozzle Angle	Deg.	N/A	N/A	N/A	N/A	N/A	N/A	20.0	15.0	20.0	N/A	20.0	15.	20.0	0.0	15.	15.	15	10	15.
10	Bleed Exit Flap Aspect Ratio	W_f/h_f	N/A	N/A	N/A	N/A	N/A	N/A	1.0	2.0	.90	N/A	1.0	1.0	.90	N/A	1 0	1.0	1.0	1 0	0.0
11	Bleed Exit Flap Area	A_f/A_c	N/A	N/A	N/A	N/A	N/A	N/A	.10	.10	.50	N/A	.10	.10	.20	N/A	20	.20	20	20	0.0
12	Bypass Exit Nozzle Type	Conv. or C-D	N/A	N/A	N/A	N/A	N/A	N/A	N/A	Conv.	C-D	N/A	Conv.	Conv.	C-D	C-D	C-D	C-D	C-D	C-D	C-D
13	Bypass Exit Nozzle Angle	Deg.	N/A	N/A	N/A	N/A	N/A	N/A	N/A	15.0	20.	N/A	20.	15.	20.	15.	15	15	15	10	15.
14	Bypass Exit Flap Aspect Ratio	W_f/h_f	N/A	N/A	N/A	N/A	N/A	N/A	N/A	2.0	.67	N/A	1.0	1.0	1.0	2.0	1.0	1 0	1 0	1 0	1.11
15	Bypass Exit Flap Area	A_f/A_c	N/A	N/A	N/A	N/A	N/A	N/A	N/A	.20	.268	N/A	.20	.20	.20	.20	20	.20	.20	20	.767
16	Subsonic Diffuser Area Ratio	A_2/A_1	1.40	1.40	1.25	1.25	1.305	1.305	1.373	1.50	1.89	1.44	1.83	2.0	1.40	2.8	4 7	1.57	2 1	4 97	2.77
17	Diffuser Total Wall Angle	Deg.	2.5	3.5	12.0	12.0	4.0	4.0	5.0	10.0	8.5	6.0	9.0	15.0	9.0	12.0	11 5	7.0	12.0	9 0	14.0
18	Subsonic Diffuser Loss Coefficient	ϵ	.12	.12	.015	.015	.12	.12	.12	.12	.16	.08	.12	.14	.14	.12	14	.06	12	12	.12
19	Throat/Capture Area Ratio	A_T/A_c	N/A	N/A	.80	.90	.96	1.00	N/A	N/A	N'A	N/A	N/A	N/A	N/A	N/A	N'A	N/A	N/A	N'A	N/A
	INLET TYPE		Chin	Chin	Pitot	Pitot	Pitot (N.S.)	Pitot (N.S.)	E.C. 2-D	E.C. 2-D	E.C. 2-D	E C. AXI	E C AXI	E C. AXI	M.C 2-D	M.C 2-D	M C 2 D	M C AXI	M C AXI	M C AXI	M.C. 2-D

Table V Derivative Parameter Summary of Nozzle/Aftbody Configurations

Derivative Parameters	Definition	CONFIGURATION NAMELIST								
		208NTTY	CD2R	DRP1	DRP2	DCD2D1	DCD2D2	SING2D	ATS2DM3	ADEN
Nozzle Static Pressure Ratio	P_9/P_{AMB}	1.0	1.0	1.0	1.0	1.0	1.0	1.0	1.0	1.0
Tail Fin Configuration	(0,1,2)	2.0	2.0	2.0	2.0	2.0	2.0	2.0	2.0	2.0
Tail Fin Angle	Deg.	0.0	0.0	0.0	0.0	0.0	0.0	0.0	0.0	0.0
Tail Fin Fore-and-Aft Location Ratio	$(X-X_9) / (X_9-X_{10})$	0.29	0.1736	0.18	0.133	0.67	0.45	0.62	0.28	0.20
Base Area Ratio	A_{BASE} / A_{10}	0.0	0.0	0.0	0.0	0.0	0.0	0.0	0.0	0.0

Table VI Derivative Parameter Summary of Nozzle C_{F_G} Configurations

		CONFIGURATION NAMELIST				
Derivative Parameters	Definition	CV1	CVRP	CV2DCD	CV2D	ADENCFG
Plug Half Angle	Deg.	N/A	10.0	N/A	N/A	N/A
Wedge Half Angle	Deg.	N/A	N/A	N/A	10.0	12.0
Aspect Ratio	W_9 / H_9	N/A	N/A	1.0	1.0	1.0
Divergence Half Angle	Deg	11.45	N/A	22.0	N/A	6.0

2.3.3.1 DERIVATIVE PROCEDURE FOR INLETS

The purpose of the inlet derivative procedure is to modify a baseline inlet configuration and define the resulting performance characteristics in a format that can be used as a direct input to the INSTAL program. Baseline inlet geometry and performance characteristics will be represented by elements of a set of inlet geometries and performance characteristics contained in the library of map files. The inlet geometric characteristics represented by the inlet configurations contained in the basic library of inlet maps are shown in Table IV. The derivative procedure provides a first-order prediction of the new inlet performance based on the baseline map file and changes in derivative parameters from those of the baseline inlet.

This procedure is based on two key assumptions:

(1) Generally applicable functions exist which relate changes in inlet performance characteristics to chances in inlet design parameters; and

(2) The derivative procedure will not alter the sophistication, technology, design philosophy, or mission related design trades that are represented by the baseline inlet. As a result, the inlet level of technology, type of application, complexity and design philosophy are removed as variables in the derivative procedure. It is important to note that as a result of this approach, a new inlet with given design variables will not have completely unique performance characteristics if it is generated by pertubations from different baseline map files. Each result will reflect the design of the chosen baseline inlet.

The derivative procedure is structured as an analytical technique as much as possible. Physically based analyses are used to relate parameter changes to the various performance map changes. The effects on all maps and map variables are included. The analyses and governing assumptions provide a procedure that is first order accurate or better. The approach

is structured so that all map effects are included in seven consecutive steps that require no iteration between the various steps. In general for each step, those effects which relate to modified geometry are determined first at the existing design Mach number. Then the effect of design Mach number change is determined.

Three types of inlets are included:

1. Two-dimensional
2. Axisymmetric
3. Pitot

The two-dimensional and axisymmetric inlets are treated similarly, though a coneflow solution is required for axisymmetric inlets while wedge flow is used for two-dimensional inlets. These inlets are assumed to have a design Mach number greater than one. The pitot inlet is treated differently because it may have a design Mach number of any value, and the derivative procedure must handle a change from subsonic to supersonic and vice versa. As a result, no simple Mach number scaling is used. For two-dimensional and axisymmetric inlets, Mach number scaling is employed if the design Mach number is changed. This Mach number scaling is accomplished as follows:

if $M_o < 1.0$,

$M_{o\,new} = M_{o\,old}$

} FOR BOTH MIXED AND EXTERNAL COMPRESSION INLETS

if $M_{o\,start\,old} > M_{o\,design\,old}$,

$$M_{o\,new} = 1.0 + (M_{o\,old} - 1.0)\frac{(M_{o\,design\,new} - 1.0)}{(M_{o\,design\,old} - 1.0)}$$

} EXTERNAL COMPRESSION INLETS

if $M_{o\,start\,old} < M_{o\,design\,old}$,

$M_{o\,start\,new} = M_{o\,start\,old}$

for $1.0 < M_o < M_{o\,start}$, (EXTERNAL COMPRESSION MODE)

$M_{o\,new} = M_{o\,old}$

for $M_{o\,new} > M_{o\,start}$, (MIXED COMPRESSION MODE)

$$M_{o\,new} = M_{o\,start} + (M_{o\,old} - M_{o\,start})\frac{(M_{o\,design\,new} - M_{o\,start})}{(M_{o\,design\,old} - M_{o\,start})}$$

} MIXED COMPRESSION INLETS

The starting Mach number is unchanged for mixed compression inlets. The range of starting Mach number is relatively small, and does not vary directly with design Mach number. The assumption of fixed starting Mach number is at least first-order accurate. The terminology for the various inlet flows is illustrated below.

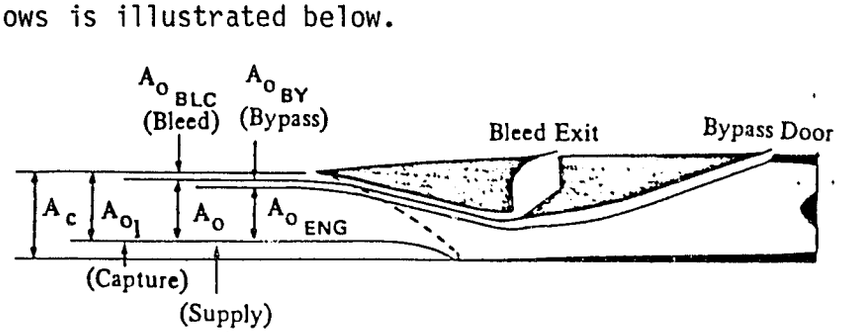

Step 1. New Inlet Capture

The first thing done is to establish the matched capture for the existing inlet:

$$\left(A_{O_I}/A_c\right)_{2CT} = \left(A_O/A_c\right)_{2C} + \left(A_{O\,BLC}/A_c\right)_{6B}$$

The remainder of this step will deal with this matched capture. For pitot inlets the existing capture is multiplied by the ratio, new-to-old, of throat-to-capture area ratio. Then if the new design Mach number is less than the old, the table is simply truncated. If the new design Mach number is greater than the old, the matched capture is extended past the previous maximum Mach number using the relation

$$\left(A_{O_I}/A_c\right)_{M_{O\,new}} = \left(A_{O_I}/A_c\right)_{M_{O\,max\ old}} \times \frac{\left(A/A^*\right)_{M_{O\,new}}}{\left(A/A^*\right)_{M_{O\,max\ old}}} \frac{\left(P_{T_2}/P_{T_1}\right)_{M_{O\,new\ NORMAL\ SHOCK}}}{\left(P_{T_2}/P_{T_1}\right)_{M_{O\,max\ old\ NORMAL\ SHOCK}}}$$

which assumes a fixed throat area and throat Mach number represented by the previous highest Mach Number.

For two-dimensional inlets, the Petersen-Tamplin analysis (Reference 14) is used, for $M_0 > 1.0$, to determine the effects of geometry changes with the existing design Mach number. This analysis, for single ramp inlets, includes the effect of aspect ratio, ramp angle, and side plate shape, and includes side spillage effects. It is assumed that ramp scheduling will be similar enough between the old and new geometries that the variation in capture will be represented by the relative variations in capture for single ramp inlets. To dimensionalize the inlet it is assumed that the ramp tip shock (old and new) is on the lip at the existing design Mach number. For this existing Mach number range, the maximum capture is determined from the analysis for the old and new geometry:

$$\left(A_{o_I}/A_c\right)_{\substack{2CT \\ new}} = \left(A_{o_I}/A_c\right)_{\substack{2CT \\ old}} \frac{\left(A_{o_I}/A_c\right)_{P\ -T_{new}}}{\left(A_{o_I}/A_c\right)_{P\ -\ T_{old}}}$$

For axisymmetric inlets, at $M_0 > 1.0$, a coneflow solution is used for the old and new initial cone angle for Mach numbers up to the old design Mach number. The cone tip shock is assumed to be on lip at the old design Mach number. A translation schedule is determined ($f(M_0)$) for the old cone angle such that the maximum capture is the matched capture determined previously. The new cone angle uses the same translation schedule to determine the new capture.

For all three types of inlets, at $M_0 < 1.0$, the effects on capture of cowl lip bluntness, takeoff door area, and subsonic diffuser modifications are determined. For cowl lip bluntness and takeoff door area the ratio of inlet airflows is equal to the ratio of effective throat areas. For the subsonic diffuser the compressor face Mach number is assumed fixed so that diffuser recovery affects capture directly ($M_{Th} < 1.0$).

Then for two-dimensional or axisymmetric inlets if the design Mach number is changed, the inlet capture is adjusted. If the design Mach number is increased the design (minimum) throat area goes down (and vice versa). Since geometric variation is limited, the maximum throat size will be changed accordingly. It is assumed that the inlet mass flow ratio at the design Mach number is the same (new and old) while at Mach 1.0

$$\left(A_{o_I}/A_c\right)_{new} = \left(A_{o_I}/A_c\right)_{old} \times \frac{(M_{o\ design})_{old}}{(M_{o\ design})_{new}}$$

This relationship has been shown to be generally valid for several axisymmetric inlets (References 15, 16, 17), but may be conservative for two-dimensional inlets.

Step 2. New Inlet Bleed

Pitot inlets are assumed generally to have no bleed, since present examples are unbled. However, in anticipation of a pitot inlet with bleed, the bleed rate tables will not be altered. No other approach would be well-founded since system characteristics are as yet undefined.

Two-dimensional and axisymmetric inlets have the effect of design change on bleed rates determined similarly, except that two-dimensional inlets can have a wetted area ratio change with fixed initial ramp angle, due to changes in aspect ratio and/or sideplate area, that axisymmetric inlets do not have. For two-dimensional inlets the bleed rates are multiplied by the ratio (new-to-old) of wetted areas.

The inlet design point, (specified in terms of design Mach number and geometric variables) is assumed to be the critical sizing point for the bleed system. It may be that some off-design condition caused a modification in the system, but that will be reflected in the design point bleed for the existing inlet. There are two criteria which may be generally used to determine the relative amount of boundary layer control: (1) the adverse gradient the boundary layer must traverse and (2) the Reynolds

number. The adverse gradient is the dominant effect. Oblique shock reflection results indicate that the allowable pressure ratio ($P_{SURFACE}/P_T$) divided by the upstream Mach number is a reasonable measure of the likelihood of separation (Reference 18) in the range of interest. Using this as a basis, and assuming a fixed downstream Mach number (throat or compressor face) and neglecting the secondary effects of recovery, the following expression may be derived (remembering that it is the surface pressure gradient the boundary layer must undergo):

$$\left[\left(\frac{A_{o_{BLC}}}{A_c}\right)_{new}\right]_{M_{o\,new}} = \left[\left(\frac{A_{o_{BLC}}}{A_o}\right)_{old}\right]_{M_{o\,old}} \cdot \left[\frac{\left(\frac{P_{surface}}{P_T}\right)_{M_{surface}\ @M_{o\,design\,old}} \cdot \left(M_{surface}\right)_{M_{o\,design\,old}}}{\left(\frac{P_{surface}}{P_T}\right)_{M_{surface}\ @M_{o\,design\,new}} \cdot \left(M_{surface}\right)_{M_{o\,design\,new}}}\right]$$

This expression works reasonably well when applied to existing inlets. Note that the pressure gradient term is affected by initial ramp or cone angle and design Mach number. The surface condition is obtained from simple wedge flow for two-dimensional inlets, and from cone flow for axisymmetric inlets. The results improve if this expression is multiplied (on the right-hand side) by

$$\left[\frac{\left(Re/ft/P_{T_o}\right)_{M_{o\,design\,new}}}{\left(Re/ft/P_{T_o}\right)_{M_{o\,design\,old}}}\right]^{1/7}$$

where the $Re/ft/P_{To}$ values come from Chart 25 of Reference 19, using the $T = 100^{o}F$ curve. This last step accounts for the Reynolds number change with Mach number.

It was determined that the expression discussed above provided excellent prediction of forward bleed in mixed compression inlets. This is quite reasonable since it implies that the bleed rate will go up or down with pressure ratio divided by initial surface Mach number to provide a constant throat entry condition.

It was found on further examination that terminal shock bleed (throat bleed for mixed compression or total bleed for external compression) scaled as

$$\left(\frac{A_{o_{BLC}}}{A_c}\right)_{new} = \left(\frac{A_{o\ BLC}}{A_c}\right)_{old} \cdot \frac{\left(A/A^*\right)_{M_{surface\ new}}}{\left(A/A^*\right)_{M_{suface\ old}}} \cdot \left[\frac{\left(Re/ft/P_{T_o}\right)_{M_{o\ design\ new}}}{\left(Re/ft/P_{T_o}\right)_{M_{o\ design\ old}}}\right]^{1/7}$$

The bleed rate split for mixed compression inlets was based on the mixed compression inlet design guidelines of Reference 20, where it is assumed that forward bleed equals throat blockage, and throat bleed is 2/3 of throat blockage. This translates to

$$\left(A_{o_{BLC}}/A_c\right)_{forward} = \frac{A_{o\ BLC}/A_c}{1.67}$$

and, as demonstrated in the Appendix, this bleed splitting provides excellent results.

It is assumed that for all inlets the variation in bleed rate with inlet supply is a variation in terminal shock bleed alone.

Step 3. New Engine Supply

Engine supply is inlet supply minus inlet bleed. Since inlet supply and inlet bleed have been determined for the new inlet in an independent manner, the resultant inlet supply does not simply scale by a shift. In fact non-linear scaling of inlet supply may well result.

$$\left(A_o/A_c\right)_{\substack{new \\ 2A}} = \left[\left(A_o/A_c\right)_{\substack{old \\ 2A}} + \left(A_{o\ BLC}/A_c\right)_{\substack{old \\ 6A}}\right] \cdot \left[\frac{\left(A_{o_I}/A_c\right)_{new}}{\left(A_{o_I}/A_c\right)_{old}}\right] - \left(A_{o\ BLC}/A_c\right)_{\substack{new \\ 6AT}}$$

An equivalency of supply, new-to-old, as a function of M_o is determined in this step so that all old tables with supply axes may be rescaled to new supply values.

Step 4. New Inlet Recovery

In this step the matched recovery will be modified, and the recovery variation with supply will simply be shifted by the same amount as the matched recovery.

For all Mach numbers less than or equal to 1.0 the ratio of new to old recovery is determined for cowl lip bluntness, takeoff door area, and subsonic diffuser changes. The existing recovery in this Mach number range is multiplied by these recovery ratios (new-to-old) to determine the new recovery. For pitot inlets this correction is applied at all existing Mach numbers.

New effective terminal shock Mach numbers are determined for two-dimensional and axisymmetric inlets at Mach numbers greater than 1.0 and less than or equal to the starting Mach number (external compression), The new values are calculated from the existing terminal shock Mach number and new and old inlet capture (prior to design Mach number change). The recovery difference for a normal shock at the old and new effective terminal shock Mach numbers is determined. The matched recovery is incremented by one-half this amount, since it is assumed ramp scheduling, or centerbody translation scheduling could be used to control this Mach number.

For two-dimensional and axisymmetric inlets at all Mach numbers greater than 1.0 the increment in initial ramp or cone shock recovery is determined for altered initial ramp or cone angle. Wedge flow is used for two-dimensional inlets and a cone flow solution for axisymmetric inlets. The matched recovery is incremented by one-half of the difference, assuming that altered inlet operation can be used to mitigate this effect.

For these same inlets and for this Mach number range the effects or recovery of subsonic diffuser geometry changes are determined for new and old geometries and the existing recovery is multiplied by the ratio new-to-old subsonic diffuser recoveries.

For two-dimensional and axisymmetric inlets, if the design Mach number is changed it is assumed that the loss coefficient $\frac{\Delta P_T/P_{T_o}}{q_o} = f(M_o)$ is still valid. Therefore the new recovery is simply

$$\left(P_{T_2}/P_{T_o}\right)_{new} = 1.0 - \left\{\left[1.0 - \left(\frac{P_{T_2}}{P_{T_o}}\right)_{old}\right] \cdot \left(\frac{M_{o\,new}}{M_{o\,old}}\right)^2\right\}$$

using Mach number equivalence. This is probably optimistic for external compression inlets with large design Mach number shifts, but has otherwise proven quite accurate (see the Appendix).

For pitot inlets if the design Mach number is reduced, the existing curve is simply truncated. If the design Mach number is increased the curve is extended by multiplying the recovery of the previous maximum Mach number by the ratio of the normal shock recovery at M_o divided by the normal shock recovery at the previous maximum Mach number.

The recovery as a function of mass flow curves are simply shifted by the difference in matched recoveries at equivalent Mach numbers. For pitot inlets this involves duplicating the previous maximum Mach number curve and shifting it so that the matched point agrees with the new M_o matched supply and recovery, or simply deleting some curves if design Mach number is decreased.

The buzz and distortion limit tables are assumed to be physically keyed to recovery, so at the same shift from the matched recovery as in the old inlet, at equivalent Mach numbers, a new inlet supply is determined and the new buzz and distortion limit tables result.

Step 5. New Spillage Drag

An inlet capture equivalence is determined

$$\left(A_{o_I}/A_c\right)_{\substack{\text{old \&}\\ \text{new}}} = \left(A_o/A_c\right)_{\substack{2A\\ \text{old \& new}}} + \left(A_{o\ BLC}/A_c\right)_{6A\ \text{old \& new}}$$

using the point-to-point equivalence in Table 2A. This allows simple rescaling of all inlet capture axes, old-to-new.

Next an absolute drag level is established by adding the reference drag levels to the power sensitive drags.

$$C_{D_{3T}} = C_{D_3} + C_{D_{3A}}$$

The drag calculation for two-dimensional inlets is done with the Petersen-Tamplin analysis (See Reference 14), which includes the effect of side spillage. The drag analyses in this program are based on momentum equations.

The drag calculation for axisymmetric inlets utilizes a cone flow solution, and the drag calculation procedures are equivalent to those in Petersen-Tamplin, except for side spillage, which has no axisymmetric counterpart.

The drag calculations for pitot inlets are equivalent to the subsonic and detached shock calculation procedures for two-dimensional and axisymmetric inlets, except that no external compression surface exists. Momentum balance equations are used with the upstream condition being freestream or behind a normal shock at freestream Mach number.

In general

$$C_{D_{new}} = C_{D_{old}} \cdot \left(\frac{C_{D_{\text{calculated new}}}}{C_{D_{\text{calculated old}}}}\right)$$

the new drag is determined as the old drag times the ratio (new-to-old) of calculated drags. The exception is for two-dimensional and axisymmetric inlets between Mach 1.0 and the starting Mach number where the ramp or cone tip shock is not detached. For those cases

$$C_{D_{new}} = C_{D_{\substack{max \\ A_{o_I}/A_c \text{ old}}}} \cdot \left[\frac{C_{D_{\substack{max \\ A_{o_I}/A_c \\ \text{calculate new}}}}}{C_{D_{\substack{max \\ A_{o_I}/A_c \\ \text{calculate old}}}}} \right] + \left[\left(C_{D_{old}} - C_{D_{\substack{max \\ A_{o_I}/A_c \\ old}}} \right) \cdot \left(\frac{\Delta C_{D_{\substack{\text{calculate} \\ \text{new N.S.}}}}}{\Delta C_{D_{\substack{\text{calculate} \\ \text{old N.S.}}}}} \right) \right]$$

the maximum capture drag is determined by multiplying by the ratio of calculated maximum capture drags, but the drag at reduced capture is determined incrementally from the maximum capture drag. This is because the drag increment is due to normal shock spillage, a different mechanism than the maximum capture drag, and the relative contributions in the old and new inlet may not be the same.

For two-dimensional inlets an equivalent single ramp angle as a function of M_0 is determined from the existing tip location to match the maximum inlet capture as a function of M_0. The drag is calculated using these equivalent ramp angles.

For axisymmetric inlets the actual cone angle is used and the tip is translated to match the maximum capture. The drag is calculated using these translation schedules.

The effect of cowl external angle on spillage drag is included as a multiplier. The ratio of K_{ADD} has been determined empirically (References 5, 14) as a function of cowl external angle, and the updated drags are multiplied by the ratio of K_{ADD} values to determine the final drag.

Then for the specified reference mass flow in 3B, Table 3A is the 3B intercepts in 3T. Table 3 is 3T - 3A.

Step 6. New Bleed Drag

The new drag is determined from the old at equivalent M_o and bleed area ratio, $A_{o\ BLC}/A_C$, making use of the point to point equivalency between Table $6A_{OLD}$ and Table $6A_{NEW}$.

$$(C_{D_{BLC}})_{new} = (C_{D_{BLC}})_{old} \cdot \frac{\left(C_{D\,BLC}\right)_{\text{new calculate}}}{\left(C_{D\,BLC}\right)_{\text{old calculate}}}$$

The PITAP (Reference 5) plenum pressure data are used, with the high pressure and low pressure bleed mass flow splits as defined in Step 2 for $M_o > M_{o\ START}$. For all other Mach numbers the high pressure curve is used. The calculated drag coefficients are determined from the flap drag and momentum drag procedures (Reference 5).

$$C_{D_{CALC}} = C_{D_{FLAP}} + C_{D_{MOM}}$$

Step 7. New Bypass Drag

This step is very similar to Step 6. The new bypass drag is determined from the old at equivalent M_o and $A_{o_{BYP}}/A_C$ as

$$(C_{D_{BYP}})_{new} = (C_{D_{BYP}})_{old} \cdot \left[\frac{\left(C_{D_{BYP}}\right)_{\text{calculate new}}}{\left(C_{D_{BYP}}\right)_{\text{calculate old}}}\right]$$

using the flap and momentum drag procedures as above. The nozzle plenum pressure is the matched inlet recovery multiplied by the PITAP plenum pressure multiplier, which is a function of bypass flow (Reference 5).

2.3.3.2 NOZZLE/AFTBODY DERIVATIVE PROCEDURE

The nozzle/aftbody derivative procedure consists of two parts: (a) nozzle/aftbody drag ($C_{D_{AB}}$) calculation procedure and (b) nozzle internal performance (C_{F_G}) calculation procedure. Each of these calculation procedures is discussed separately in the subsections which follow.

The purpose of the nozzle/aftbody drag calculation derivative procedure is to provide a rapid first-order computerized calculation method for obtaining the incremental changes in drag due to changes in nozzle and afterbody geometric variables and nozzle static pressure ratio. The basic premise in the development of the nozzle/aftbody drag derivative procedure is that a set of baseline nozzle/aftbody configurations and their estimated (or measured) drag characteristics are available in PIPSI format. The format of the nozzle/aftbody drag maps is illustrated in Figure 37.

The derivative procedure provides a means for calculating the changes in drag that are caused by changes in certain geometric parameters. These geometric parameters are defined by the list of derivative parameters in Section 2.3.3. The nozzle/aftbody derivative parameters are summarized below.

1. Aft end area distribution	Includes the effects of rectangular nozzle aspect ratio, nozzle boattail angle, twin nozzle spacing
2. Tail position	Includes the effects of radial tail orientation and longitudinal tail location
3. Base area	

All the parameters required to calculate the above relation are readily available except A_9/A_8. To obtain A_9/A_8 values, the user of the derivative procedure must input a variation of A_9/A_8 as a function of M_o or the program will default to a typical area variation schedule.

The typical area variation schedule built into the program is shown in figure 44. Using the above equation, incremental changes in drag due to pressure ratio effects will be calculated and stored as tables that can be used as input for the PIPSI program.

Drag Due to Aft End Area Distribution

The approach used to calculate the effects of changes in parameters which affect the aft-end area distribution is the truncated integral mean shape IMS_T method documented in References 21 and 22. This calculation procedure is summarized in Figure 42. The calculation of the IMS_T parameter requires that the nozzle/aftbody area distribution be determined as a function of several different nozzle positions ranging from minimum nozzle exit area (A_9) position to maximum nozzle exit area. A typical area distribution such as that required by the IMS_T procedure is shown in Figure 43. The calculated IMS_T parameter for a particular area distribution is used as input to data correlations of nozzle/aftbody drag as a function of IMS_T parameter and free-stream Mach number to obtain the nozzle/aftbody drag coefficient, $C_{D_{A10}}$. Examples of the drag data correlations are presented in Figures 44, 45, and 46.

The computer program is structured to have built-in drag correlation tables such as the data shown in Figures 44, 45, and 46. At the present time, only a limited amount of data has been found to provide the table look-up data required for all configurations. Until such time as better data are available, the same data will be used for 2-D wedge nozzles and 2-D C-D nozzles. Similarly, the only data correlations available for round plug nozzles are for twin round plug nozzles. These data correlations will also be used for single round plug nozzles until better data correlations are available. Twin round C-D nozzle drag correlations will likewise be used for single round C-D nozzles. The basic drag correlations are for a fully-expanded nozzle ($P_9/P_o = 1.0$). The effects of

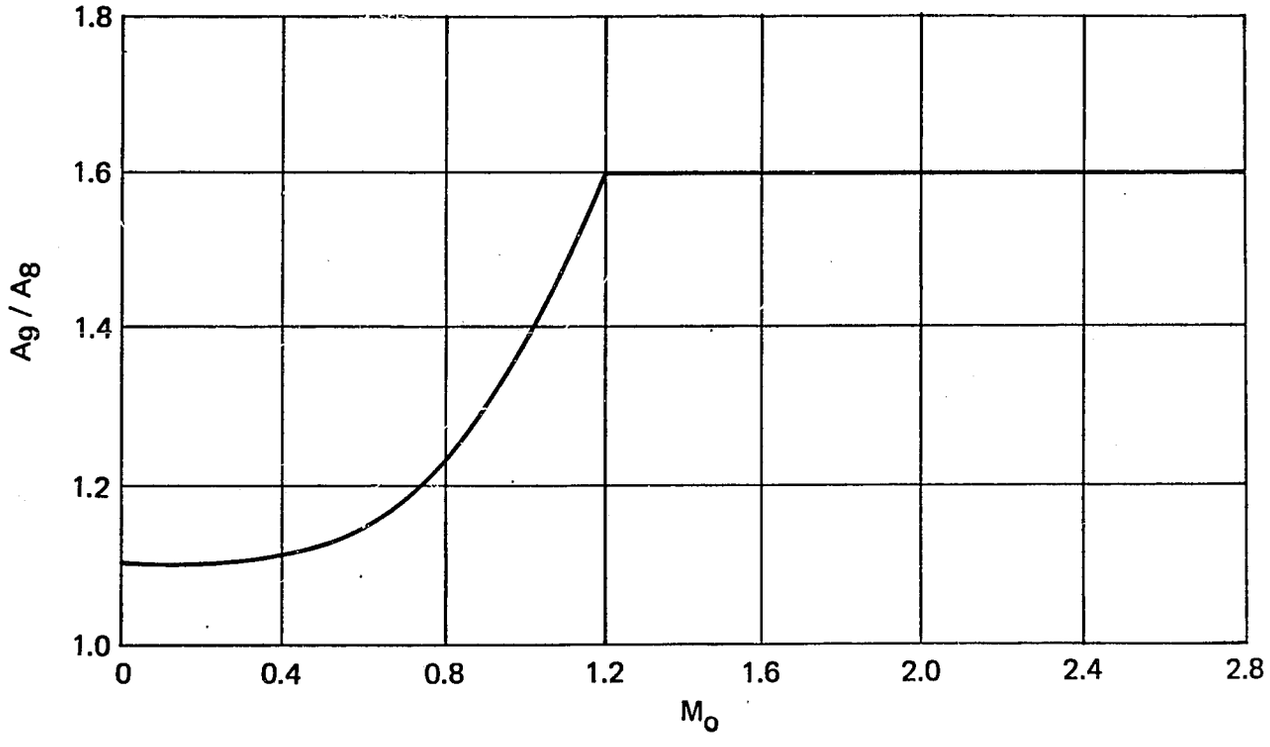

Figure 41. Default Nozzle Area Ratio Schedule

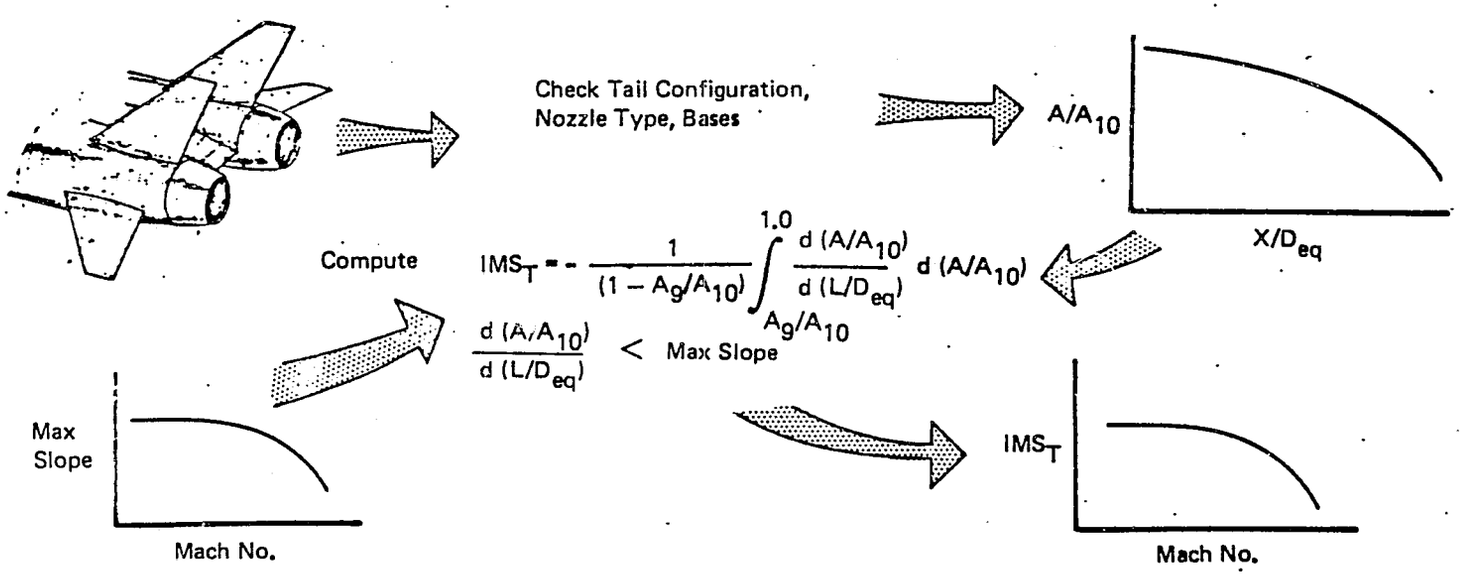

Figure 42 IMS_T Calculation Procedure

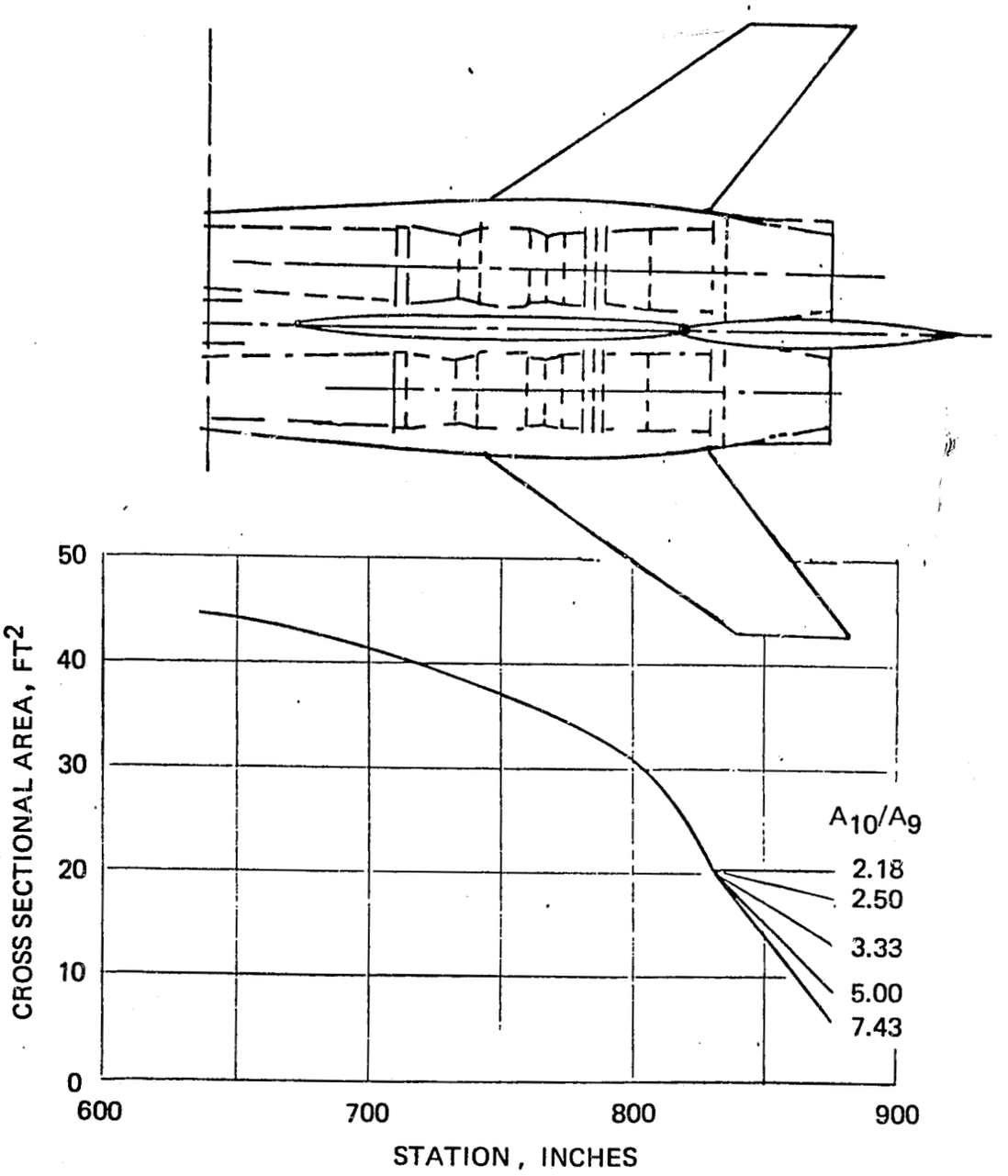

Figure 43. Nozzle/Aftbody Area Distribution for a Twin Round Nozzle Configuration

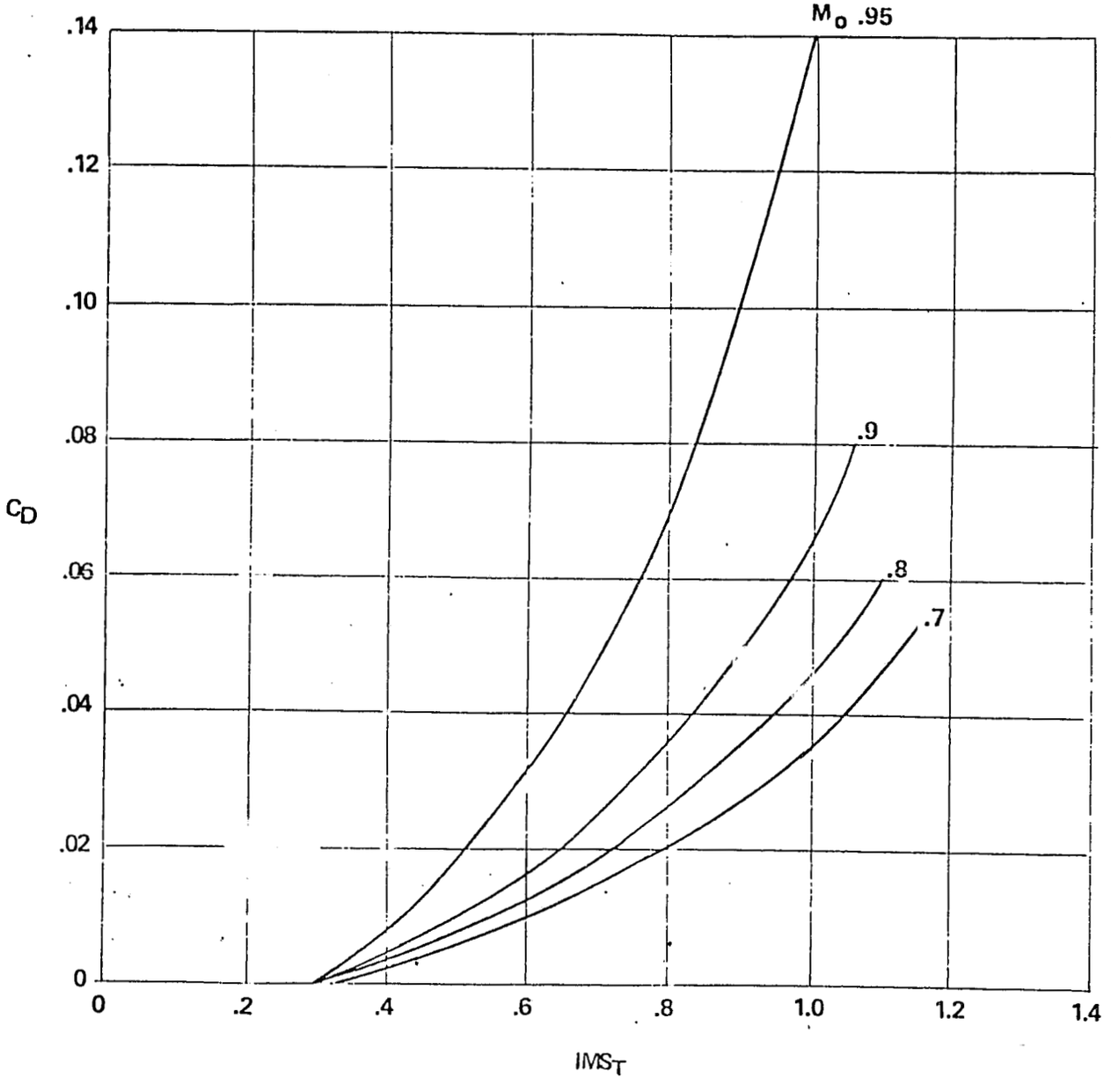

Figure 44. Nozzle/Aftbody Drag Correlations for a Twin C-D Axisymmetric Nozzle Configuration

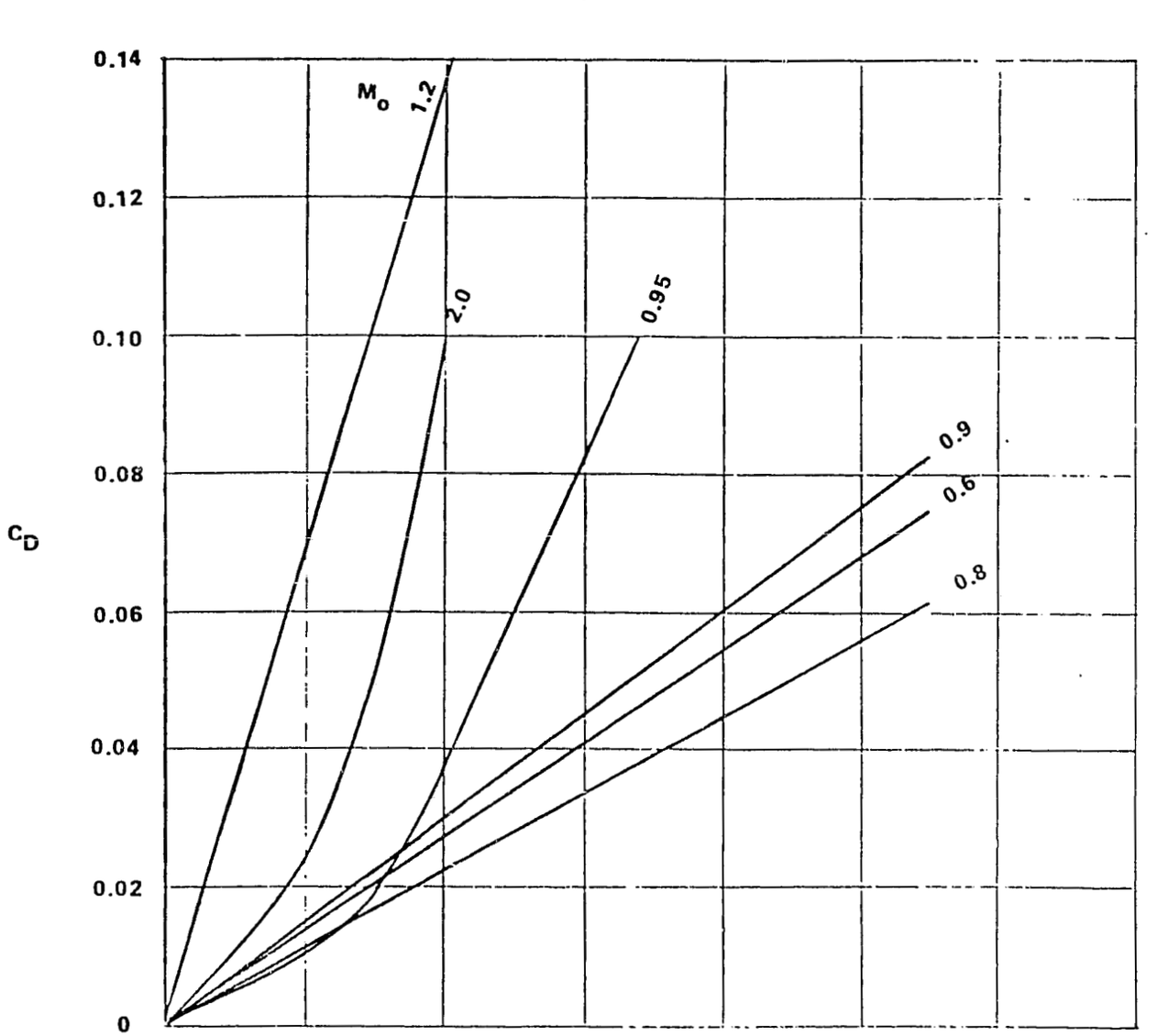

Figure 45. Nozzle/Aftbody Drag Correlations for Twin and Single 2-D Wedge Nozzle Configurations

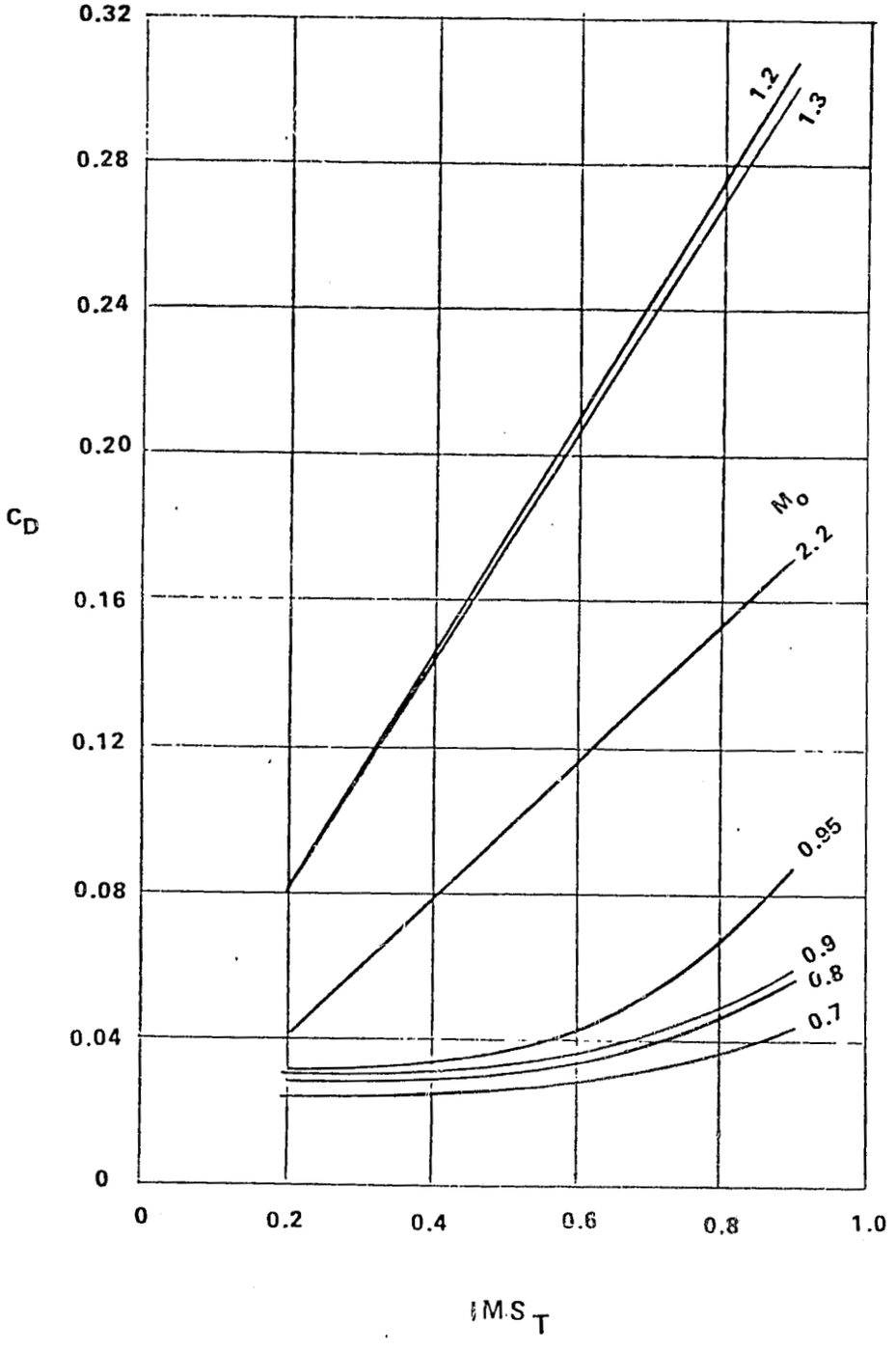

Figure 46 Pressure Drag Coefficient for Twin-Jet Axisymmetric Plug Nozzles

nozzle exit static pressure ratio (other than 1.0) on drag are calculated using a drag correlation developed during the Exhaust System Interaction Program (Reference 21). This correlation is:

$$C_{D_{A_{10}-A_9}} = C_{D_{\substack{A_{10}-A_9 \\ @\ P_9/P_o = 1.0}}} + \left[4.5\, e^{-M_o^2} \left(1 - \frac{P_9}{P_o}\right) \cdot \left(1.1\, \frac{A_9}{A_8} - 1.0\right) \cdot \left(\frac{A_9}{A_{10}}\right)^{3/2} IMS_T \right]$$

$$\Delta C_D = \left(C_{D_{\substack{A_{10}-A_9 \\ @\ P_9/P_o = 1.0}}} \right) - \left(C_{D_{A_{10}-A_9}} \right)$$

Drag Due to Tail Effects and Base Area

After the calculation of drag due to aft-end closure effects (previously described) drag increments are added to account for the radial orientation of tails, longitudinal location of tails and base drag. The program is structured to contain a table of incremental drag corrections (ΔC_{D_R}) as a function of free-stream Mach number, M_o, and radial tail orientation angle, Θ_R. However, due to the lack of experimental data to show the effect on drag of radial tail orientation, it has not been possible to construct a satisfactory correction table. Therefore, the table structure was coded to contain $\Delta C_{D_R} = 0$ for all Mach numbers and tail angles. When adequate data are available to construct a satisfactory table of corrections, the data can be entered in the computer program code. The format of the table is shown in Figure 47.

An incremental drag correction to account for the effects of fore-and-aft movement of the tail surfaces on aftbody drag has been developed from analysis of the data contained in Reference 23. These data were for single engine installations. Figure 48 shows the variation of $\Delta C_{D_{PAP}}$ as a function of the tail fore and aft location for a nozzle static pressure ratio, $P_9/P_o = 1.0$. The computer program is structured to contain the incremental tail location drag data shown in Figure 48. If better data become available, the computer code can be changed to incorporate the data tables.

The first-order effects of base area on drag are calculated by using input tables of base pressure coefficient as a function of free-stream

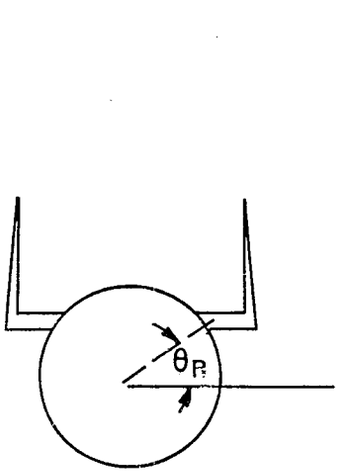

NOTE: TO ILLUSTRATE DATA TABLE FORMAT ONLY

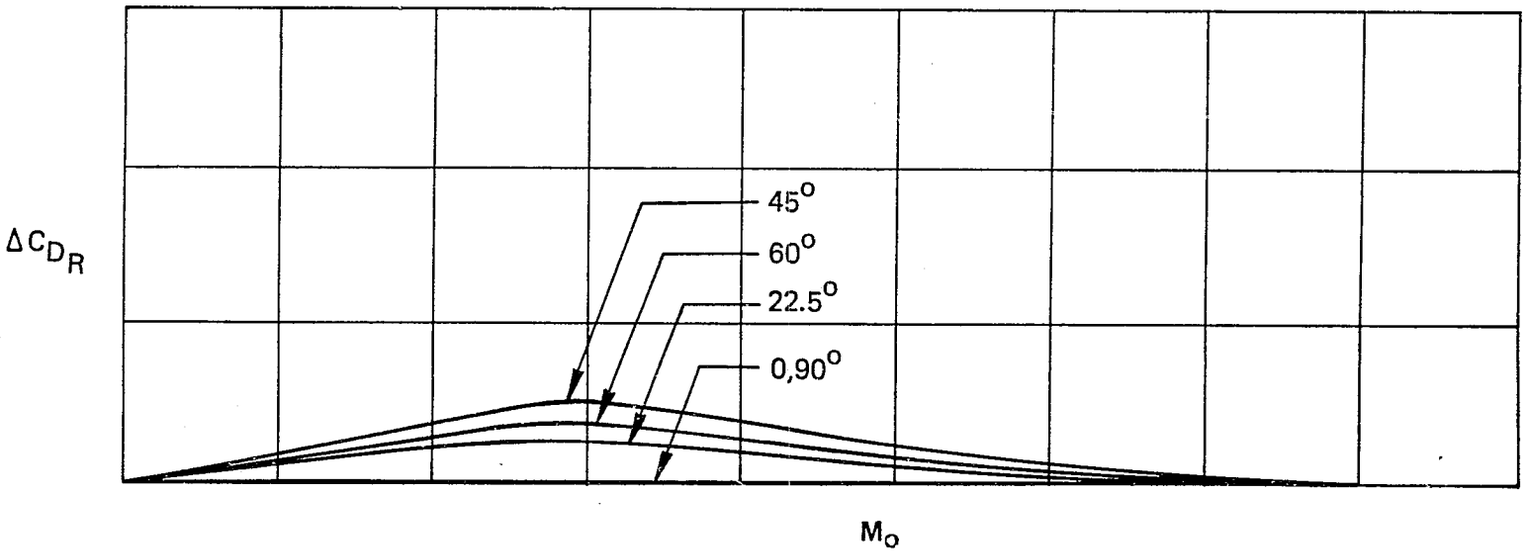

Figure 47 Correction for Radial Orentation of Tail

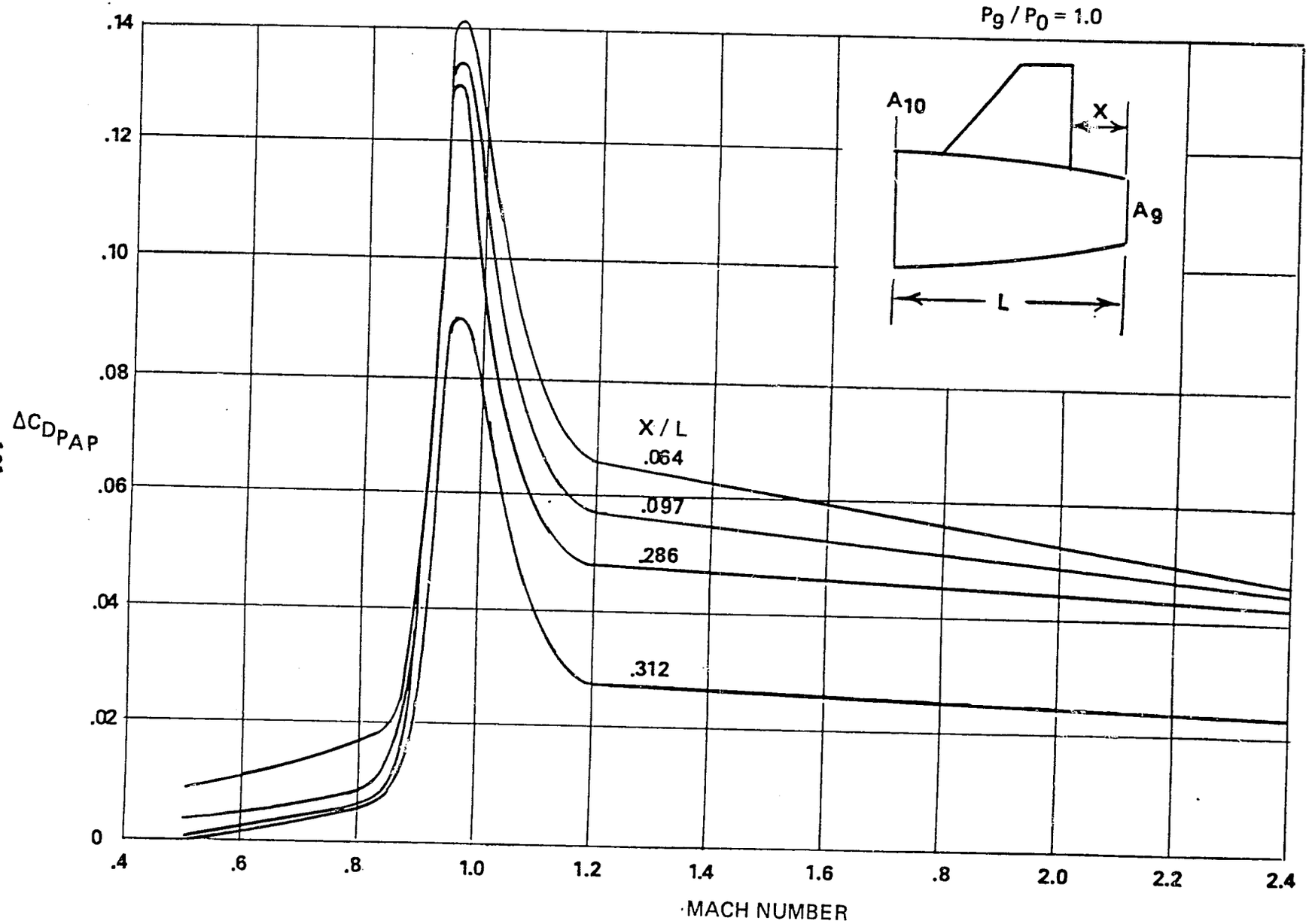

Figure 48. Incremental Drag Coefficient Due to Tail Fore-and-Aft Location

Mach number, M_0, and nozzle type (either axisymmetric or two-dimensional). The base pressure coefficient in the program is shown in Figure 49. Using the base pressure coefficient, C_{P_B}, and the base area ratios, the incremental base drag coefficient is calculated by the following relation:

$$\Delta C_{D_B} = C_{P_B} \cdot \left[(A_{base}/A_{10})_{new} - (A_{base}/A_{10})_{old} \right]$$

The total of the incremental changes in drag due to geometry are added and the resultant drag increment applied to the input drag map to obtain the new nozzle/aftbody drag map.

2.3.3.3 NOZZLE GROSS THRUST COEFFICIENT DERIVATIVE PROCEDURE

The calculation methods employed to determine the effects on nozzle gross thrust coefficient (C_{F_G}) of changes in nozzle geometric variables depend greatly on the type of nozzle being used. Separate calculation flow paths were constructed to handle each of the following nozzle types:

(1) Axisymmetric Convergent-Divergent
(2) Axisymmetric Plug
(3) Two-Dimensional Convergent-Divergent
(4) Two-Dimensional Plug (Wedge)

For all the above nozzle types, the approach used in developing the derivative procedure was to utilize as much as possible the data from experimental results, with theoretical calculations used where there were data voids or where it was necessary to calculate geometric relationships for typical trends of nozzle variations.

The derivative parameters for each nozzle type are summarized in Table VII:

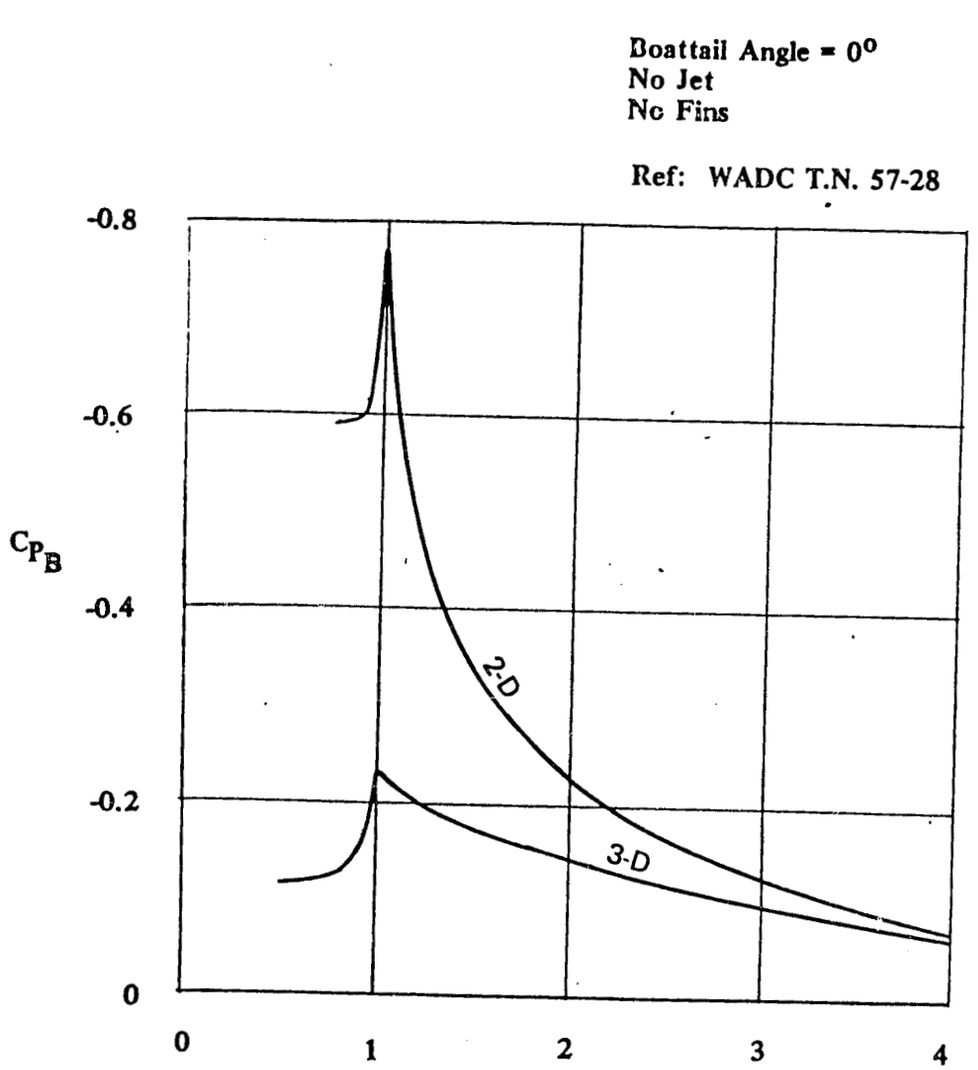

Figure 49 Base Pressure Coefficient

TABLE VII

DERIVATIVE PARAMETERS FOR NOZZLE C_{F_G} CALCULATION

NOZZLE TYPE		DERIVATIVE PARAMETERS
AXI C-D	Θ_{DIV}	DIVERGENCE HALF-ANGLE
AXI PLUG	Θ_P	PLUG HALF-ANGLE
2-D C-D	W_9/H_9	ASPECT RATIO
	Θ_{DIV}	DIVERGENCE HALF-ANGLE
2-D WEDGE	W_9/H_9	ASPECT RATIO
	Θ_N	RAMP (WEDGE) HALF-ANGLE

The user of the derivative procedure has the options available to calculate the effect on the input C_{F_G} map of any of the derivative parameters shown in the right hand column of Table V. The methods and data used to calculate the effects of variations in each of the derivative parameters are described in the sections which follow.

Effect of Divergence Half-Angle on C_{F_G} for a Round C-D Nozzle

The input map format for round C-D nozzles used by the PIPSI program is illustrated in Figure 50. This map provides C_{F_G} as a function of nozzle pressure ratio, P_{T8}/P_o, for various nozzle expansion ratios, A_9/A_8. To provide a method whereby the effect of Θ_{DIV} could be related to area ratio, a typical round C-D nozzle Θ_{DIV} variation as a function of A_9/A_8 was examined. Based on the results of this examination the simplified variation shown in Figure 51 was adopted for programming into the procedure. With a knowledge of A_9/A_8 and Θ_{DIV}, it is possible to determine the angularity loss, using the angularity loss coefficient data from Reference 1. These experimental data are shown in Figure 52.

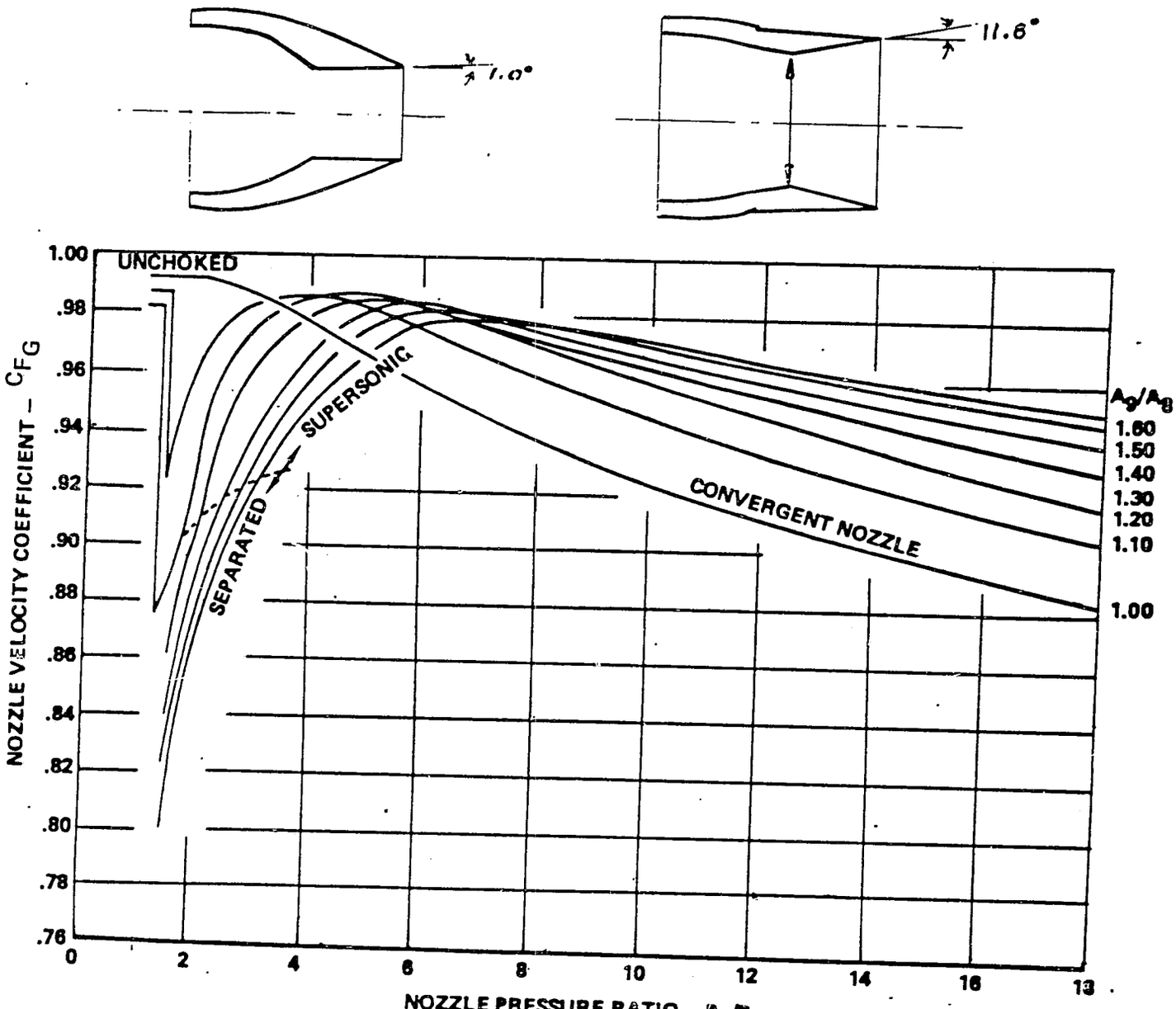

Figure 50. Gross Thrust Coefficient for a Round C-D Nozzle

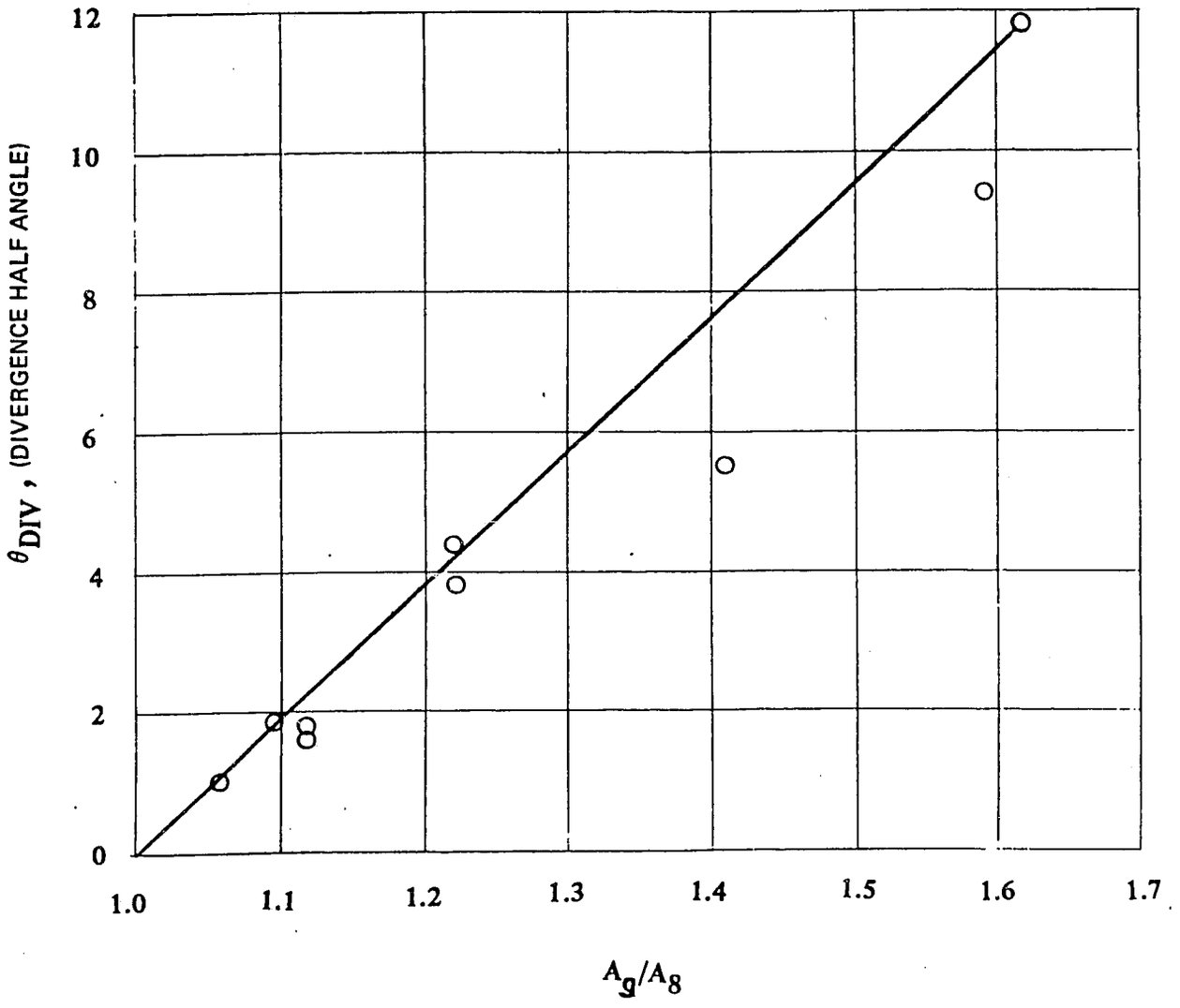

Figure 51. Divergence Angle/Area Ratio Relationship for a Round C-D Nozzle

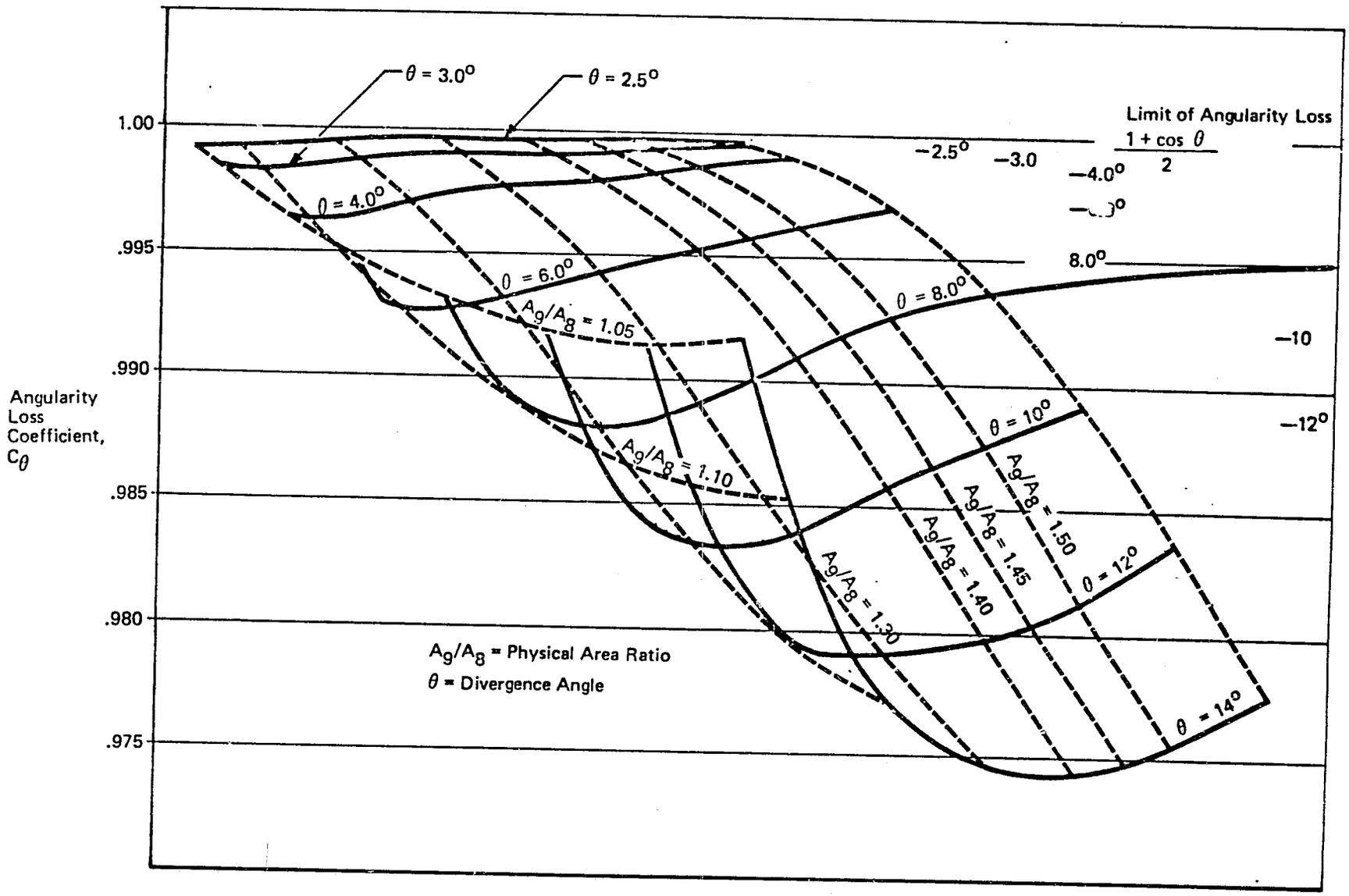

Figure 52. Angularity Loss Coefficient for Convergent-Divergent Nozzles

Effect of Plug Half-Angle on C_{F_G} for a Round Plug Nozzle

The input map format for an axisymmetric plug nozzle is shown in Figure 53. This format provides nozzle gross thrust coefficient, C_{F_G}, as a function of nozzle pressure ratio P_{T8}/P_o for various area ratios, A_9/A_8. To obtain the relationship of A_9/A_8 and plug half angle, a two-dimensional table look-up set of data was prepared that represents the geometric relationships between lip angle, plug half angle, Θ_p, and area ratio, A_9/A_8, for a typical plug nozzle configuration. These data, presented in Figure 54, is programmed into the code to provide inputs necessary to calculate the parameter $(\alpha - \Theta_p)$. The parameter $(\alpha - \Theta_p)$ is then used to enter Figure 54 to obtain the plug nozzle performance loss. Figure 55 documented in Reference 3, is based on experimental data.

Effect of Aspect Ratio and Divergence Half-Angle on C_{F_G} for a Two-Dimensional Convergent-Divergent Nozzle

The methods used in developing the computer code for the 2-D C-D nozzle internal performance calculations are based primarily on the experimental data gathered during the AFAPL Installed Turbine Engine Survivability Criteria contract documented in Reference 24. These tests provided data on a variety of 2-D nozzles of various aspect ratios and divergence angles.

The input map format for the 2-D C-D nozzle C_{F_G} is shown in Figure 56. This format provides nozzle C_{F_G} as a function of pressure ratio and nozzle jet area. Two jet area schedules are provided, minimum jet area and maximum jet area, corresponding to the experimental configurations tested. An optimum schedule of area ratio is used for each of the jet area settings. This area ratio schedule is presented in Figure 57. The area ratio schedule is truncated at a maximum area ratio of 1.60, corresponding to the maximum area ratio used in the tests. A divergence angle schedule was also obtained from the test configurations, as shown

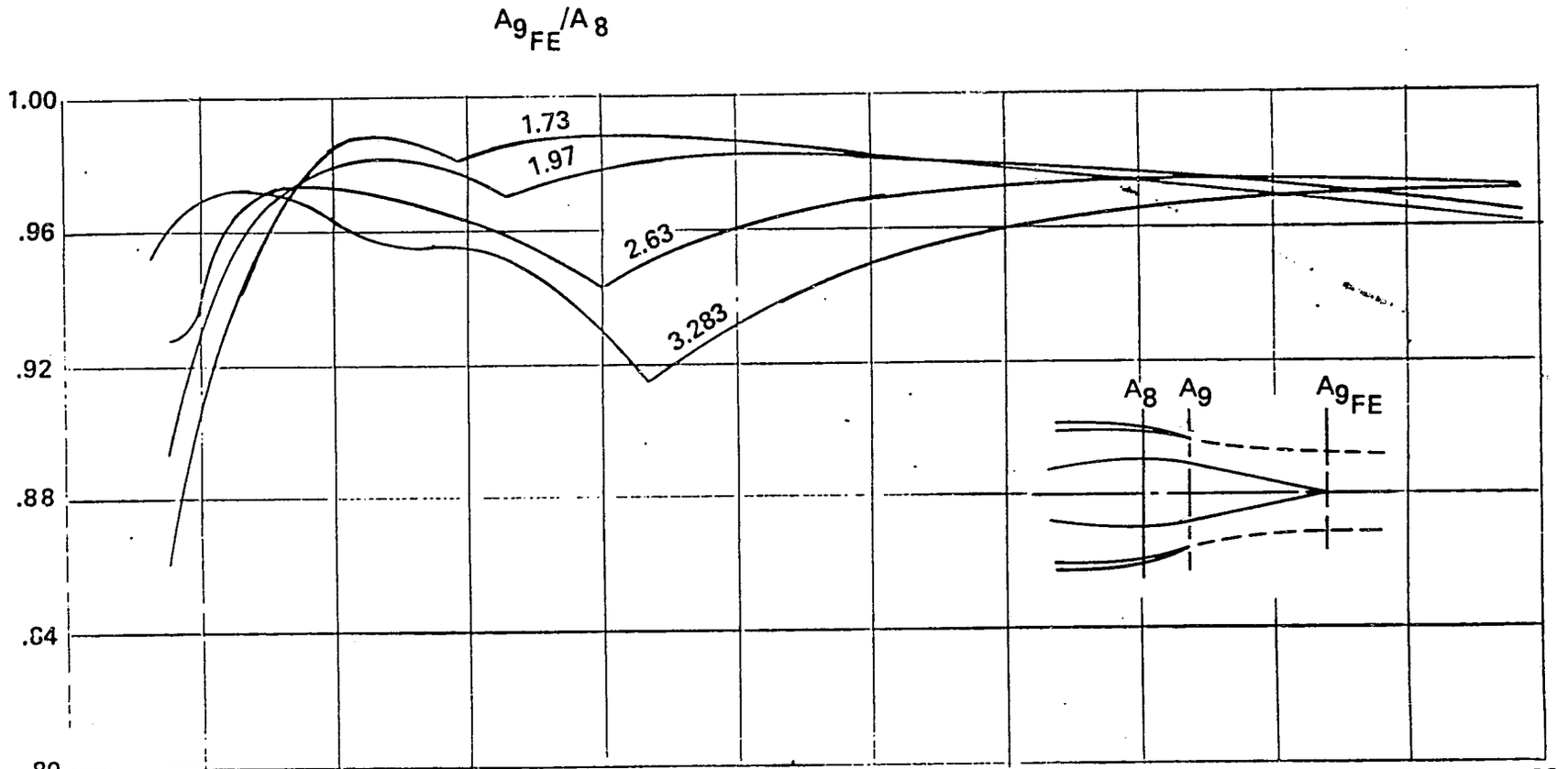

Figure 53 Gross Thrust Coefficient for Axisymmetric Plug Nozzles

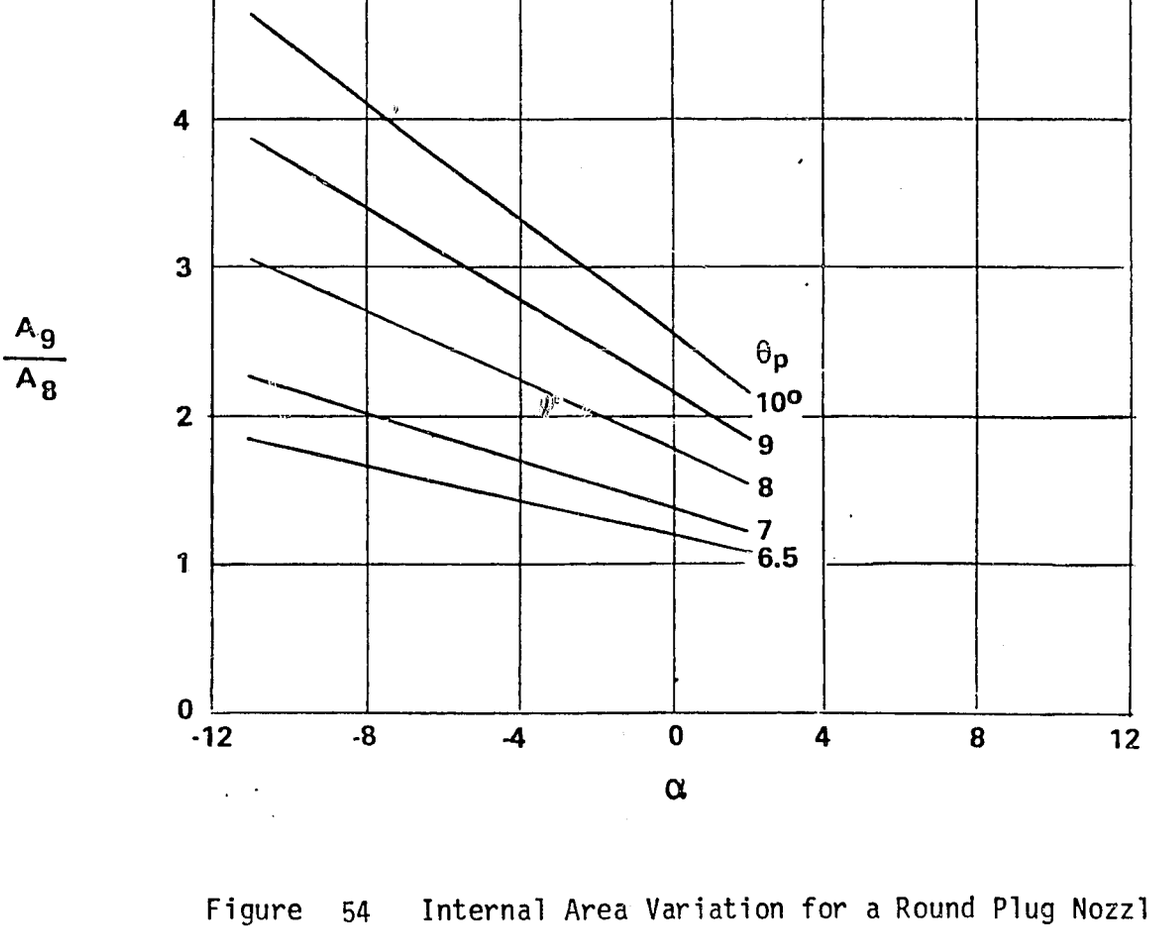

Figure 54 Internal Area Variation for a Round Plug Nozzle

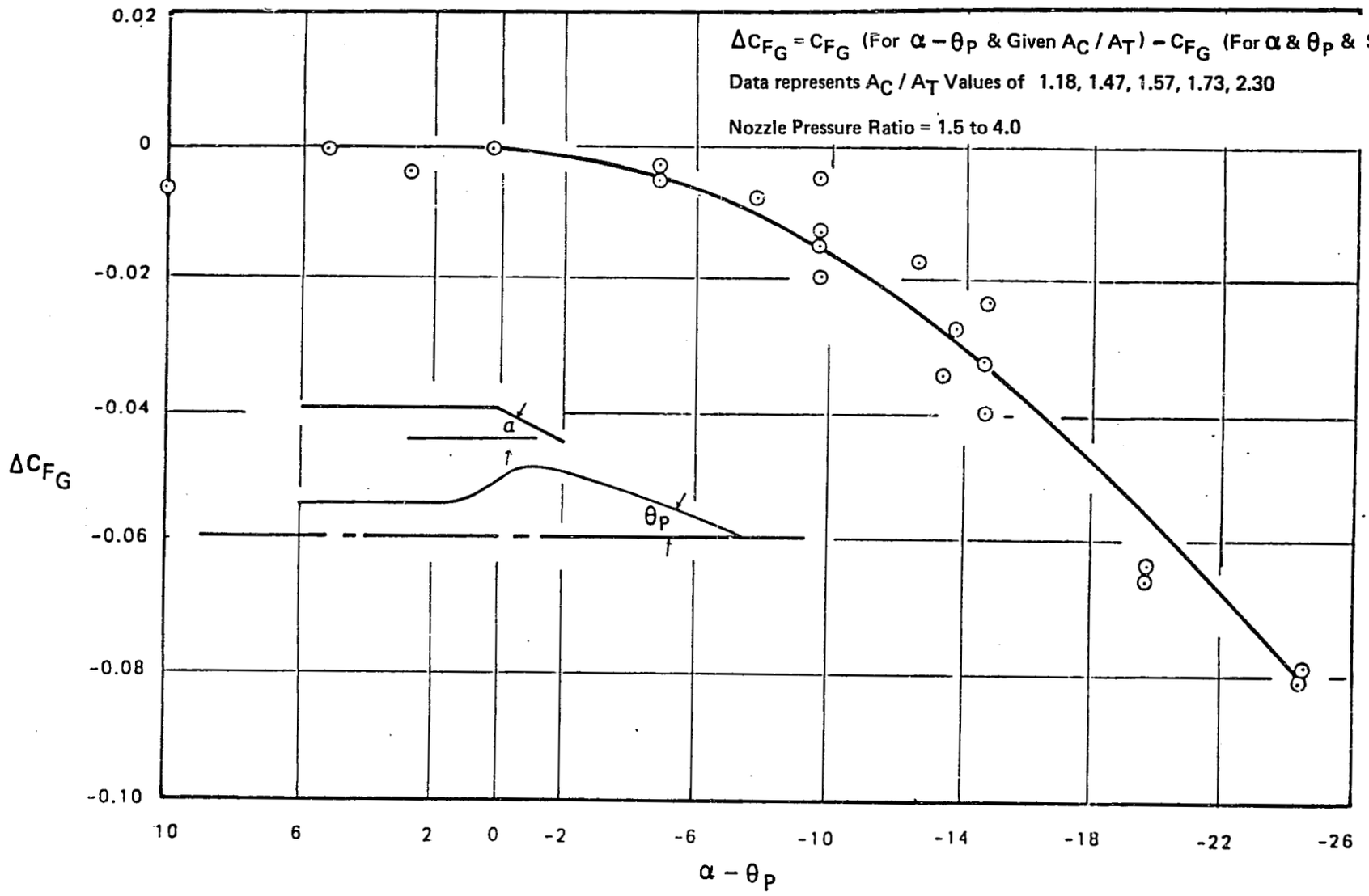

Figure 55 Performance Loss Due to Difference Between Cowl Angle and Plug Angle

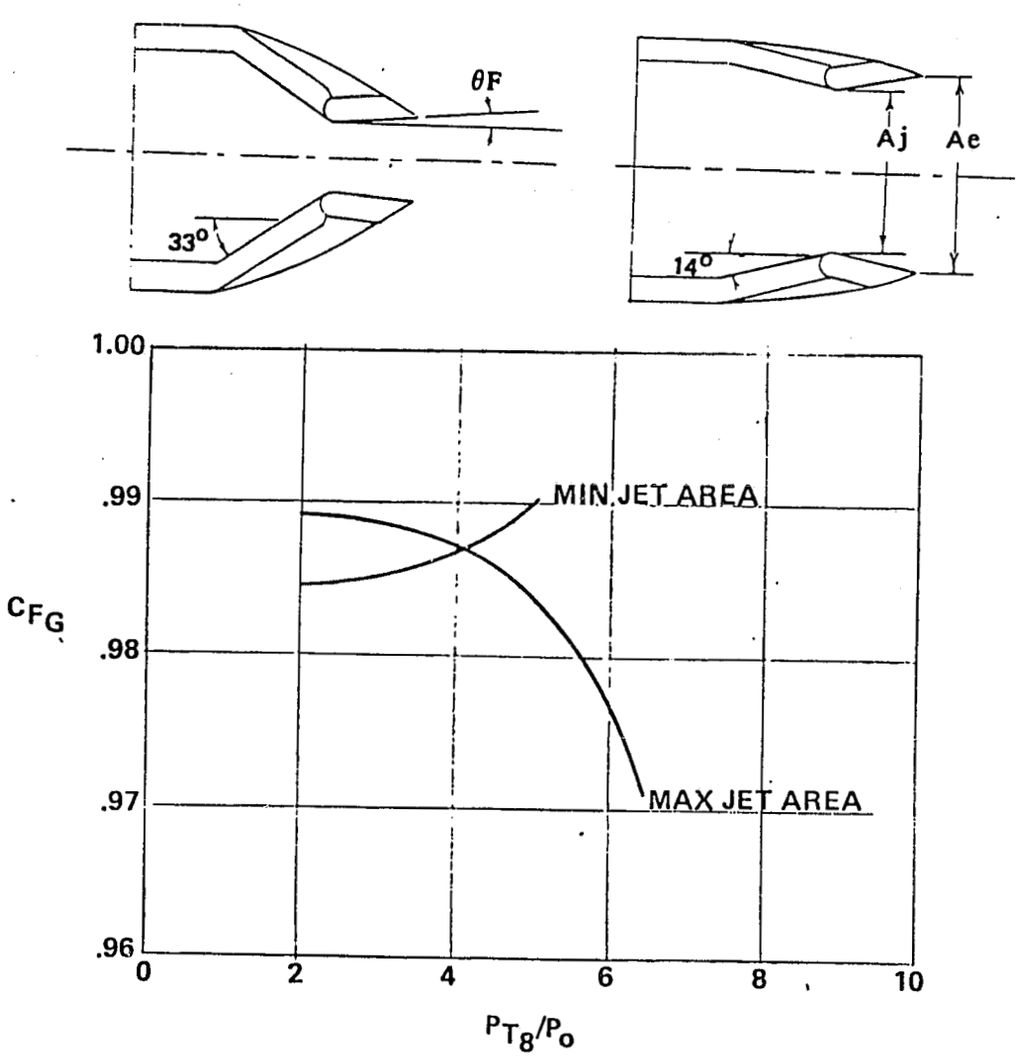

Figure 56 Gross Thrust Coefficient for a 2-D/C-D Nozzle

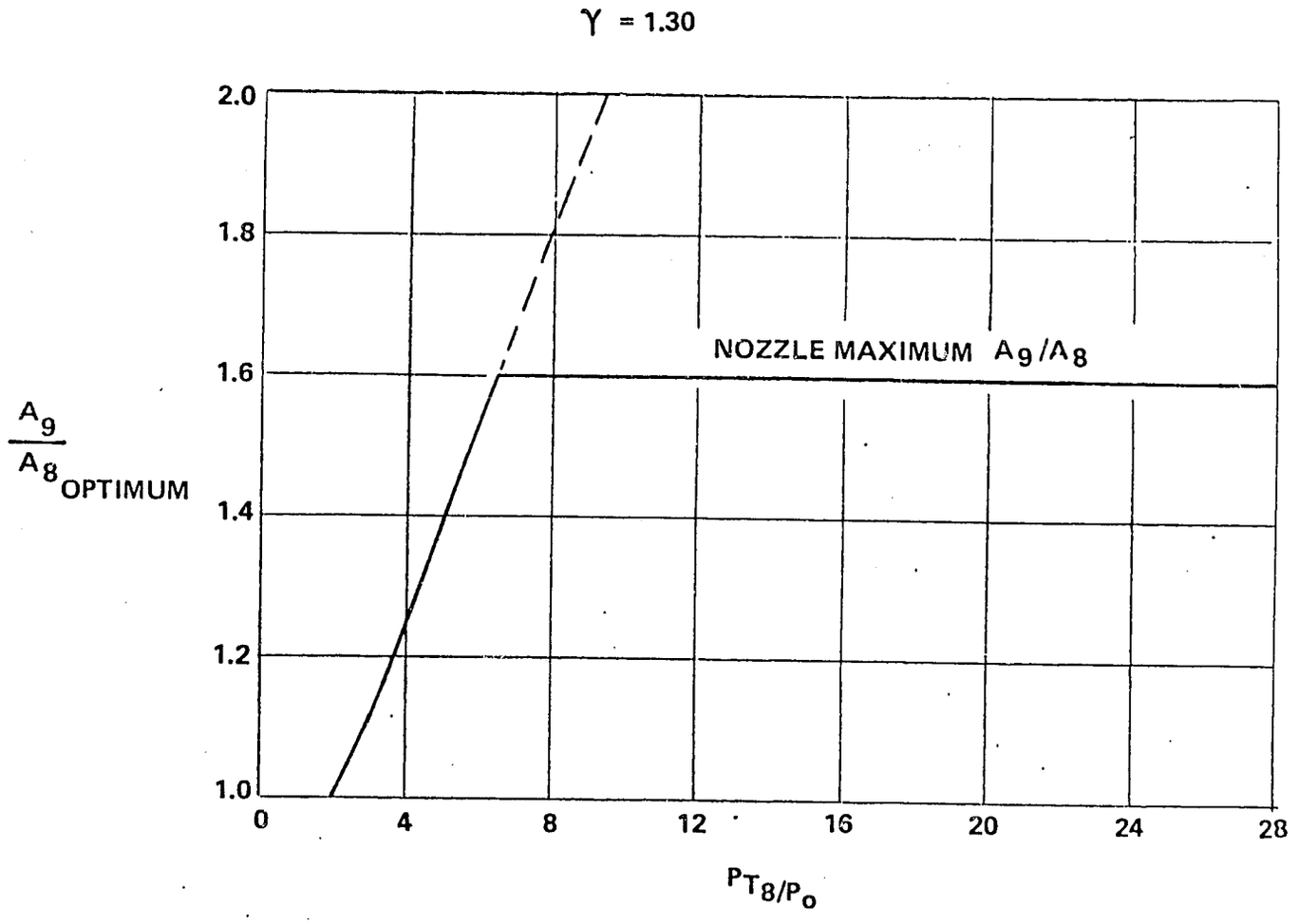

Figure 57 Optimum Area Ratio for a 2-D/C-D Nozzle

in Figure 58. With the geometric relationships provided by the previous A_9/A_8 and Θ_{DIV} schedules, the necessary input parameters are available to obtain $C_{F_{G\ PEAK}}$ as a function of A_9/A_8 and θ_{DIV} from the correlation of experimental data presented in Figure 59. The $C_{F_{G\ PEAK}}$ values for old and new configurations provide the data needed to obtain the ΔC_{F_G} resulting from the geometric change in θ_{DIV}. Presently, the code will treat divergent half angle effects on the ADEN gross thrust coefficient as if it were a 2-D convergent divergent nozzle. If more accuracy is required, this effect should be programmed for an ADEN type nozzle.

The experimental data from Reference 24 were also used to obtain the effect of nozzle aspect ratio. These data, presented in Figure 60, provide a correction factor, $C_{F_{G/}} C_{F_{G\ AR\ =\ 1}}$ as a function of Log AR for minimum and maximum jet settings.

Effect of Aspect Ratio and Wedge Half-Angle on C_{F_G} of a 2-D Wedge Nozzle

The format for 2-D wedge nozzle PIPSI input data maps is shown in Figure 61. This format provides C_{F_G} as a function of nozzle pressure ratio, P_{T8}/P_0, for two nozzle area ratio schedules, one for non-afterburning operation and one for maximum afterburning operation. These schedules assume that variable area nozzle geometry is available such that the nozzle area ratio can be scheduled to operate at the optimum value until the geometric limits of nozzle travel are reached.

The experimental data from Reference 24 were used to provide the correction factors for 2-D wedge nozzle aspect ratio and wedge angle. The data used in the computer program were prepared as correction factors relative to the baseine values of a wedge angle, θ_p, of 10^o and an aspect ratio,AR , of 1.0. The resulting correction factors are presented in Figures 62 and 63.

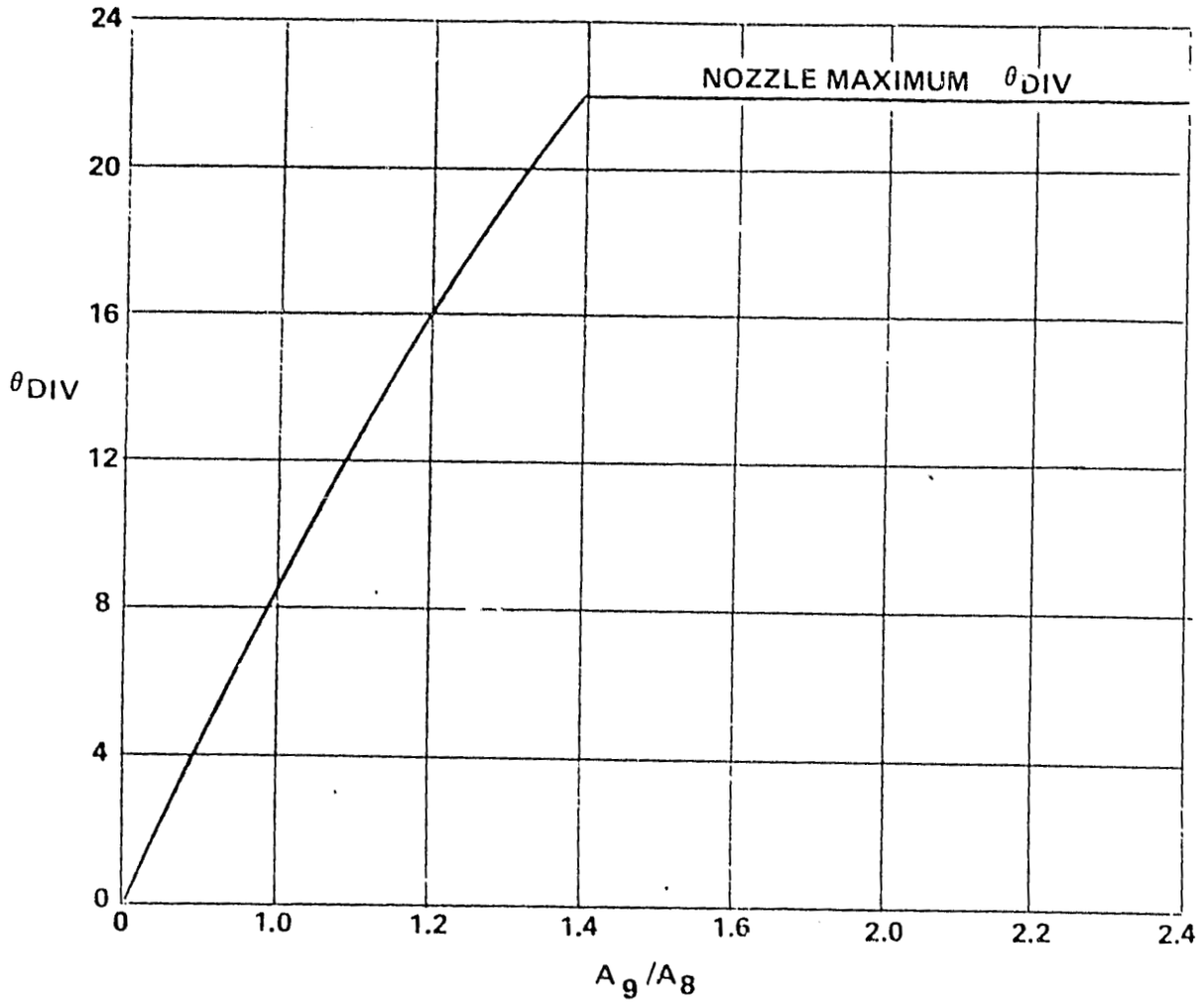

Figure 58 Optimum Divergence Angle as a Function of 2-D/C-D Nozzle Area Ratio

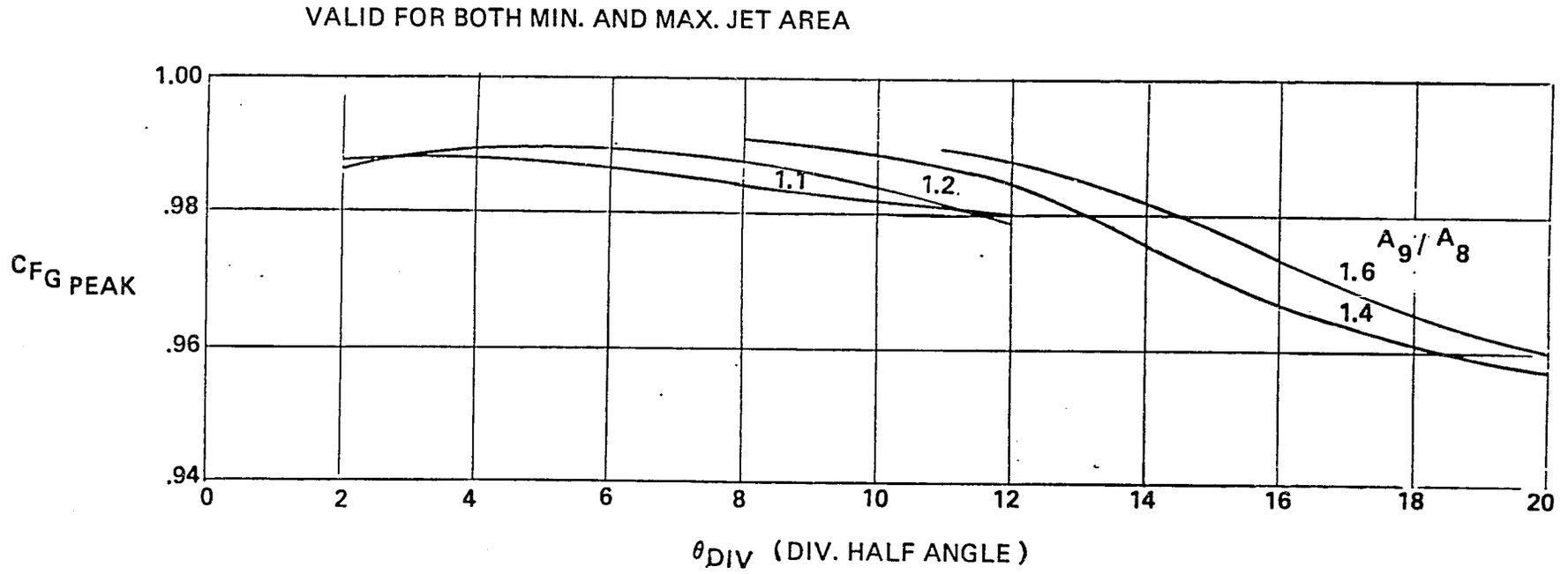

Figure 59 Effect of Divergence Angle on C_{F_G} for a 2-D/C-D Nozzle

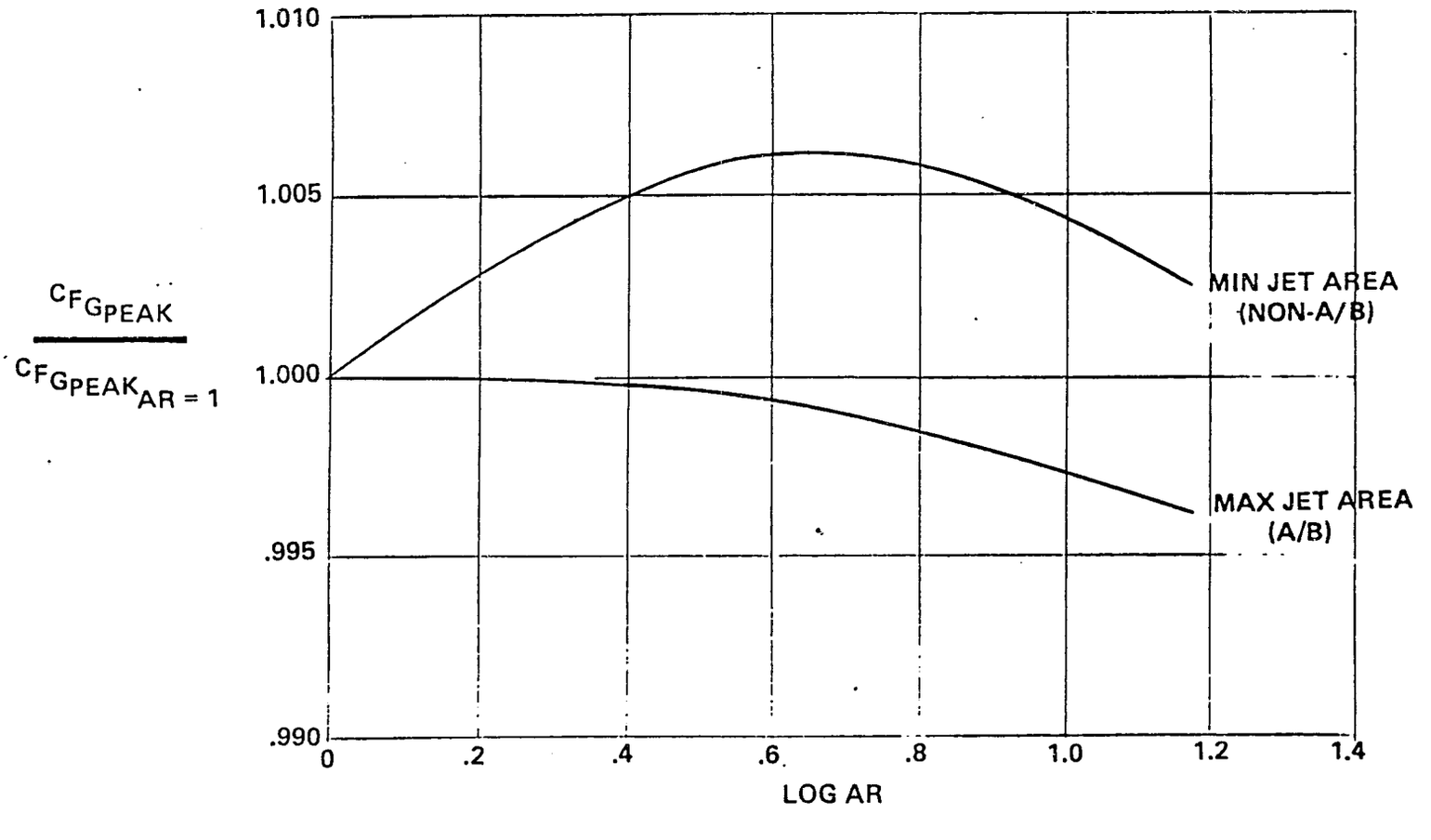

Figure 60 Effect of Aspect Ratio on 2-D/C-D Nozzle Performance

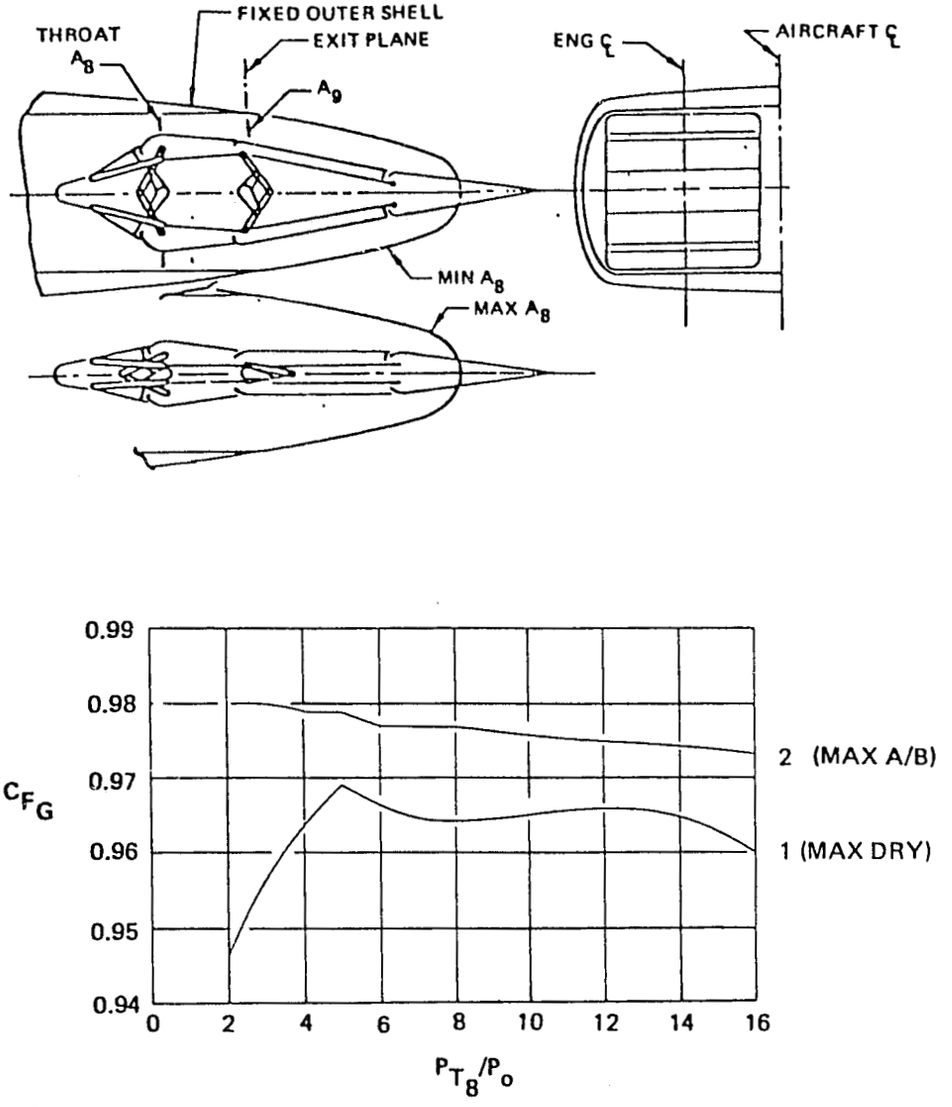

Figure 61 Gross Thrust Coefficient for a 2-D Wedge Nozzle

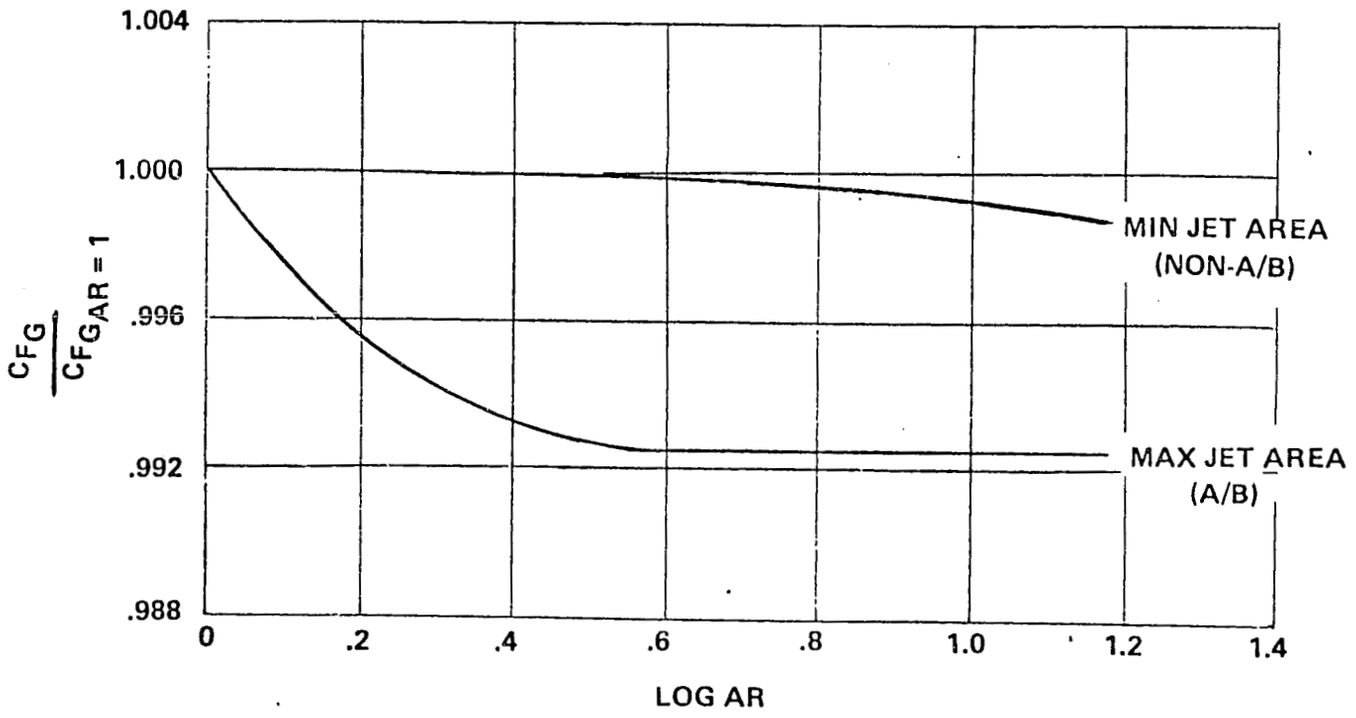

Figure 62 Effect of Aspect Ratio on 2-D Plug Nozzle Performance

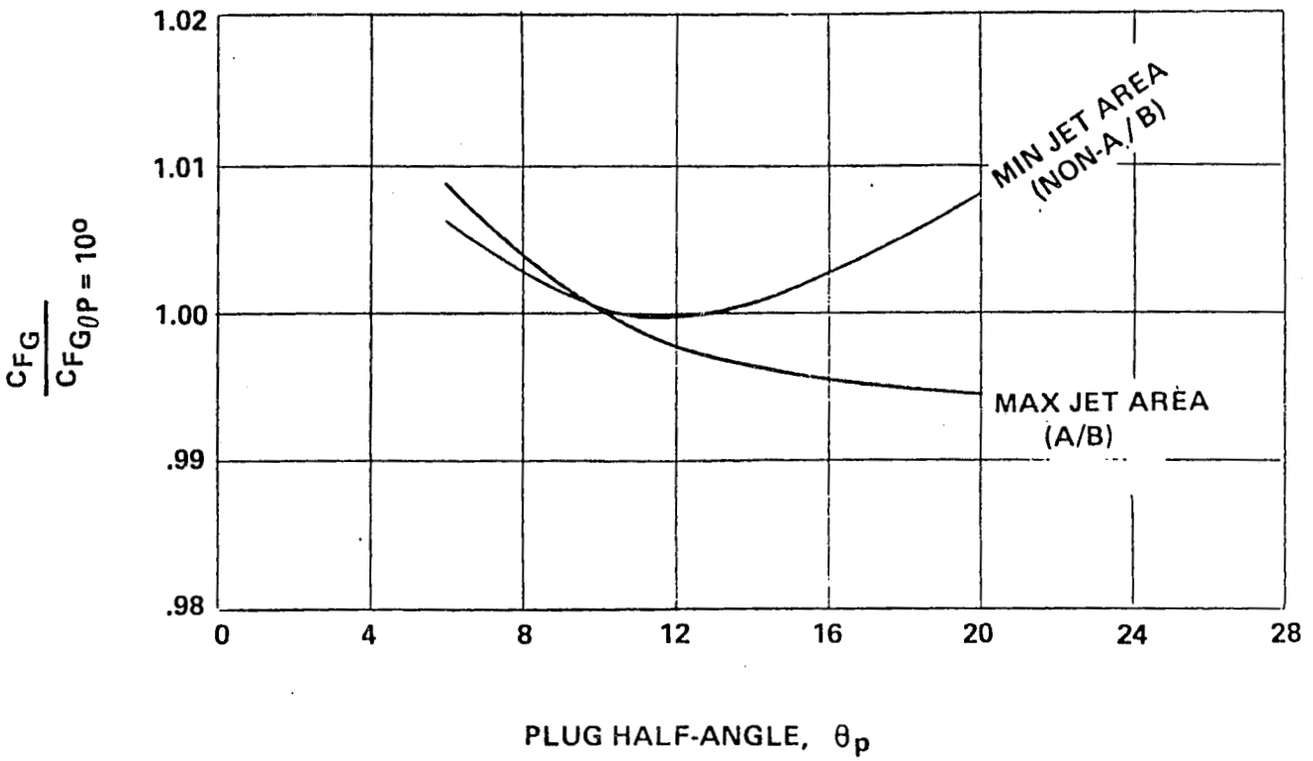

Figure 63 Effect of Plug Angle on 2-D Plug Nozzle Performance

2.3.4 NACELLE AND INLET WEIGHT

Boeing Military Airplane Development Weight Technology Staff engineers have developed weight prediction methods for nacelles and inlets (see Reference 25). These methods are currently being used in support of conceptual design, configuration development and technology assessment studies. At this stage of airplane development, only general airplane design parameters are known: mission requirements, general arrangement drawing (a three view), basic engine dimensions and location (podded-wing or body mounted, body buried, etc.), engine airflow and thrust (SLST) and engine inlet and nozzle type. These weight prediction methods are well suited for this type of study when there is limited design information available. When used by experienced weight engineers, these methods typically produce within $\pm$10% of the actual weight of inlets and/or nacelles. Figure 64 shows the correlation of estimated versus actual nacelle weight for the current data base of 42 currently operational airplanes. Figure 65 shows the estimated versus actual correlation for air induction (inlet) weight for a data base of 24 currently operational airplanes.

Nacelle weight for a podded installation is generally considered to include weight allowance for engine mounts, non-structural firewall, nacelle cowling and struts. For a body buried installation nacelle cowling and struts are not applicable. Engine mount weights are determined as a function of maximum sea level static thrust.

$$(\text{ENGINE MOUNTS})_{WT} = .003\ \text{SLST}$$

Firewall weights are based on a statistical average unit weight;

$$\text{FIREWALL}_{WT} = \pi\ \text{DIA}_{ENG}\ L_{ENG}$$

Nacelle cowl weights (see figures 66 through 68) are determined as a function of cowl dimensions. Cowling weight as estimated by this method has been modified to eliminate the correction factor for dynamic pressure. Using this revision, the method accurately predicts an axisymmetric pod weight but underpredicts the two dimensional dual pod weight.

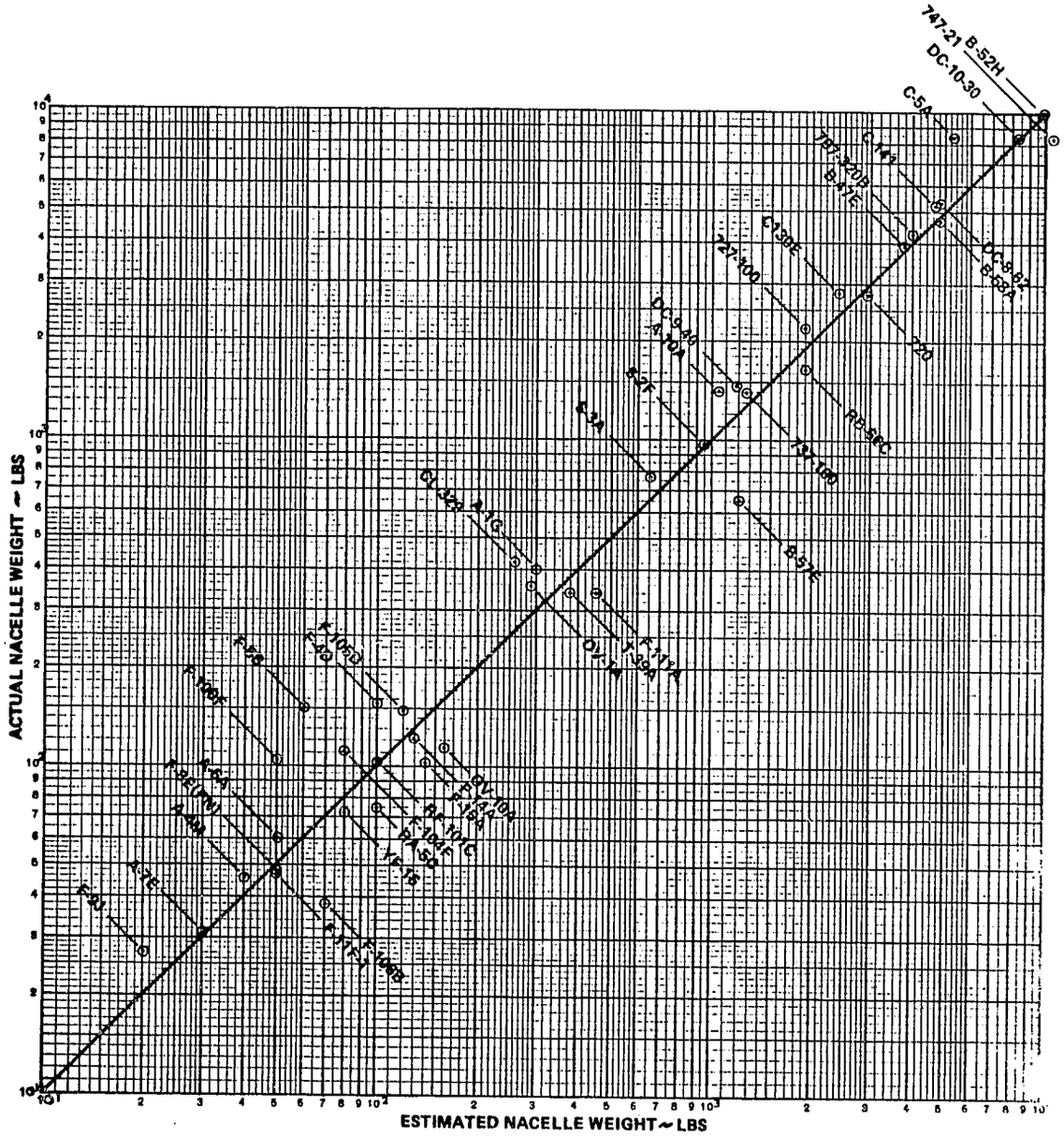

Figure 64 Nacelle Weight Correlation

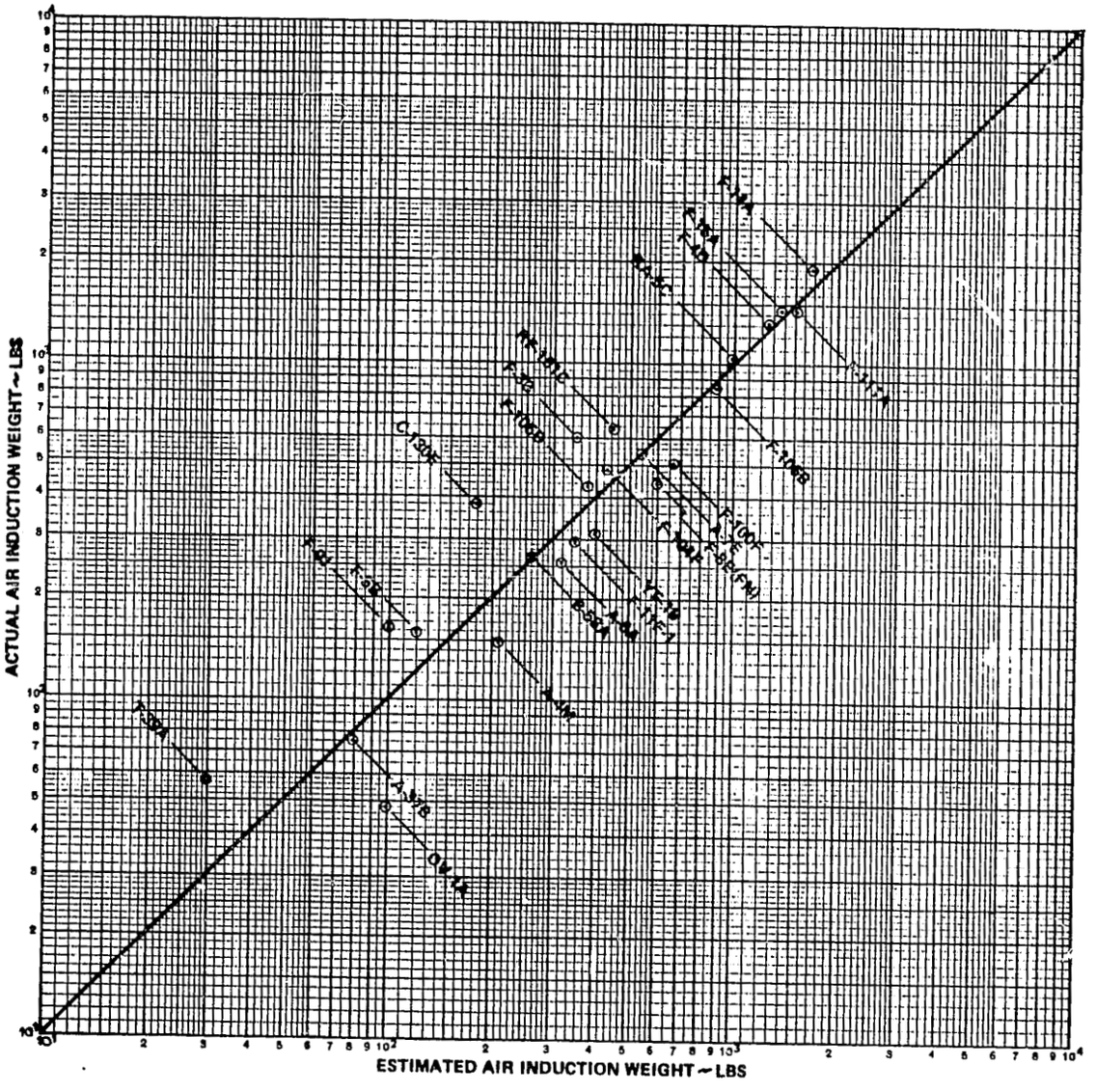

Figure 65 Air Induction Weight Correlation

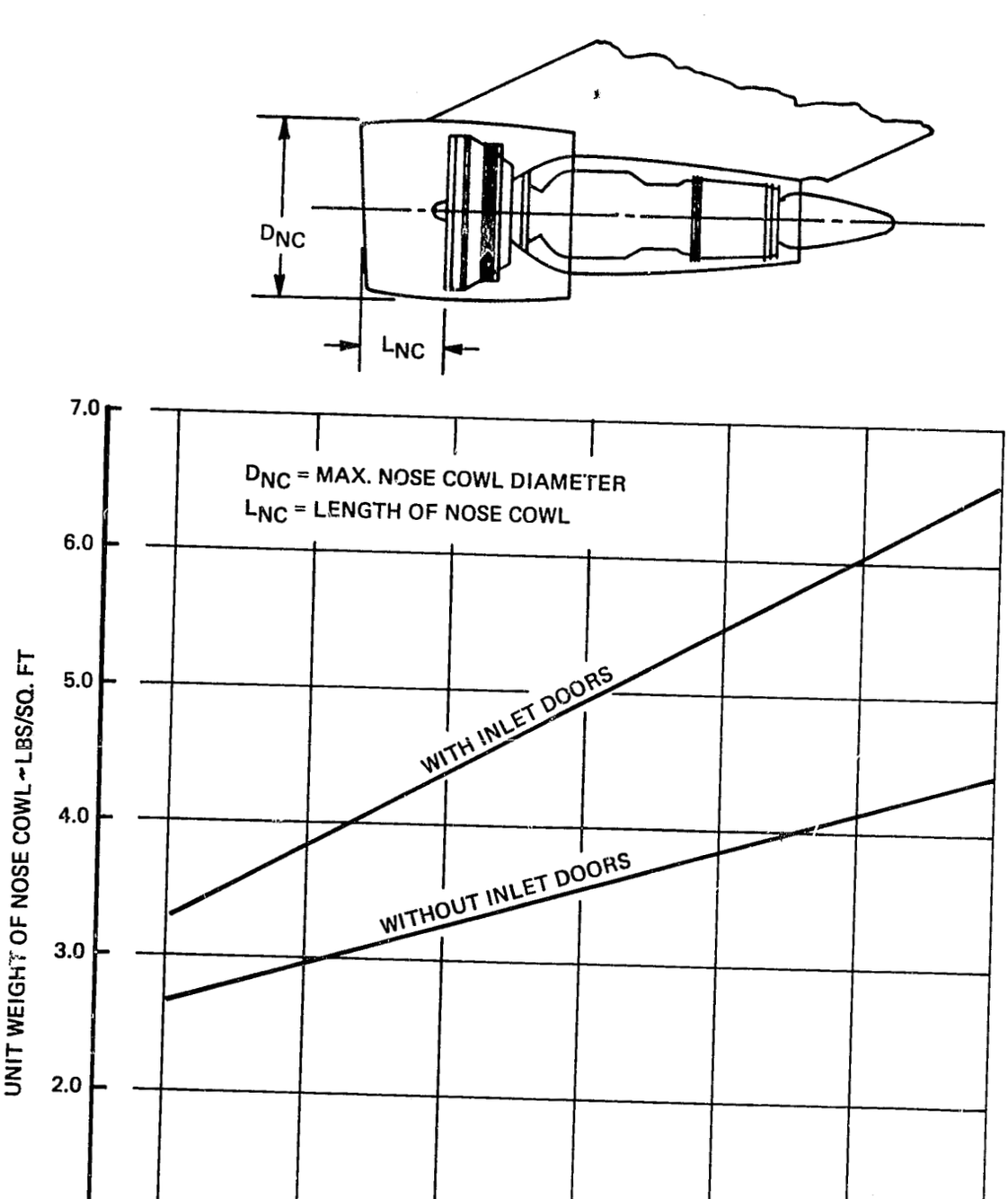

Figure 66 Nose Cowl Weights

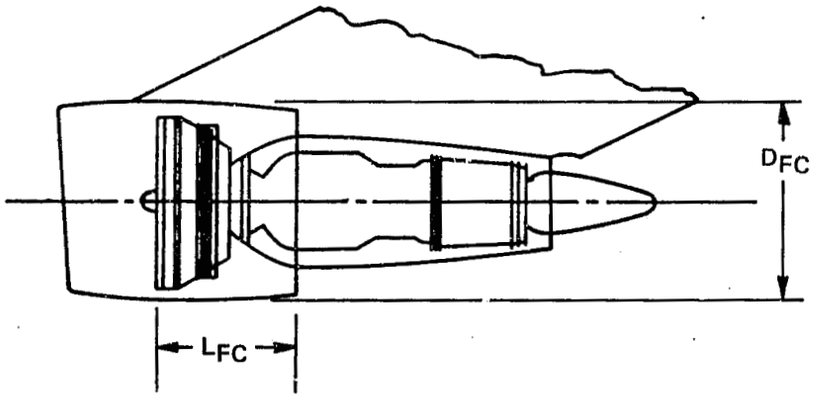

D_{FC} = MAXIMUM FAN COWL DIAMETER
L_{FC} = FAN COWL LENGTH

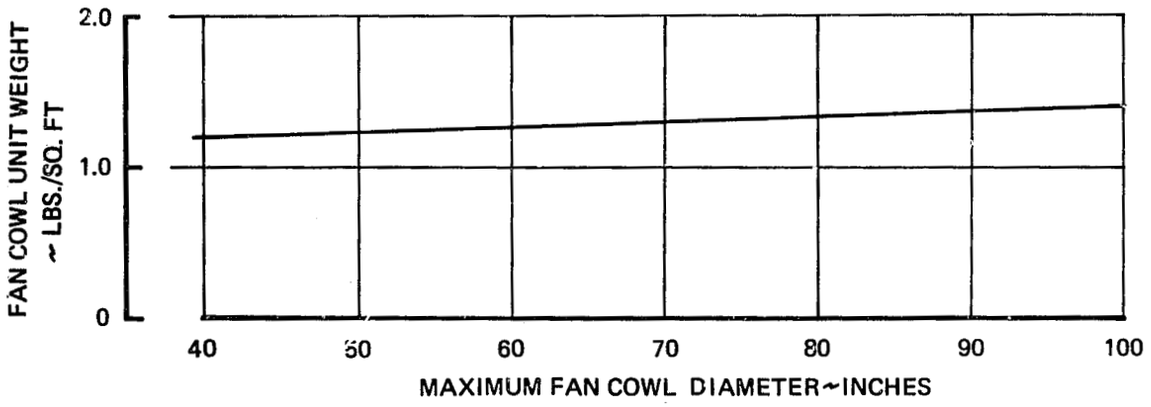

Figure 67 Fan Cowl Weight

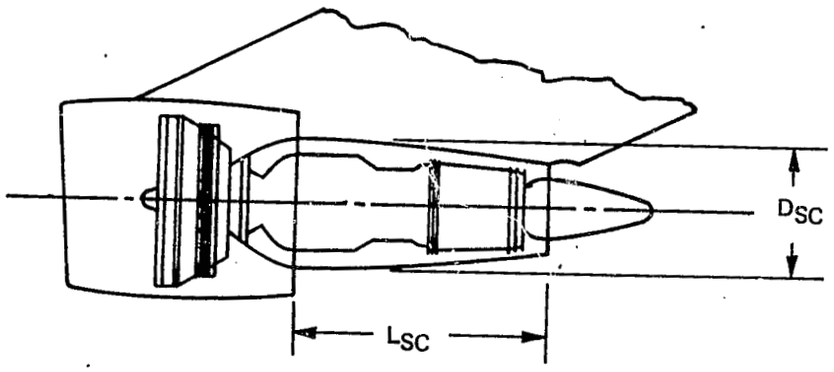

D_{SC} = MAXIMUM SIDE COWL DIAMETER
L_{SC} = SIDE COWL LENGTH

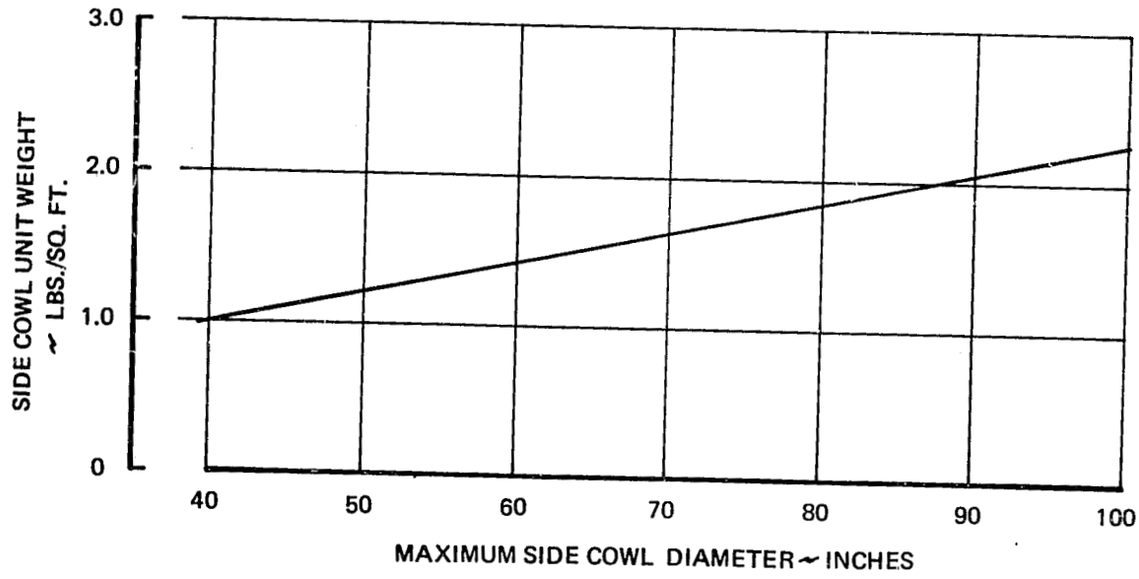

Figure 68 Side Cowl Weight

Inlet weight, by current accepted standards, includes only the internal surfaces that are wetted by the inlet flow. The nose cowl weight for podded engine installation on subsonic airplanes is normally considered to include the internal and external cowl structure, while on body submerged engine installation configurations of supersonic airplanes, the inlet weight is called air induction weights and the outer cowl is part of structural weight. Air induction weight predictions using the existing methods include allowances for inlet, movable ramps and/or plugs and intake ducting, but does not include allowances for exterior structure. Weight predictions are based on inlet type (external or mixed compression or fixed ramp/plug), fixed or variable geometry, shape (two-dimensional or axisymmetric), engine front flange diameter, airplane maximum dynamic pressure and air induction system total length. The analysis base for the inlet weight prediction methods allowed for hammer shock loading of airplanes required to operate at high dynamic pressures.

For each inlet type shown below, the calculated inlet weight includes the weight of a duct which has the assumed L/D (see Figures 69 through 76).

(1)	2-D Mixed Compression	L/D = 5.88 AR = 1.06
(2)	2-D External Compression	L/D = 3.85
(3)	2-D Fixed Ramp	L/D = 4.89
(4)	Axisymmetric Fixed Center Body	L/D = 0.88
(5)	Axisymmetric External Compression Expandable Center Body	L/D = 2.02
(6)	Axisymmetric External Compression Translating Center body	L/D = 2.56
(7)	Axisymmetric Mixed Compression Translating Spike	L/D = 2.36
(8)	Axisymmetric Mixed Compression Expandable Centerbody	L/D = 1.48

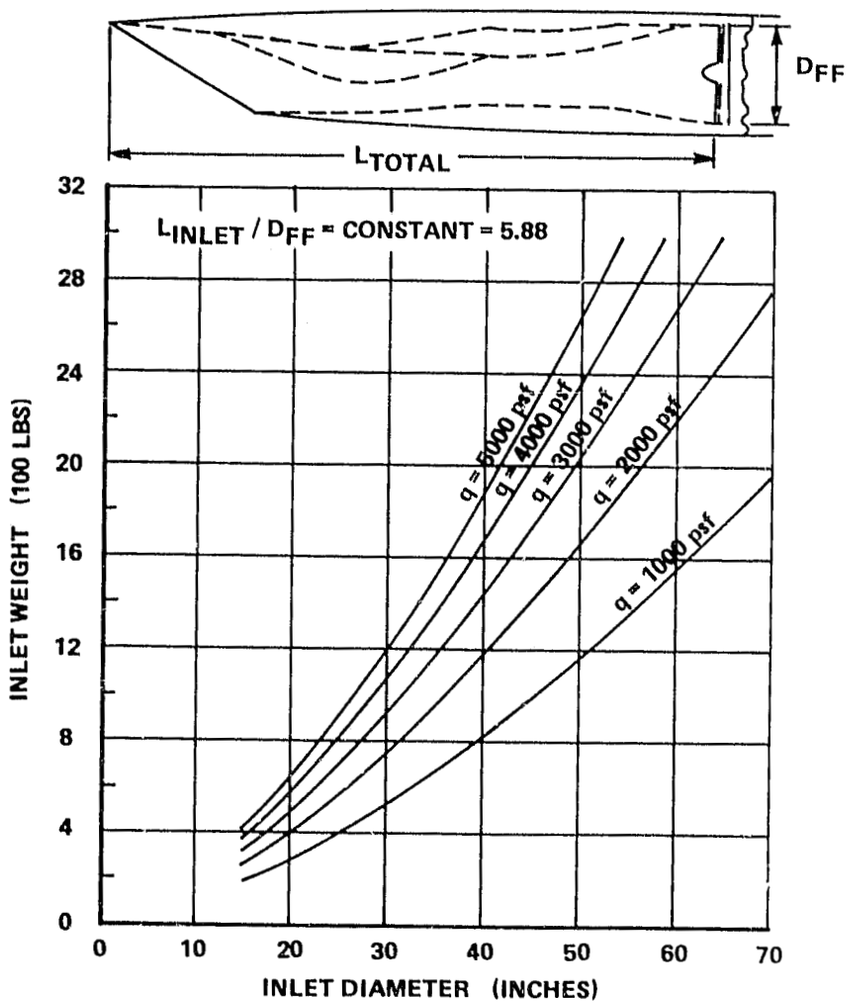

Figure 69 Two-Dimensional Mixed Compression Inlet Weight

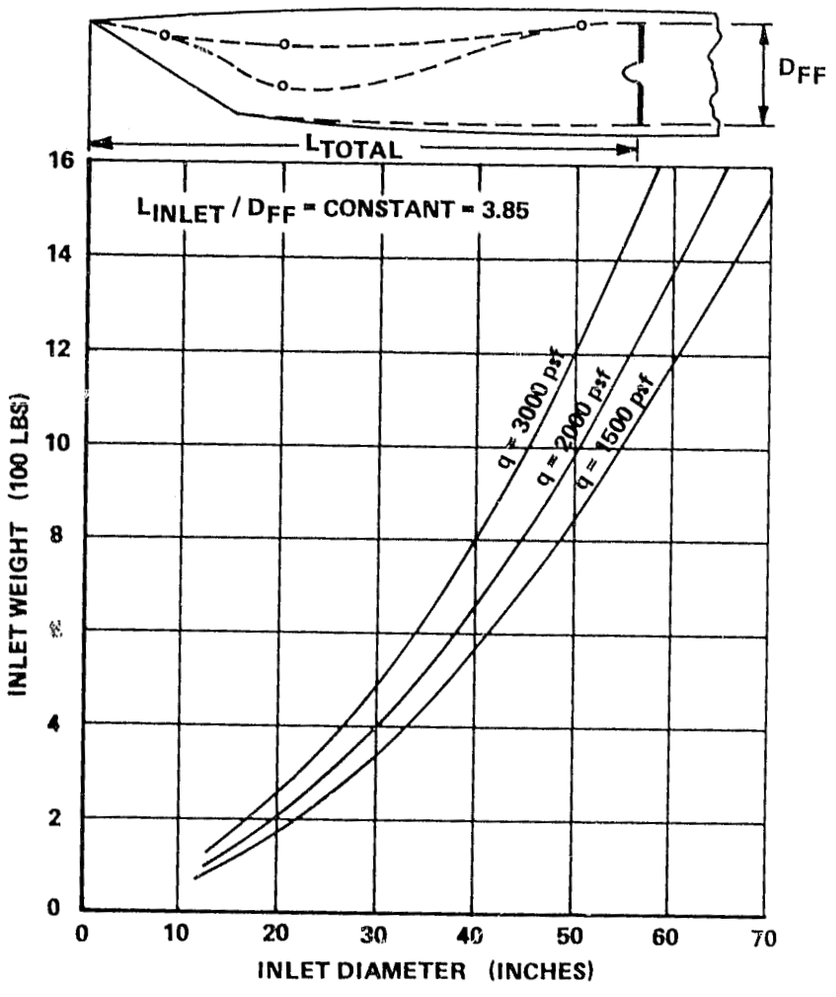

Figure 70 Two-Dimensional External Compression Inlet Weight

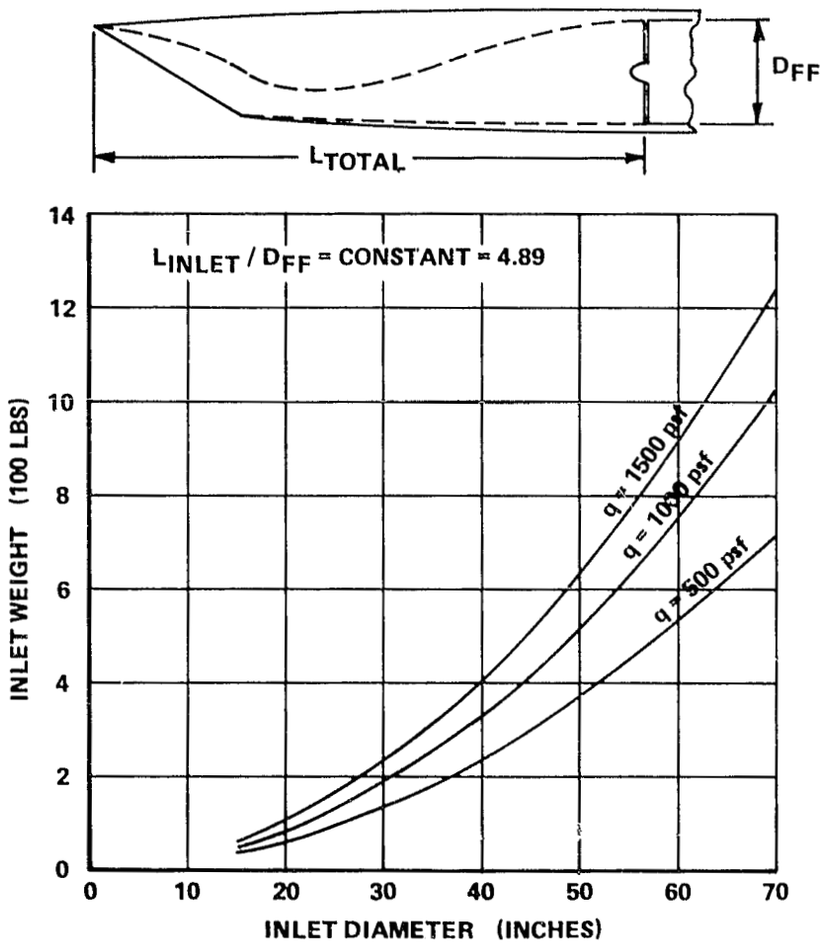

Figure 71 *Two-Dimensional Fixed Ramp Inlet Weight*

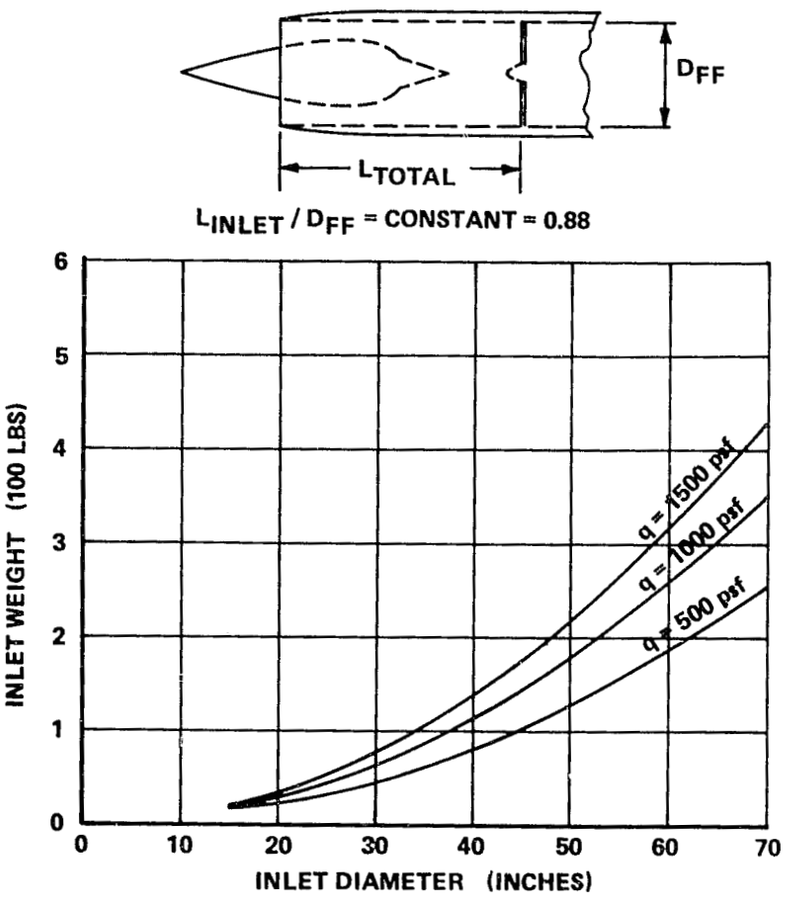

Figure 72 Axisymmetric Fixed Centerbody Inlet Weight

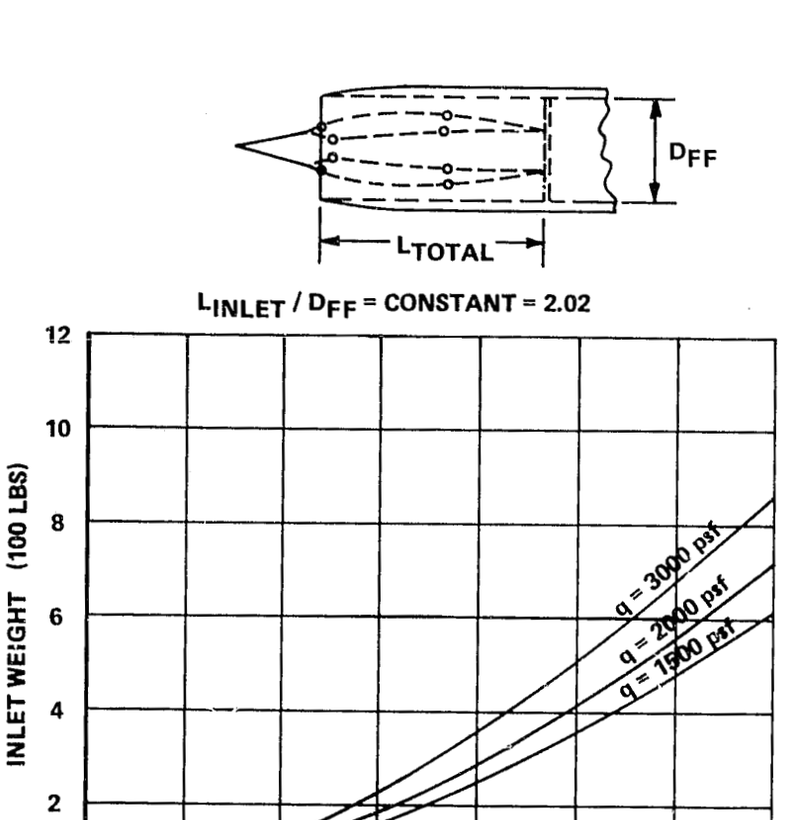

Figure 73 *Axisymmetric External Compression Expandable Centerbody Inlet Weight*

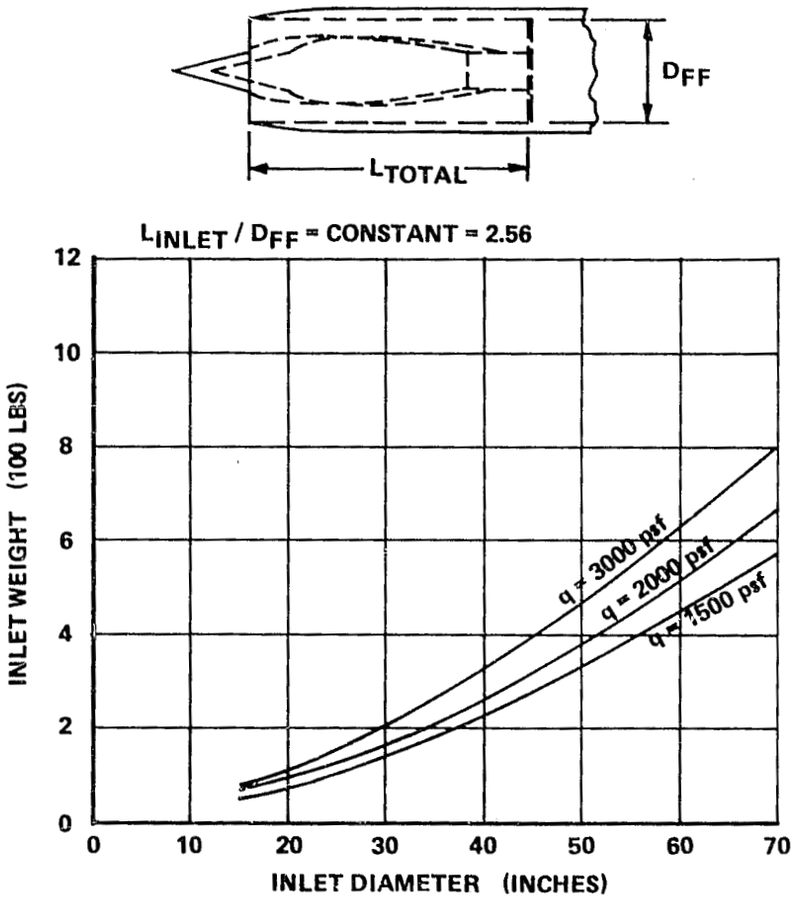

Figure 74 *Axisymmetric External Compression Translating Centerbody Inlet Weight*

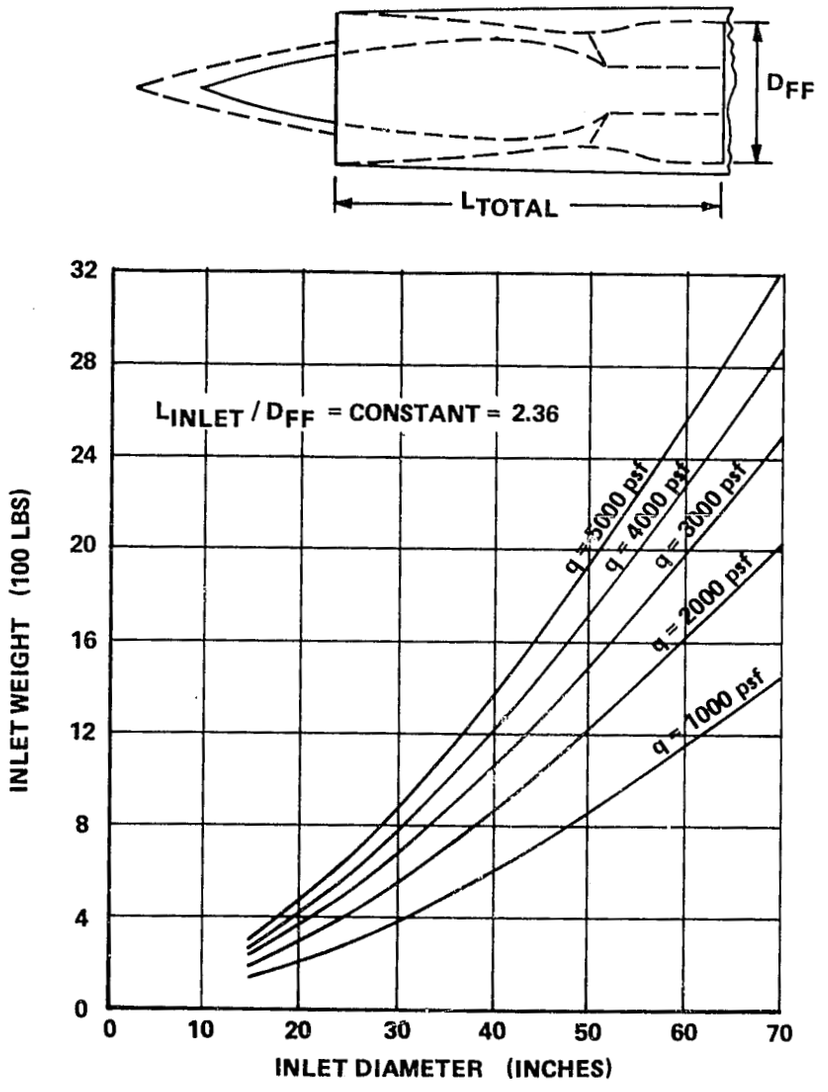

Figure 75. Axisymmetric Mixed Compression Translating Spike Inlet Weight

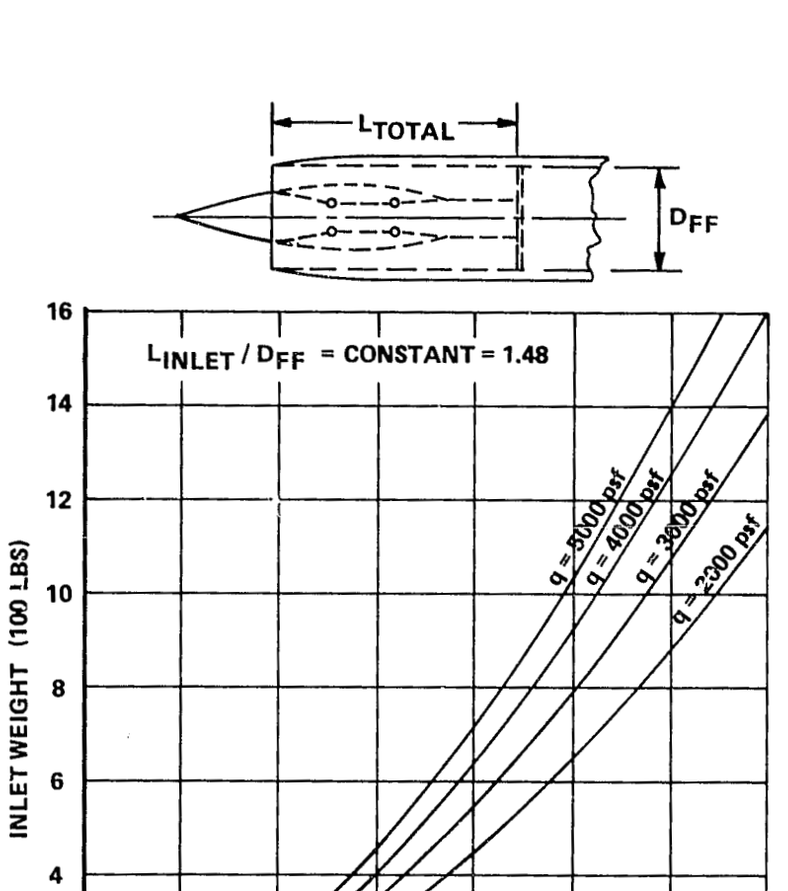

Figure 76 *Axisymmetric Mixed Compression Expandable Centerbody Inlet Weight*

Weight estimating methods for two-dimensional mixed compression inlets (inlet type 1) and axisymmetric mixed compression inlets with translating spikes (inlet type 7) were revised. The revisions to the axisymmetric inlet methodology are based on reported weight data for the Boeing designed SST singly podded engine installation. Revisions to the two dimensional inlet methods are based on the weight reported by North American for their design of a dual podded engine installation for the Boeing SST (see Figures 69 and 75 respectively).

Both the axisymmetric and the 2-D inlet weight methods were modified on the basis of paper study inlets. Reasonable results were achieved when used to predict the two development inlets. The methods have not been verified by using them to estimate flying in service hardware due to the unavailability of data; therefore, confidence in the revised methodology is not as high as might be desired.

The revised weight estimating method for axisymmetric mixed compression inlets now includes allowances for throat and bypass doors (see Figures 77 and 78). Similarly, the revised weight estimating method for 2-D mixed compression inlets now includes allowances for bypass doors (see Figure 79). These increments were developed using the reported weights as a basis for adjusting the basic inlet weight, the incremental weight of throat and bypass doors, respectively, as a function of inlet diameter and dynamic pressure.

The weight of each inlet type (1 through 8) includes duct weight corresponding to the designated L/D. During the installation, if the calculated L/D differs, the duct weight will be adjusted (see Figure 80).

2.3.5 NACELLE DRAG

The following is a list of the nacelle drags calculated for a podded installation:

- o Skin friction (subsonic & supersonic)
- o Form drag (subsonic)
- o Wave drag (supersonic)

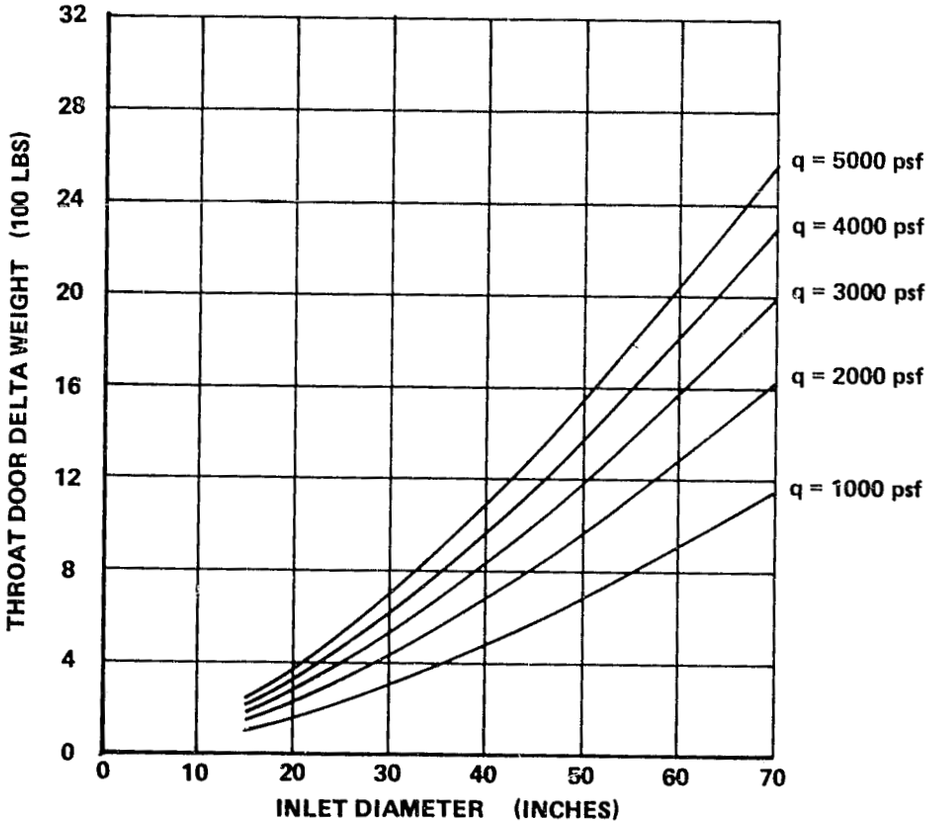

Figure 77 *Delta Weight for Throat Doors, Axisymmetric Mixed Compression Inlets*

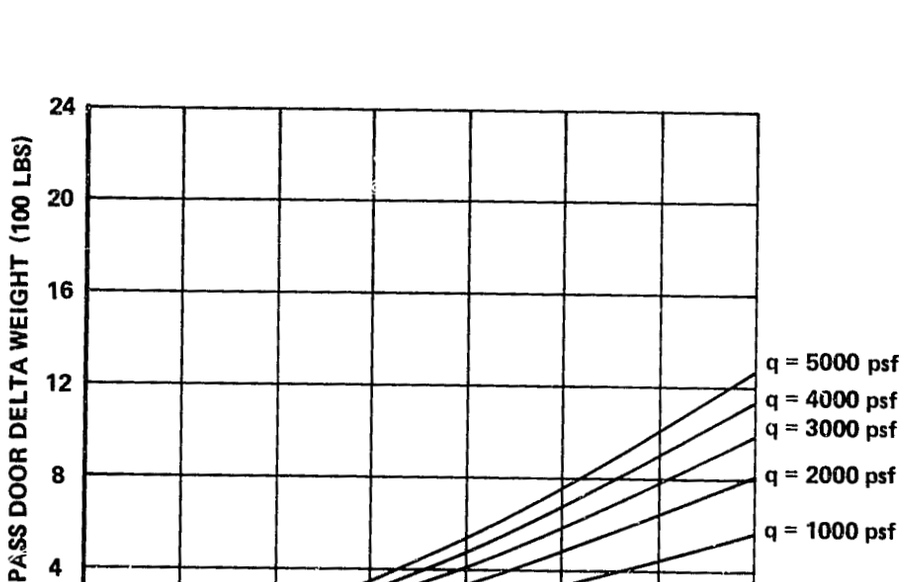

Figure 78 *Delta Weight for Bypass Doors, Axisymmetric Mixed Compression Inlets*

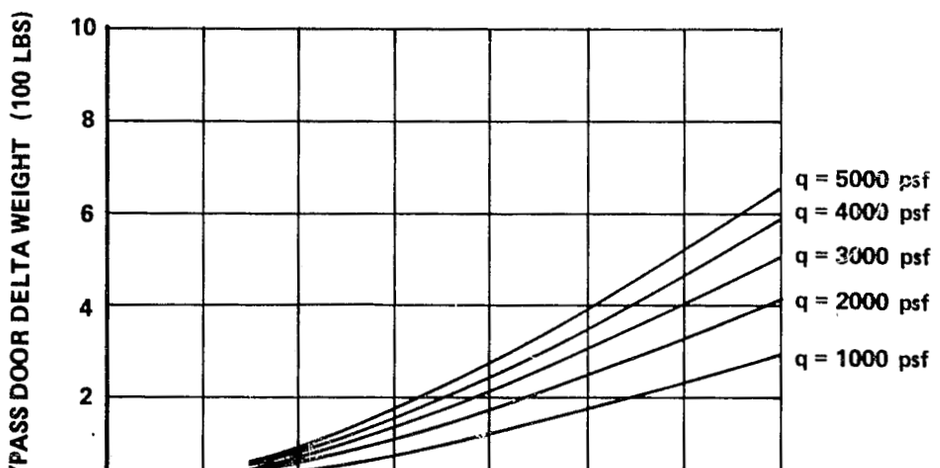

Figure 79 *Delta Weight for Bypass Doors, 2-D Mixed Compression Inlets*

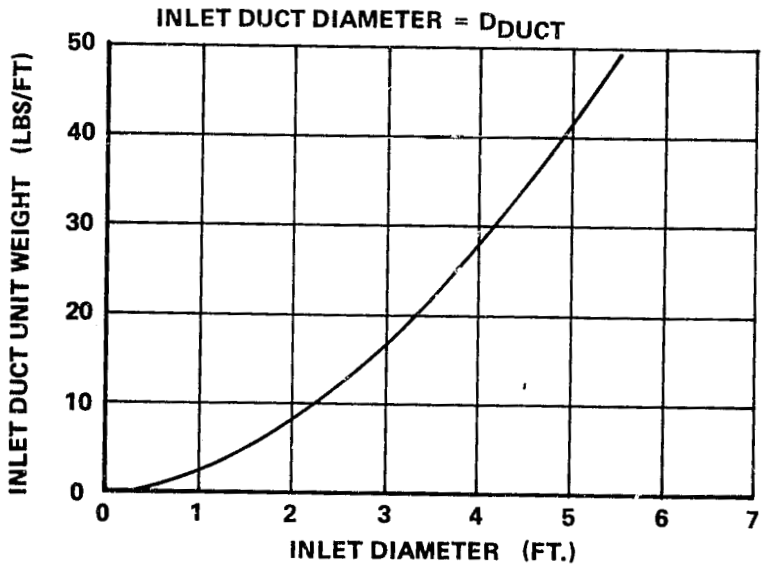

Figure 80 Inlet Duct Unit Weight

Skin Friction Drag

Friction drag is the integral of the shearing stresses taken over the exposed surface (wetted area) of the vehicle. In practice the friction drag is dependent on the amount of exposed surface, the average skin friction coefficient and the surface roughness. The major portion of subsonic minimum parasite drag can be attributed to skin friction.

The average skin friction coefficient and friction drag coefficient used in his document are derived by standard techniques. The calculations and curves presented assume the following:

1. Turbulent flow
2. Smooth flat plate
3. Zero heat transfer
4. Free stream static temperature $400^{o}R$
5. Ratio of specific heats and recovery factor are allowed to vary with the reference temperature corresponding to the mean enthalpy across the boundary layer.

The assumption of turbulent flow requires the majority of the boundary layer to be turbulent. For most configurations this condition is satisfied, however, at low Reynolds numbers ($<10^{6}$) it is possible to have considerable areas with laminar flow so a correction factor has been included. Since the effects of heat transfer are sufficietly complex they will be neglected in the scope of preliminary design. Flight conditions of present day configuration studies do not warrant extensive heat transfer investigation. The selection of a free stream static temperature of $400^{o}R$ was based on a compromise which introduces negligible error over expected operating conditions of present day configurations.

The following method describes the method for determining the friction drag coefficient.

(1) Calculate the wetted area and length of the nacelle that is exposed to free stream air.

(2) Using Figure 81, determine the Reynolds number per foot per Mach number as a function of the flight conditions altitude.

(3) Calculate the effective Reynolds number by multiplying the Reynolds number of part (2) by Mach number and nacelle length.

(4) Determine the admissible roughness /k where is the nacelle length of part (1) and k is the surface roughness height in inches. Representative values of k (based on measurements of a wide variety of aircraft) are shown in Table VIII.

(5) Calculate the cutoff Reynolds number associated with surface roughness from Figure 82 as a function free stream Mach number and admissible roughness, /k.

(6) Obtain the average skin friction coefficient for the nacelle from Figure 83 using the free stream Mach numer and the lesser of the Reynolds numbers calculated in parts (2) and (5). The cutoff Reynolds number will ordinarily be a factor only at combined low altitude and high speed flight conditions.

$$DRAG_{\substack{SKIN \\ FRIC}} = C_{D_{\substack{SKIN \\ FRIC}}} q A_{WET}$$

A_W = Nacelle wetted area
q = dynamic pressure

Form Drag (MN<1)

The component of parasite drag often referred to as form drag or "profile" drag results from the aircraft overall shape or profile which is submitted to the free stream. The form drag presented in this section is designed to be applied at subsonic speeds only.

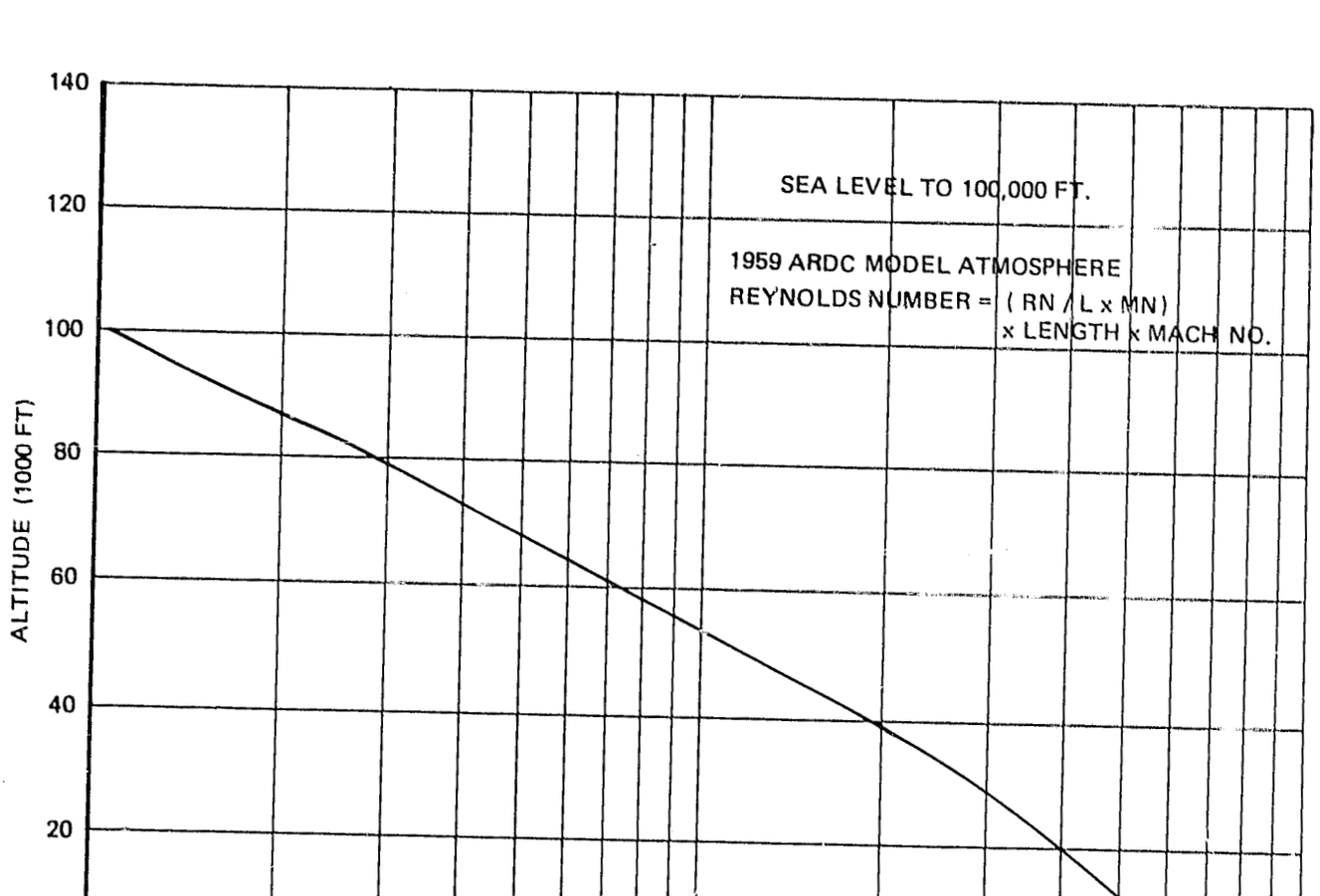

Figure 81 *Reynolds Number / Foot / Mach Number (Sea Level to 100.000 FT.)*

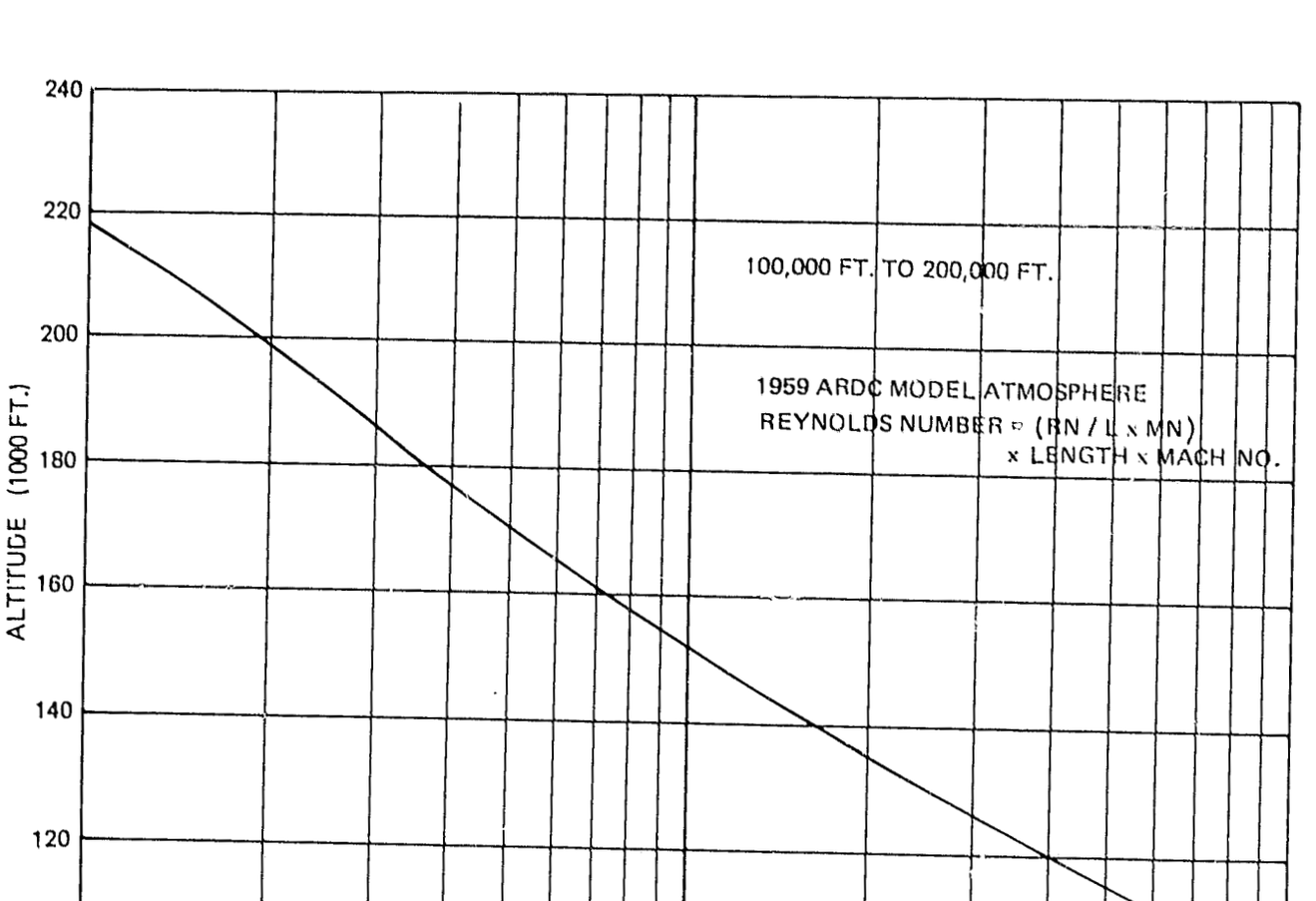

Figure 81 *Reynolds Number / Foot / Mach Number (100 000 to 200 000 FT.)*

TABLE VIII REPRESENTATIVE VALUES OF SURFACE ROUGHNESS HEIGHT

TYPE OF SURFACE	k – IN.
NATURAL SHEET METAL	0.16×10^{-3}
SMOOTH PAINT	0.105×10^{-3}
STANDARD CAMOUFLAGE PAINT	0.25×10^{-3}
CAMOUFLAGE PAINT, ROUGHLY APPLIED	0.40×10^{-3}

*BASED ON WEO MEASUREMENTS

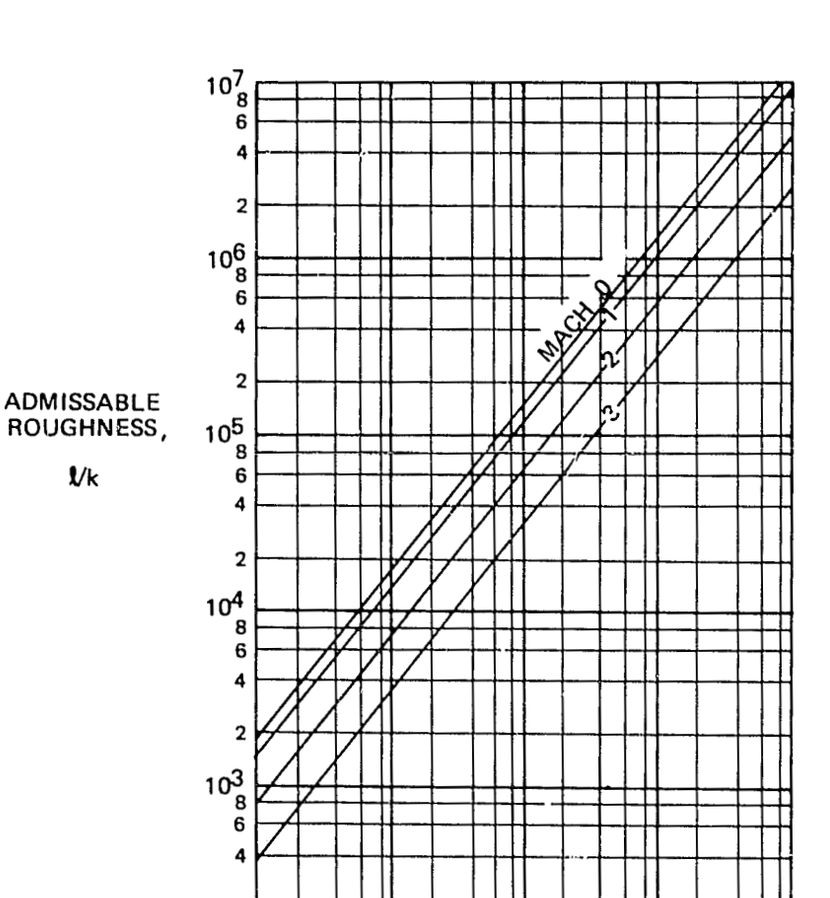

Figure 82 Cutoff Reynolds Number

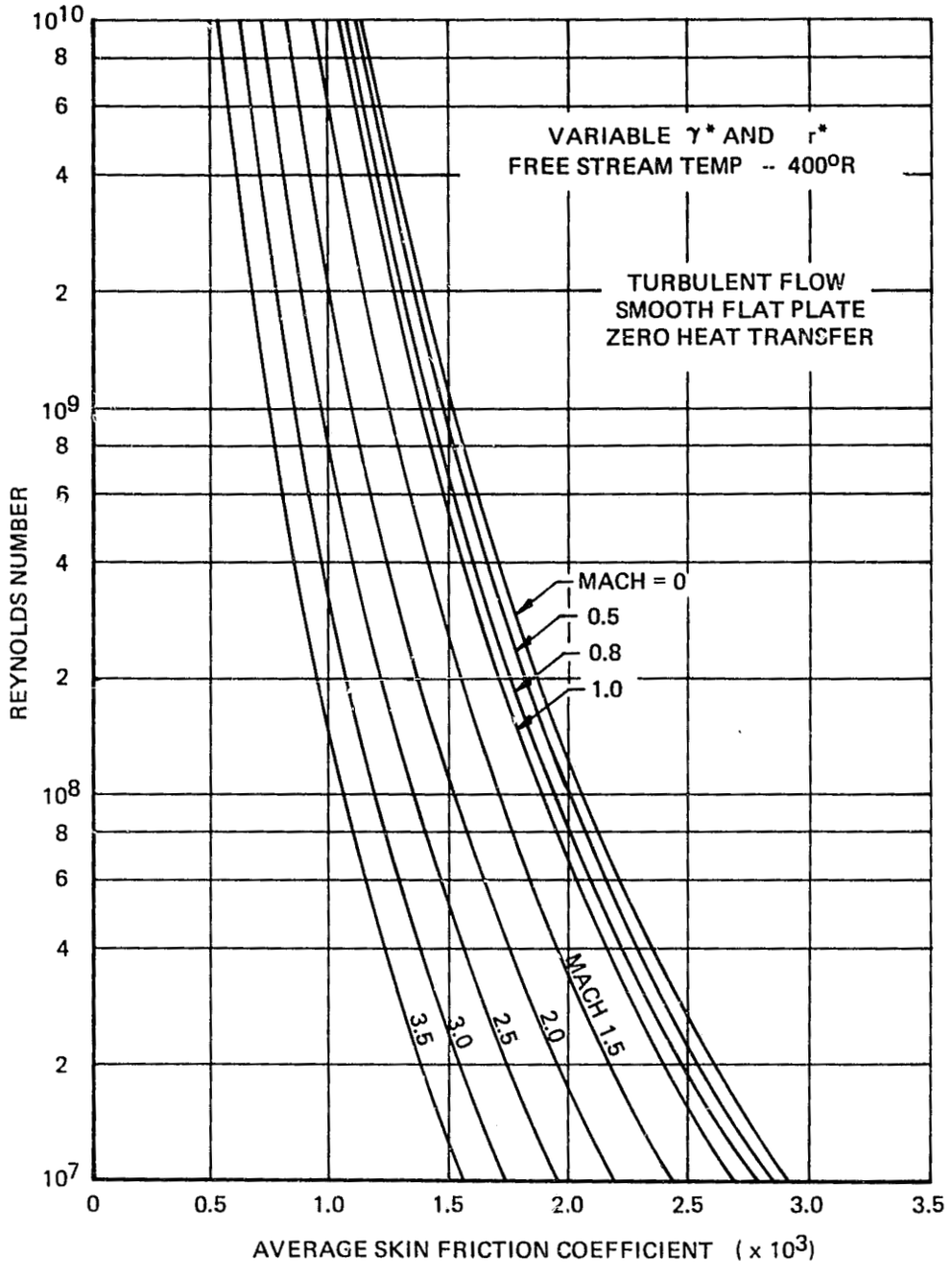

Figure 83 Average Skin Friction Coefficients

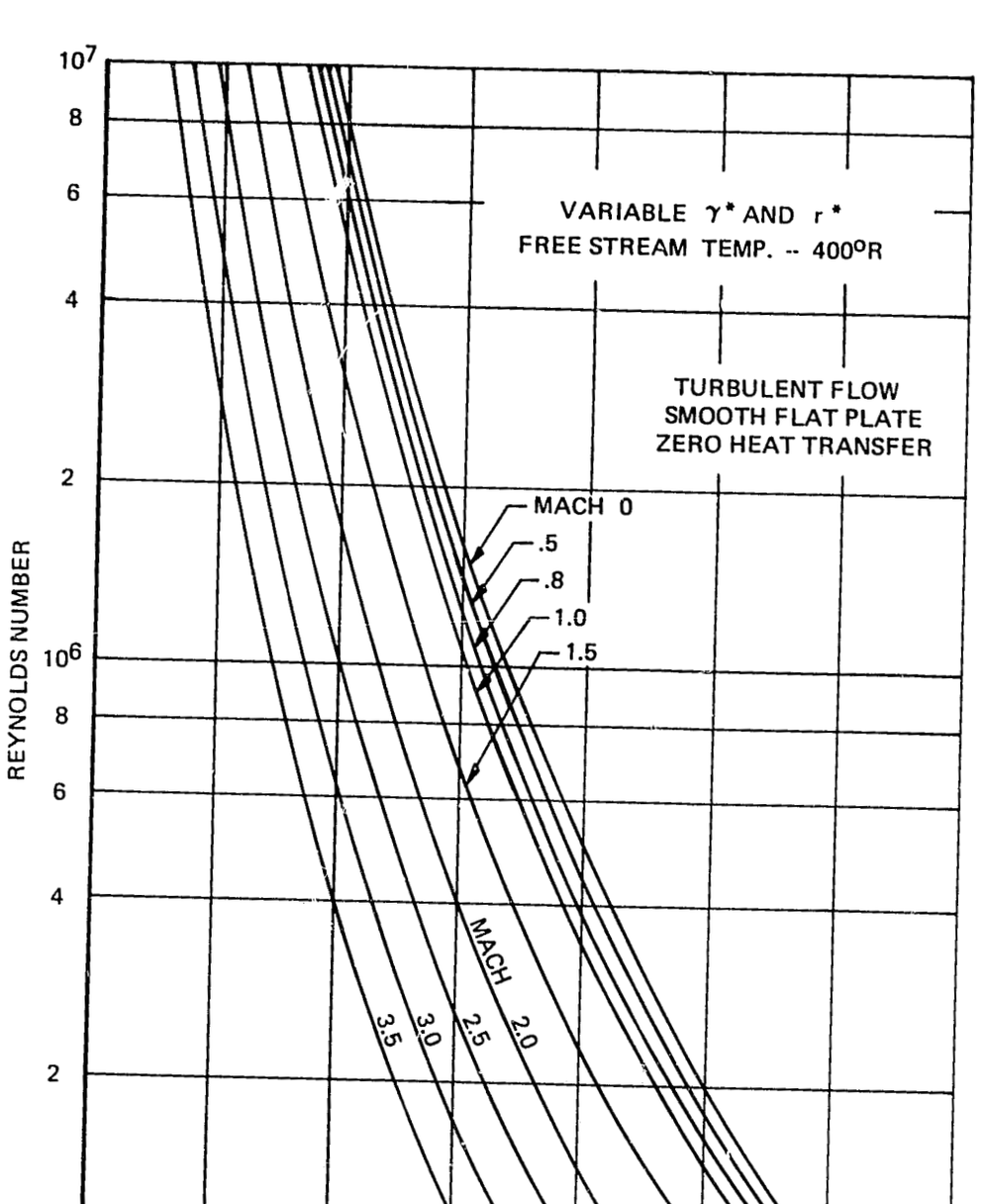

Figure 83 Average Skin Friction Coefficients

Nacelle form drag is influenced by a variety of factors such as inlet mass flow ratio, nacelle curvature and nozzle boattail angle. However, since the reference drag nacelle condition is a large mass flow ratio and an open nozzle (small boattail angle), a rather simple coefficient of form drag equation will be used for the nacelle.

$$C_{D_{FORM}} = K_N C_{D_f}$$

where

$K_N = 0.5/(l/d)$

l = nacelle length

Δd = the difference between the maximum nacelle diameter and the average of the inlet diameter and the nozzle exit diameter

C_{D_f} = nacelle flat plate skin friction drag coefficient

Nacelle form drag will thus be defined by:

$$DRAG_{FORM} = C_{D_{FORM}} A_W q$$

where

A_W = Nacelle wetted area

q = dynamic pressure

Wave Drag (MN>1)

Wave drag is the zero lift pressure drag resulting from the formation of shock systems associated wth the supersonic flow of compressible fluid around an object of finite thickness.

To determine the nacelle wave drag, data from wind tunnel and free flight sources have been represented in Figure 84. The coefficient C_D has been plotted versus an equivalent ratio d/l. Figure 85 is a nacelle schematic used to determine d/l, where:

C_{D_π} = $0.7(d/l)^{5/3}_{Equiv}$

d_x = diameter at station x

l_x = length at station x

A_x = area at station x

$$(d/l)_{Equiv} = \frac{\left(\frac{d_2 - d_1}{l_2}\right)(A_2-A_1) + \left(\frac{d_3-d_2}{l_3-l_2}\right)(A_3-A_2) + ...}{A_{MAX}}$$

A_{MAX} = maximum nacelle area

2.3.6 NACELLE WETTED AREA

To determine nacelle drag and weight, the wetted area of the nacelle is required. A user input under the &WET namelist is required to describe the flow paths for any components that are visible. Figure 86 gives an example of a short duct turbofan. The inputs for this example would be:

ITERFP(1) = 1,2,3,4,5,0

ISECFP(1) = 1,2,3,6,7,8,9,10,11,12,0

The last component number of each flowpath must be zero to inform the computer of a flow path's termination. The ITERFP array must be comprised of the engines outermost flow path.

The capability of adding "X" inches to the radii of each component exists to determine the outside dimension of the nacelle, thus allowing for flange heights, plumbing, ducting, etc. Using the component flowpath designations and the WATE-2 arrays of component lengths and outer radii (with "X" inches added), the nacelle wetted area is determined. The nacelle is considered to be axisymmetric and each component is considered to be a frustrum of a right circular cone (see Figure 87). Splitters are ignored because of their zero length.

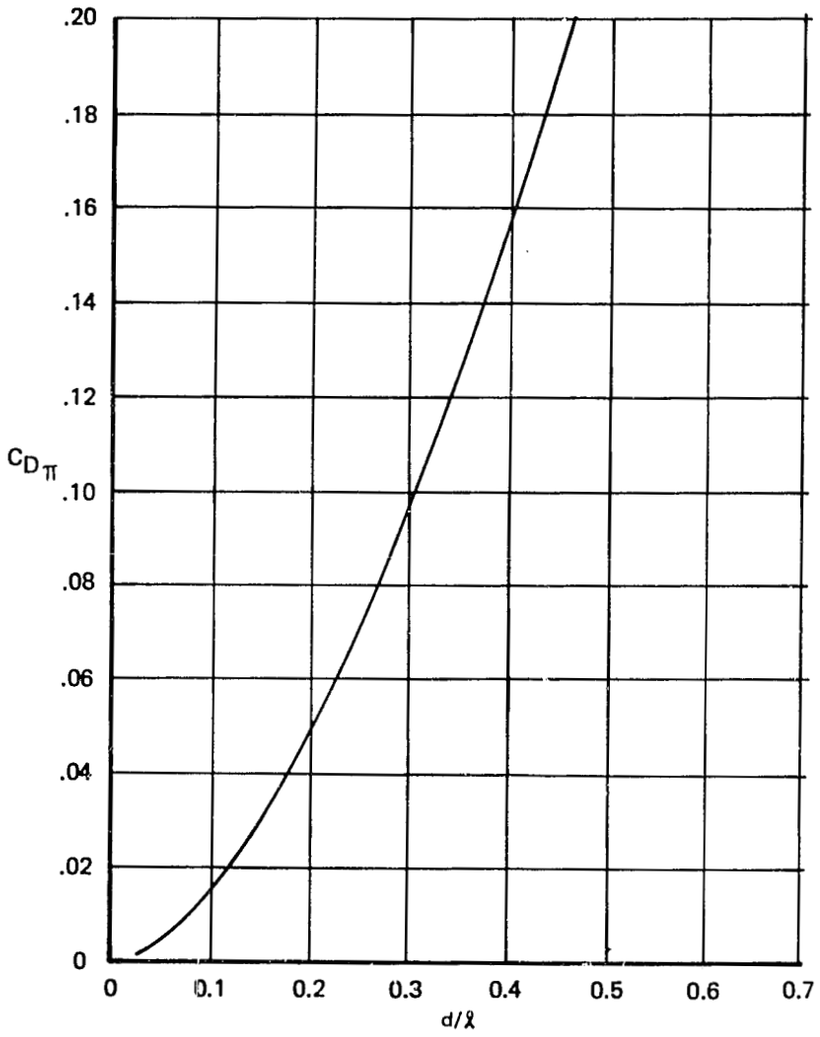

Figure 84 Maximum Body Wave Drag

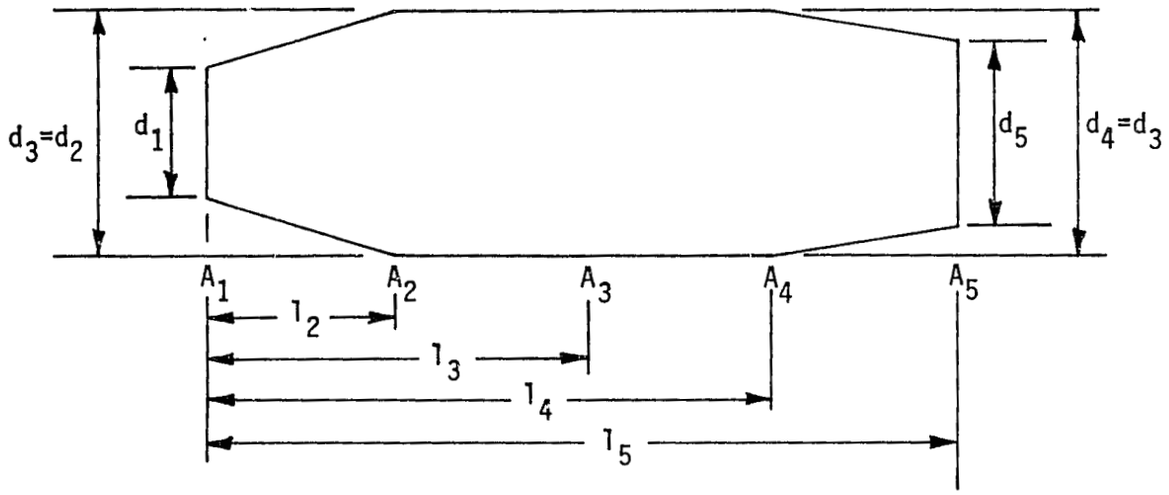

$$DRAG_{WAVE} = C_{D_\pi}{}^* \; A_{MAX} \; ^* \; q$$

q = Dynamic pressure

Figure *85* Nacelle Schematic for Determination of Wave Drag

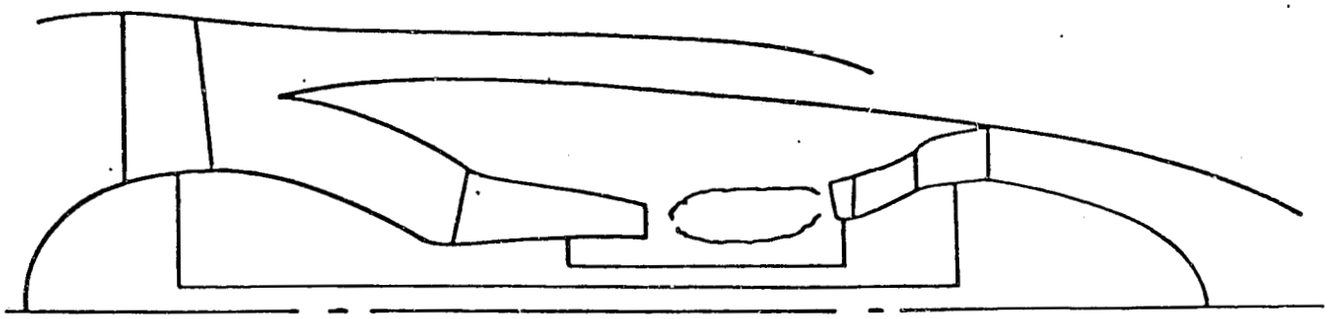

ENGINE LAYOUT

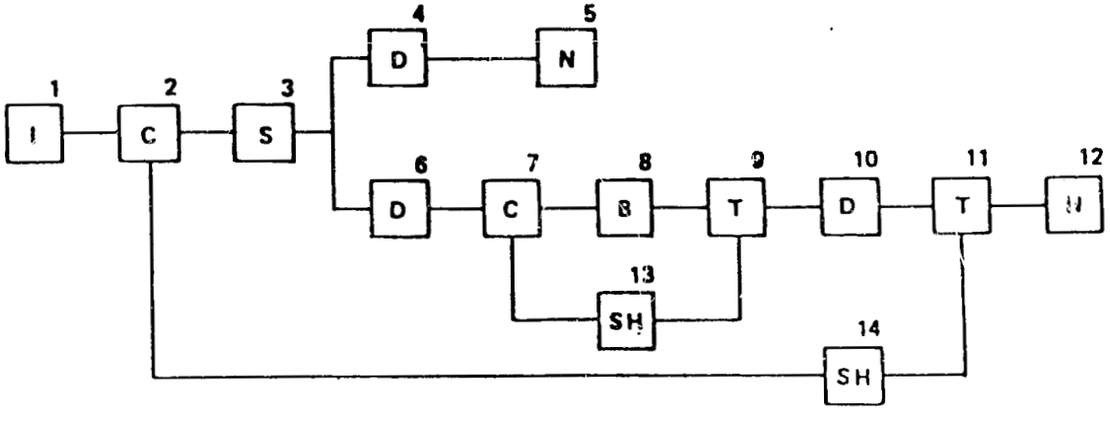

ITERFP (1) = 1, 2, 3, 4, 5, 0

ISECFP (1) = 1, 2, 3, 6, 7, 8, 9, 10, 11, 12, 0

Figure 86 *Typical Inputs for A Nacelle Wetted Area Calculation*

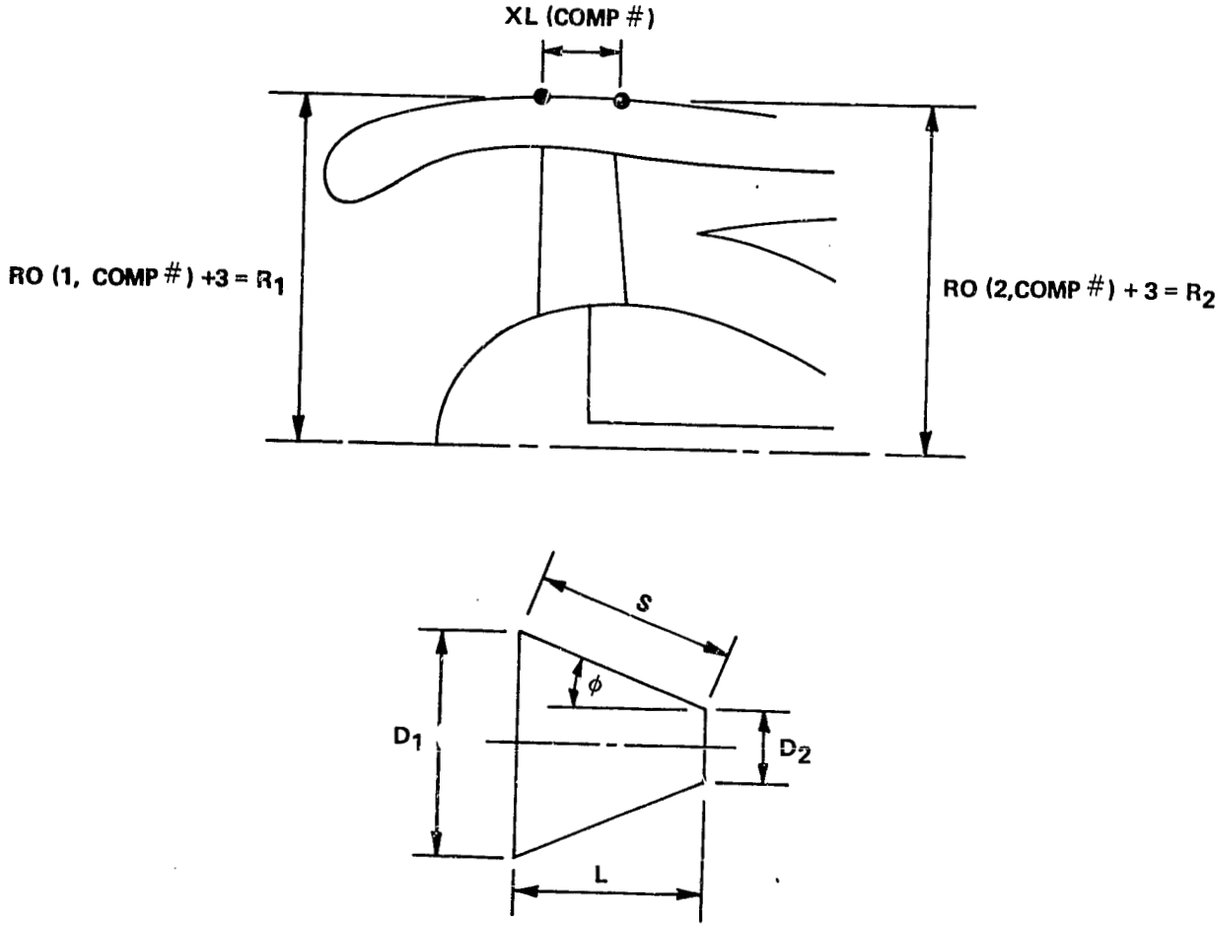

$$\text{SURFACE AREA} = \pi S (D_1 + D_2) / 2$$

$$D_1 = 2R_1$$

$$D_2 = 2R_2$$

$$L = XL$$

$$\tan \phi = (D_1 - D_2) / 2 / L = A$$

$$\phi = \arctan A$$

$$\cos \phi = L / S$$

$$S = L / \cos \phi$$

$$\text{SURFACE AREA} = \pi \; L / \cos \phi \quad (D_1 + D_2) / 2$$

Figure 87 Wetted Area Calculation

Using the inputed length of the inlet, its capture area and the radius of the engine front face (its component number is a &I input), the wetted area of the inlet is determined.

The total fan cowl wetted area is comprised of the inlet wetted area and that of the outermost flow path (ITERFP for our example). A_{MAX} and $(d/l)_{equiv}$ are also calculated in this routine to be used with the fan cowl wetted area and fan cowl length in the nacelle drag routine.

The total engine cowl wetted area is comprised of the fan cowl wetted area plus that of the innermost flowpath. The engine wetted area and engine length are used in the nacelle weight routine.

3.0 APPENDIX

CHECK OF SOME DERIVATIVE PROCEDURE METHODS

This appendix will show results for a limited number of inlets, using the inlet derivative procedure methods for bleed rates, and inlet design point recovery with varied inlet design Mach number. The attempt will be made to transform from one known inlet to the parameters of another known inlet.

Two groups of inlets are considered. The first consists of three mixed compression, two-dimensional inlets, defined in the following table. All values are given for the design Mach number.

Design Mach No.	2.50	2.60	3.0
Recovery	0.905	0.916	0.885
Bleed Rate	0.07	0.07	0.105
Initial Ramp Angle	7.0°	5.0°	7.0°
Aspect Ratio	1.0	0.91	1.0
Side Plate Cutback	0.0	0.0	0.0
Ramp Surface Mach No.	2.179	2.381	2.65
Reference	1	26	7

Since there is very little difference in aspect ratio, its effect will be neglected in the following. Bleed rate calculations will be made for these inlets, then recovery calculations will be considered.

Two bleed predictions methods will be used. The first will use the equation

$$\left(\frac{A_{o_{BLC}}}{A_c}\right)_{new} = \left(\frac{A_{o\ BLC}}{A_c}\right)_{old} \cdot \left[\frac{\left(\frac{P}{P_T}\right)_{M_S} \cdot (M_S)_{old}}{\left(\frac{P}{P_T}\right)_{M_S} (M_S)_{new}}\right] \cdot \left[\frac{(Re)_{M_{o\ design\ new}}}{(Re)_{M_{o\ design\ old}}}\right]^{1/7}$$

C-3

The second will use this same equation for the low pressure bleed, where

$$\left(\frac{A_{o_{BLC}}}{A_c}\right)_{LP} = \left(\frac{A_{o_{BLC}}}{A_c}\right)_{old} \cdot \frac{1}{1.67} \cdot \left(\frac{A_{o_{BLC}}}{A_o}\right)_{HP} = \left(\frac{A_{o_{BLC}}}{A_c}\right) - \left(\frac{A_{o_{BLC}}}{A_c}\right)_{LP}$$

and it will use

$$\left(\frac{A_{o_{BLC}}}{A_c}\right)_{new} = \left(\frac{A_{o_{BLC}}}{A_o}\right)_{old} \cdot \left[\frac{(A/A^*)_{M_{surface\ old}} \cdot (M_{surface})_{old}}{(A/A^*)_{M_{surface\ new}} \cdot (M_{surface})_{new}}\right] \cdot \left[\frac{(Re/P_{T_o})_{M_{o\ design\ new}}}{(Re/P_{T_o})_{M_{o\ design\ old}}}\right]$$

for the high pressure bleed.

For the Mach 2.5 inlet transformed to the Mach 2.6 inlet design variables, the following results were obtained:

Mach 2.5 $\quad \frac{A_{o_{BLC}}}{A_c} = 0.07$

Mach 2.6 Method 1 $\quad \frac{A_{o_{BLC}}}{A_c} = 0.087$

Method 2 $\quad \frac{A_{o_{BLC}}}{A_o} = 0.085$ (vs. 0.07)

For the Mach 2.5 to Mach 3.0 design variables

Method 1 $\quad \frac{A_{o_{BLC}}}{A_c} = 0.116$

Method 2 $\quad \frac{A_{o_{BLC}}}{A_c} = 0.111$ (vs. 0.105)

For the Mach 2.6 to Mach 3.0 design variables

Method 1 $\quad \frac{A_{o_{BLC}}}{A_c} = 0.092$

Method 2 $\frac{A_{o\,BLC}}{A_c} = 0.90$ (vs. 0.105)

These results do not seem initially to be consistent. If one were to say that they are due to differences in maneuverability (angle-of-attack capability), with higher bleed rate equating to higher maneuverability, then we would rate the inlets with the Mach 2.6 as least maneuverable, the Mach 2.5 as most maneuver- able, and the Mach 3.0 inlet between. This was done by comparing bleed rates at a Mach 3.0 design for each inlet. Examining the references it was found that the Mach 2.5 inlet was for a fighter-bomber, the Mach 2.6 inlet for a commercial SST, and the Mach 3.0 inlet for a bomber. The maneuverability characteristics would indeed rank the inlets as listed from the prediction.

It is likely that high maneuverability brings lowered recovery to achieve stable operation. Knowing the ranking above, it would be expected that for a Mach 3.0 design, the Mach 2.6 base would have highest recovery, the Mach 2.5 lowest recovery, and the Mach 3.0 between them.

The recovery calculation assumes that the inlet loss co-efficient, $\frac{\Delta P_T/P_{T_o}}{q_o} = f(M_o)$ is valid. Thus when design Mach number changes, q_o changes. The equation is

$$\frac{P_{T_2}}{P_{T_{o\,new}}} = 1 - \left[\left(1 - \frac{P_{T_2}}{P_{T_{o\,old}}}\right)\cdot\left(\frac{M_{o\,new}}{M_{o\,old}}\right)^2\right]$$

For the Mach 2.5 to Mach 2.6 design

$$\frac{P_{T_2}}{P_{T_{o\,new}}} = 0.897 \text{ (vs. } 0.916)$$

For the Mach 2.5 to Mach 3.0 design

$$\frac{P_{T_2}}{P_{T_{o\,new}}} = 0.863 \text{ (vs. } 0.885)$$

For the Mach 2.6 to Mach 3.0 design

$$\frac{P_{T_2}}{P_{T_o\ new}} = 0.888 \quad \text{(vs. 0.885)}$$

These predictions of recovery would, in fact, order the inlets in the same manner as previously ranked. The result of these comparisons is that the bleed and recovery analyses show the correct trends. It also illustrates the effect and importance of the selection of the baseline inlet map file. Further demonstration of the methods requires evaluation among a family of inlets with similar designs and applications.

The second group of inlets consists of four mixed compression, axisymmetric inlets, all designed for supersonic cruise application. The following table provides information at the design Mach number.

Design Mach No.	2.35	2.65(A)	2.65(B)	3.5
Recovery	.93	.927	.907	.837
Bleed Rate	.0553	.0662	.07	.134
Initial Cone Angle	10.3°	11.2°	9.0°	10.0°
Cone Surface Mach No.	2.174	2.326	2.439	3.125
Reference	13	11	11, 27	12

The two bleed rate prediction methods used previously are used again.

For the Mach 2.35 to the Mach 2.65(A) design

Method 1 $$\frac{A_{o\ BLC}}{A_{c\ new}} = 0.0643 \quad (-2.8\%)$$

Method 2 $$\frac{A_{o\ BLC}}{A_{c\ new}} = 0.0635 \quad (-4.1\%)$$

For the Mach 2.35 to the Mach 2.65(B) design

Method 1 $\frac{A_{o_{BLC}}}{A_{c_{new}}} = 0.0732 \ (+4.6\%)$

Method 2 $\frac{A_{o_{BLC}}}{A_{c_{new}}} = 0.0715 \ (+2.1\%)$

For the Mach 2.35 to the Mach 3.5 design

Method 1 $\frac{A_{o_{BLC}}}{A_{c_{new}}} = 0.153 \ (+14.0\%)$

Method 2 $\frac{A_{o_{BLC}}}{A_{o_{new}}} = 0.141 \ (+5.4\%)$

For the Mach 2.65(A) to the Mach 3.5 design

Method 1 $\frac{A_{o_{BLC}}}{A_{c_{new}}} = 0.157 \ (+17.4\%)$

Method 2 $\frac{A_{o_{BLC}}}{A_{c_{new}}} = 0.147 \ (+9.8\%)$

For the Mach 2.65(B) to the Mach 3.5 design

Method 1 $\frac{A_{o_{BLC}}}{A_{c_{new}}} = 0.146 \ (+9.05\%)$

Method 2 $\frac{A_{o_{BLC}}}{A_{c_{new}}} = 0.138 \ (+2.95\%)$

These comparisons show that Method 2 produces less than 10% error in bleed rate for all these design modifications, when compared to the actual inlet. Generally the error is considerably smaller than that. Method 2 is used in the derivative procedure for mixed compression inlets. These results are better than first order accurate.

The recovery calculation is as described previously in this Appendix.
For the Mach 2.35 to Mach 2.65(A) design

$$\frac{P_{T_2}}{P_{T_o}}_{new} = 0.911 \quad (-1.7\%)$$

For the Mach 2.35 to Mach 2.65(B) design

$$\frac{P_{T_2}}{P_{T_o}}_{new} = 0.911 \quad (+0.44\%)$$

For the Mach 2.35 to Mach 3.5 design

$$\frac{P_{T_2}}{P_{T_o}}_{new} = 0.845 \quad (+0.92\%)$$

For the Mach 2.65(A) to Mach 3.5 design

$$\frac{P_{T_2}}{P_{T_o}}_{new} = 0.873 \quad (+4.26\%)$$

For the Mach 2.65(B) to Mach 3.5 design

$$\frac{P_{T_2}}{P_{T_o}}_{new} = 0.838 \quad (+0.09\%)$$

These results show excellent agreement, certainly better than first order accuracy.

4.0 REFERENCES

1. Fishbach, L. H., Caddy, M. J., NNEP-The Navy NASA Engine Program, NASA TM X-71857, December 1975.

2. Onat, E., and Klees, G. W., A Method to Estimate Weight and Dimensions of Large and Small Gas Turbine Engines, CR159481, January 1979.

3. Ball, W. H., and Hickcox, T. E., Rapid Evaluation of Propulsion System Effects, AFFDL-TR-78-91, July 1978.

4. Sharp, B. M., and Howe, J. P., "Procedures for Estimating Inlet External and Internal Performance", NWC TP 5555, Naval Weapons Center, China Lake, California, April 1974.

5. Ball, W. H., Propulsion System Installation Corrections, AFFDL-TR-72-147, Volumes I-IV, Air Force Flght Dynamics Laboratory, December 1972.

6. Gerend, R. P., and Roundhill, J. P., "Correlation of Gas Turbine Engine Weights and Dimensions", AIAA Paper 70-669, June 1970.

7. Cawthon, J. A., et al, Supersonic Inlet Design and Airframe-Inlet Integration Program (Project TailorMate), Volume III, Composite Inlet Investigation, AFFDL-TR-71-124, Vol. III, Air Force Flight Dynamics Laboratory, WPAFB, Ohio, May 1973.

8. Rejeske, J. V., and Porter, J. L., Inlet/Aircraft Drag Investigation, AFFDL-TR-74-34, Air Force Flight Dynamics Laboratory, WPAFB, Ohio, April 1974.

9. Gould, D. K., and Eastman, D. W., Methods Used to Determine Aerodynamic Drag and Installed Propulsion Thrust for the Boeing Lightweight Fighter, D199-10003-1, The Boeing Company, 1972.

10. Randall, L. M., The XB-70A Air Induction System, AIAA Paper No. 66-634, AIAA Second Propulsion Joint Specialist Conference, Colorado Springs, Colorado, 13-17 June 1966.

11. Randall, L. M., et al, Experimental Investigation to Determine the Effect of SEveral Design Variables on the Performance of the F-100 Duct Inlet, NA-53-26, North American Aviation, Inc., 7 January 1953.

12. Bates, D. L., and Welling, S. W., Engine Inlet Pressure Survey - 747 Airplane, Boeing Report No. D6-30622, The Boeing Company, Seattle, Washington, 17 November 1969.

13. Syberg, J., and Koncsek, J. L., "Low Speed Tests of a Fixed Geometry Inlet for a Tilt Nacelle V/STOL Airplane", NAS2-9215, January 1977.

14. Petersen, Martine W., and Tamplin, Gordon C., Experimental Review of Transonic Spillage Drag of Rectangular Inlets, Air Force Report No. APL-TR-66-30, May 1966.

15. Syberg, J., and Koncsek, J. L., "Transonic and Supersonic Test of the SST Prototype Air Intake", FAA-SS-72-50, April 15, 1972.

16. Syberg, J., and Koncsek, J. L., "Experimental Evaluation of a Mach 3.5 Axisymmetric Inlet", NASA CR-2563, Prepared by Boeing Commercial Airplane Company for NASA Ames Research Center, July 1975.

17. Syberg, J., "Analytic Design of AST Inlet", Boeing Company Document D180-20551-1, The Boeing Company, Seattle, Washington, March 8, 1977.

18. Paynter, G. C., Shock and Ramp Induced Incipient Separation of a Turbulent Boundary Layer, D6-11847, The Boeing Company, November 3, 1967.

19. Equations, Tables, and Charts for Compressible Flow, NACA Report 1135, 1953.

20. Syberg, J., and Hickcox, Design of a Bleed System for a Mach 3.5 Inlet, NASA CR-2187, January 1973.

21. Exhaust System Interaction Program, Handbook, D162-10467-12, The Boeing Aerospace Company, Seattle, Washington, Contract F33615-70-C-1450, April 1973.

22. Wynosky, T. A., and Spurrell, R. M., Final Progress Report, Exhaust System Interaction Program, PWA-4745, Contract No. F33615-70-C-1450, 5 June 1973, Pratt and Whitney Aircraft, East Harford, Connecticut.

23. Berrier, B. L., Effect of Nonlifting Empennage Surfaces on Single-Engine Afterbody/Nozzle Drag at Mach Numbers from 0.5 to 2.2, NASA TN D-8326, 1977.

24. Paul, S. A., Installed Turbine Engine Survivabiliy Criteria (ITESC Program) Pratt & Whitney Aircraft Group Report FR-8824, 31 August 1977.

25. McBarron, J. P., and McKimson, J. F., "Guidelines for Mass Properties Estimating", D6-15095TN, The Boeing Company, March 1966.